

UNCLASSIFIED

FILE COPY

SECURITY CLASSIFICATION OF THIS PAGE (When Data Entered)

AD-A197 147

REPORT DOCUMENTATION PAGE		READ INSTRUCTIONS BEFORE COMPLETING FORM
1. REPORT NUMBER AFIT/CI/NR 88- 105	2. GOVT ACCESSION NO.	3. RECIPIENT'S CATALOG NUMBER
TITLE (and Subtitle) ULTRAVIOLET-INDUCED FLASHOVER OF HIGHLY-ANGLED POLYMERIC INSULATORS IN VACUUM		5. TYPE OF REPORT & PERIOD COVERED THESIS
AUTHOR(s) CARL LON ENLOE		6. PERFORMING ORG. REPORT NUMBER
PERFORMING ORGANIZATION NAME AND ADDRESS AFIT STUDENT AT: UNIVERSITY OF MICHIGAN		8. CONTRACT OR GRANT NUMBER(s)
CONTROLLING OFFICE NAME AND ADDRESS		10. PROGRAM ELEMENT, PROJECT, TASK AREA & WORK UNIT NUMBERS
14. MONITORING AGENCY NAME & ADDRESS (if different from Controlling Office) AFIT/NR Wright-Patterson AFB OH 45433-6583		12. REPORT DATE 1988
		13. NUMBER OF PAGES 155
		15. SECURITY CLASS. (of this report) UNCLASSIFIED
		15a. DECLASSIFICATION/DOWNGRADING SCHEDULE
16. DISTRIBUTION STATEMENT (of this Report) DISTRIBUTED UNLIMITED: APPROVED FOR PUBLIC RELEASE		
17. DISTRIBUTION STATEMENT (of the abstract entered in Block 20, if different from Report) SAME AS REPORT		
18. SUPPLEMENTARY NOTES Approved for Public Release: IAW AFR 190-1 LYNN E. WOLAVER Dean for Research and Professional Development Air Force Institute of Technology Wright-Patterson AFB OH 45433-6583		
19. KEY WORDS (Continue on reverse side if necessary and identify by block number)		
20. ABSTRACT (Continue on reverse side if necessary and identify by block number) ATTACHED		

DTIC
SELECTED
AUG 17 1988
S H

DD FORM 1 JAN 73 1473

EDITION OF 1 NOV 65 IS OBSOLETE

UNCLASSIFIED

SECURITY CLASSIFICATION OF THIS PAGE (When Data Entered)

88*8-16 035

ABSTRACT OF DISSERTATION

ULTRAVIOLET-INDUCED FLASHOVER OF HIGHLY-
ANGLED POLYMERIC INSULATORS IN VACUUM

by
Carl Lon Enloe
Captain, United States Air Force

PhD (Nuclear Engineering), 1988
The University of Michigan

155 pages

The flashover of electrically stressed polymeric insulators in vacuum induced by exposure to intense ultraviolet radiation was investigated. Two geometries, positive and negative 45 degrees, were studied at electric field stresses of up to 80 kV/cm. Insulating materials tested were polyethylene, polystyrene, acrylic, nylon-6, acetal, PVC, and teflon. A krypton fluoride excimer laser at a wavelength of 248 nm provided the ultraviolet illumination.

Ultraviolet-induced flashover over polymeric insulators in vacuum depends on the ultraviolet fluence (energy density) incident on the insulator surface. The negative-angle (unconventional) configuration exhibits superior ultraviolet tolerance compared to the positive-angle (conventional) configuration by approximately a factor of two in fluence. Insulating materials with high dielectric constants and low secondary electron emission coefficients exhibit superior ultraviolet tolerance. A model of ultraviolet-induced insulator flashover based on induced charging of the insulator surface is sufficient to explain the observed phenomena. The ultraviolet fluences required to initiate flashover are sufficiently low so that the contribution of neutral particles to the initiation of flashover may be disregarded, except perhaps at very low field stresses where the critical flashover fluences are correspondingly higher. Overall, of the materials tested, nylon exhibited the best performance (that is, the highest critical fluence in both polarities) because of its high dielectric constant and low secondary electron emission.

theseo. (7/19/77) ←

BIBLIOGRAPHY

R. A. Anderson, "Role of the Secondary Electron Emission Avalanche in Surface Flashover or [sic] Insulators in Vacuum," in *1974 Annual Report, Conference on Electrical Insulation and Dielectric Phenomena* (Washington, D.C.: National Academy of Sciences, 1975), 435.

R. A. Anderson, "Propagation velocity of cathode-initiated surface flashover," *J. Appl. Phys.* 48 (10), 4210 (1977).



Availability Codes

Dist Avail and/or
Special

A-1

ULTRAVIOLET-INDUCED FLASHOVER OF HIGHLY-
ANGLED POLYMERIC INSULATORS IN VACUUM

by

Carl Lon Enloe

A dissertation submitted in partial fulfillment
of the requirements for the degree of
Doctor of Philosophy
(Nuclear Engineering)
in The University of Michigan
1988

Doctoral Committee:

Associate Professor Ronald M. Gilgenbach, Chairman
Assistant Professor Mary L. Brake
Professor Terry Kammash
Assistant Professor Robert M. Ziff

To the memory of my mother, who would have wanted to see this.

ACKNOWLEDGEMENTS

It is in some ways unfair that one person's name should appear on a dissertation, when in reality no work of this magnitude can be created without the cooperation of a large number of people. I am indebted, foremost, to my advisor, Prof. Ron Gilgenbach, for the resources and the feedback he provided, and for the wholehearted manner in which he adopted this project. I would like to thank the other members of my committee as well, Prof. Mary Brake, who gave me a crash course in spectroscopy, Prof. Terry Kammash, and Prof. Robert Ziff, for their assistance in completing this work.

My fellow graduate students at the Plasma Experimental Bay made for a pleasant working environment indeed. Bob Lucey would never give anything less than the most complete answer to any question, no matter how bothersome or inconvenient. "No, that's all right, I didn't mean for you to look for it," carried almost no weight with him. Mike Cuneo had the uncanny ability to think about everyone else's projects, as well as his own, when in the vicinity of the library. Tom Repetti and Mike Passow rarely raised an eyebrow when they by rights could have raised the roof, every time I asked them to run the spectrometer for me on less than short notice. Steve Bidwell and Bob Bosch exhibited similar patience, when we all found out just how cozy a screen room could be. I owe a great deal to Joe Meachum for not being satisfied until the position sensor was fast enough (and to our technician Ron Spears, for making it that way), and I cannot forget John Tucker's helping me to break into life around the lab. I have enjoyed the

daily give-and-take with all of the group at the lab, perhaps because they let me get away with more than my fair share of the latter.

I would like also to thank my colleagues from my days in New Mexico, especially Bob Reinovsky and Norm Roderick. I feel that the background and support which they gave me is responsible, in large measure, for the success I have enjoyed here at the University of Michigan.

I gratefully acknowledge the financial support of this research and my education from the Air Force Institute of Technology, the National Science Foundation, the Air Force Office of Scientific Research, the Office of Naval Research, and the Strategic Defense Initiative Organization.

PREFACE

When I began researching this topic at the Air Force Weapons Laboratory, fresh out of my undergraduate curriculum, I had no idea that I would become as involved with it as I have. The project became personal when I found myself standing before the attendees of the Pulsed Power Conference, telling a group whom I very much considered my superiors to go back to their laboratories and turn their insulators upside-down. I think that some of my continuing interest in this topic stems from a desire to justify myself in that moment. I was delighted to find out, upon my arrival at the University of Michigan, that I would have the opportunity to make some of the improvements to the experiment which I had always wanted to make. I would like to think that the results which I have obtained shed some light outside the narrow boundaries which the title of this work would imply. For a project which sometimes seemed the most obscure I could have fastened onto, that would indeed be rewarding.

TABLE OF CONTENTS

DEDICATION	ii
ACKNOWLEDGEMENTS	iii
PREFACE	v
LIST OF TABLES	viii
LIST OF FIGURES	ix
LIST OF APPENDICES	xiv
CHAPTER	
1. INTRODUCTION	1
1.1. Historical Development	
1.2. Approach	
2. A REVIEW OF UNILLUMINATED INSULATOR FLASHOVER BEHAVIOR	8
2.1. Emperical Results	
2.2. Theory of Surface Charging of Vacuum Insulators	
2.3. Theory of Flashover of Vacuum Insulators	
2.4. Parameters of the Present Experiment	
3. EXPERIMENTAL CONFIGURATION	23
3.1. Ultraviolet Illumination Source	
3.2. Test Chamber	
3.3. Electrical Diagnostics	
3.4. Optical Diagnostics	
3.5. Timing	
4. RESULTS AND ANALYSIS	61
4.1. Ultraviolet Effects on Polymers	
4.2. Electron Emission Measurements	
4.3. Neutral Particle Emission Measurements	
4.4. Characterization of Induced Flashover	

5. THEORY OF INDUCED FLASHOVER	101
6. CONCLUSIONS	112
APPENDICES	114
REFERENCES	149

LIST OF TABLES

Table

2.1. Properties of Insulating Materials	21
4.1. Spectral Lines in Flashover Plasmas	85
4.2. Flashover Performance of Insulating Materials	100
C.1. Gas Mixtures for the KrF Excimer Laser	148

LIST OF FIGURES

Figure

1.1. Examples of insulator flashover in various situations. a) The simplest case, a plane insulator/vacuum interface between plane parallel electrodes, with the interface normal to the electrodes. b) As in (a), except that the insulator/vacuum interface is at an angle to the electrode normal. c) As in (b), except that ultraviolet radiation is incident on the insulator surface.	4
1.2. Solving the problem of ultraviolet-induced insulator flashover by isolating the insulator surface from the ultraviolet source. The straight transmission line (a) is replaced by a convoluted transmission line (b).	5
2.1. The angle convention in insulator flashover. a) Positive angle, in which an electrons are accelerated away from the insulator surface. This is the conventional configuration. b) Negative angle, in which electrons are accelerated into the insulator surface. This is the unconventional configuration.	11
2.2. Flashover strenth of several materials without ultraviolet illumination versus angle of the insulator (from Milton [Mil72]).	12
2.3. Universal secondary electron emission coefficient curve for polymers (from Burke [Bur80]).	14
2.4. Insulator surface charging. a) Uncharged insulator surface. b) Equilibrium surface charge distribution.	16
2.5. Chemical formulas for the materials used in this experiment. a) Polyethylene. b) Teflon. c) Acetal. d) PVC. e) Nylon-6. f) Acrylic. g) Polystyrene.	22
3.1. Experimental configuration. a) Carbon block calorimeter. b) Quartz converging lens. c) Attenuators. d) Excimer laser. e) Quartz window. f) Optional Collimator. g) Top electrode. h) Vacuum gauge. i) Slip seal. j) Screw-thread adjustment. k) Bottom electrode. l) BNC feed-through. m)Adjustable feet. n) Turbomolecular pump. o) Variable aperture.	24

3.2. Variation of energy in the excimer laser pulse versus shot number.	26
3.3. Normalized laser pulse shape $f(t)$ and its integral, which were the same for all shots.	27
3.4. Transmission of the excimer laser beam versus number of sheets of plastic attenuators.	28
3.5. Equipotential contours for an insulator near to (a) and far from (b) the edge of the electrodes, demonstrating that edge effects may be neglected if an insulator is inset from the edge of the electrodes by approximately its thickness.	33
3.6. Electrode configurations. a) Charged particle collector. b) Typical configuration, including voltage and current monitors.	34
3.7. Rogowski coil used in the experiment. a) cross-section of the coil, including electrostatic shield. b) Top view of the coil, including terminating resistor and passive integrating circuit.	36
3.8. Calibration of the Rogowski coil used in the experiment. Sensitivity 0.055 V/A.	39
3.9. Capacitive V-dot probe used in the experiment. a) Physical implementation. b) Equivalent circuit, including terminating resistor and passive integrating network.	41
3.10. Calibration of the capacitive V-dot probe used in the experiment. Sensitivity 0.046 V/kV.	44
3.11. High-speed passive integrator used to integrate Rogowski coil and capacitive V-dot probe signals without introducing ringing. a) BNC feed-through connectors. b) Copper foil outer conductor. c) Resistor. d) Coaxial capacitor. e) Copper foil outer conductor.	46
3.12. The laser deflection technique applied to detecting neutral emission from the insulator surface. a) He-Ne probe laser. b) Insulator surface, from which neutral particles are emitted. c) Position sensor.	49
3.13. Position sensor circuit, including quadrant detector, differential stage, amplifying stage, and high-pass filter. ...	51
3.14. Comparing the output of one side of the position sensor (a) with that of a fast p-i-n diode (b) yields a circuit risetime of approximately 20 ns for the position sensor.	53

3.15. Timing chain. a) Trigger generator. b) Excimer laser. c) Ultraviolet-sensitive p-i-n diode. d) Capacitive V-dot probe. e) Rogowski coil.	58
3.16. Dedicated trigger unit with delay channels.	60
4.1. Electron emission signal versus voltage applied to the collecting plates. The knee in the curve corresponds to an electric field of approximately 50 V/cm.	64
4.2. Electron emission signal versus background pressure in the chamber.	65
4.3. Electron emission from polyethylene and teflon, indicating the conditioning effects of repeated exposure to ultraviolet radiation.	66
4.4. Electron emission from polymers under ultraviolet illumination. a) Polyethylene and polystyrene, which are simple hydrocarbons. b) Acetal, nylon, and acrylic, which are more complex polymers. c) Teflon and PVC, which are polymers containing halogens.	67
4.5. Experimental configuration for determining the lifetime of excited states in a polymer. a) Incident ultraviolet laser beam. b) Visible light (fluorescence). c) Acrylic sample. d) Photodiode.	70
4.6. a) Input ultraviolet laser pulseshape. b) Decay of prompt fluorescence. c) Convolution of (a) and (b) indicating increased pulsewidth Δw	71
4.7. Results of a coupled rate equation model of two step photoionization.	74
4.8. Neutral emission from polymers under ultraviolet illumination. a) Polyethylene and polystyrene. b) Acetal, nylon-6, and acrylic. c) Teflon and PVC.	76
4.9. Typical data from ultraviolet-induced insulator flashover. a) Incident laser pulse. b-d) Voltage (top) and current (bottom) in the interelectrode region. Shots (b) through (d) are in order of decreasing laser pulse energy.	79
4.10. Experimental configuration for emission spectroscopy, indicating the composition of each component. a) +45° (conventional) configuration. b) -45° (unconventional) configuration.	81

4.11. Emission spectra of flashover plasmas with an aluminum anode, a brass cathode, and a teflon insulator. a) +45° (conventional) configuration, early time. b) -45° (unconventional) configuration, early time. c) +45° (conventional) configuration, late time. d) -45° (unconventional) configuration, late time.	83
4.12. Burn patterns observed after ultraviolet induced flashover. The results are similar for both polarities	87
4.13. Open-shutter photographs of the flashover event. a) Conventional configuration. b) Unconventional configuration.	89
4.14. Geometry used in data analysis.	90
4.15. Typical insulator flashover behavior. a) Time to flash versus total fluence (laser pulse energy divided by illuminated area). b) Critical fluence (fluence at the time of flashover) versus total fluence.	92
4.16. Critical fluence as a function of polarity and electric field stress for insulators angled at 45 degrees. a) Polyethylene. b) Polystyrene. c) Acrylic. d) Nylon-6. e) Acetal. f) PVC. g) Teflon.	93
4.17. Critical fluence (for $E > 40$ kV/cm) versus secondary electron emission coefficient for the conventional (a) and the unconventional (b) configurations. Note the change in scale between the two graphs.	98
4.18. Critical fluence (for $E > 40$ kV/cm) versus relative dielectric constant for the conventional (a) and the unconventional (b) configurations. Note the change in scale between the two graphs.	99
5.1. Equipotential contours near the interface of a dielectric and vacuum. a and c) Uncharged surface. b and d) Charged surface.	104
5.2. Total electric field enhancement versus position on the insulator surface. Solid line: charged. Broken line: uncharged. a) $\theta = -45^\circ$ (unconventional). b) $\theta = +45^\circ$ (conventional).	105
5.3. Parallel electric field enhancement versus position on the insulator surface. Solid line: charged. Broken line: uncharged. a) $\theta = -45^\circ$ (unconventional). b) $\theta = +45^\circ$ (conventional).	106

5.4. Surface charging mechanisms. At large insulator angles, field emission from the triple point (a and c) is an unlikely source of surface charging. Ultraviolet illumination (b and d) provides a source of primary electrons across the entire insulator surface	107
5.5. Angle of the electric field to the surface of the insulator versus magnitude of surface charge for $\epsilon_r = 2$ (solid line) and $\epsilon_r = 4$ (dashed line).	109
5.6. Peak prebreakdown current/peak laser power for conventional and unconventional configurations.	111
A.1. Contour point and fictitious charge placement for the solution to the problem of an insulator in vacuum via the charge simulation technique. Crosses are contour points, while points are line charges. a) For an uncharged insulator. b) For a charged insulator.	117
B.1. LAPLACE scratchpad meshes. a) Four-sided mesh. b) Three-sided mesh. c) A trapezoidal four-sided mesh. d) A trapezoidal mesh created by truncating a three-sided mesh. e) Assembling a mesh with a circular boundary between regions.	139
B.2. Adding a scratchpad mesh to an archive mesh.	142
B.3. Simulating surface charge with thin regions of volume charge in three equivalent ways. a) By defining the potential. b and c) By defining the charge density.	143
B.4. A typical LAPLACE mesh used to solve the problem of a vacuum insulator with a uniform surface charge density.	144

LIST OF APPENDICES

Appendix

A. CHARGE SIMULATION TECHNIQUE	115
B. USING "LAPLACE"	137
C. OPERATING THE KrF EXCIMER LASER	145

CHAPTER 1

INTRODUCTION

1.1. Historical Development

It has been known for some time that the interface between a solid dielectric and a vacuum is subject to electrical breakdown if a sufficiently large electric field exists at that interface. [Gle51a, Gle51b, Bor58, Boe63] Because the breakdown appears on the surface of the dielectric, and because a hot surface plasma is formed which radiates brightly, the term "flashover" was coined to describe this breakdown phenomenon.

Understanding the flashover of insulators in vacuum is of great practical interest, since the need arises in many disciplines to apply high voltage in a vacuum region from a voltage source which remains outside the vacuum. This implies the presence on an interface somewhere in the system. It is this interface which will, in general, be the weak link in the power-flow chain and hence the determiner of system performance. The reason for this is straightforward. In an insulating material, charge carriers are not free to move, while in a vacuum charge carriers do not exist—either exhibits high breakdown strength. At the interface between the two, however, the insulator surface is a ready source of charge carriers, so that the breakdown strength of the interface is reduced. This reduction may be considerable, up to several orders of magnitude compared to the breakdown strength of either the insulator or the vacuum alone.

The problem of flashover in vacuum has been studied from the standpoint of the insulating materials used, [Gle51b, Bor58, Wat67, Haw68, Mil72, Jac83, Pil82, Pil85a] the geometry of the interface (including the polarity of the applied voltage), [Bor58, Sha65, Wat67, Haw68, Mil72, Avd77a, Tho80, Pil84] the magnitude and time-history of the voltage pulse, [Grz72, And85, Pil85a] surface charging effects, [DeT72, Bra74, Bra75, And79, Pil82] and other factors [Gle51a, Bug68, And77, Sud77, And78, Tho80, Van82, Pil85a] including coating and conditioning of the insulator surface. [Cro74, Sud76, Mil78, Mil80, Jac83, Mil85, Pil85b] Much empirical knowledge and some theoretical understanding has resulted.

With the advent of large (≥ 1 MV, ≥ 10 MA, ≥ 10 TW) pulsed-power devices, however, another factor was added to the problem—intense ultraviolet radiation. Ultraviolet radiation has a significant effect on vacuum insulators because its penetration depth is so small (typically $100\text{ }\mu\text{m}$ in polyethylene, which is one of the more transmissive polymers) that its effect is concentrated at the insulator surface. [Phi86] The presence of such radiation was found to initiate flashover over insulators even when they had been designed conservatively according to empirical criteria. The breakdown strength of insulators in such environments had to be considerably derated in order to obtain acceptable performance. [Bak78, Enl82, Enl83, Enl87a, Enl87b]

In approaching the problem of flashover of vacuum insulators, one may consider several cases. The simplest case which one may consider is the plane dielectric/vacuum interface between plane parallel electrodes, where the interface is normal to the electrodes, as in Figure 1.1(a). This case is the one which has received the most experimental and theoretical attention. The flashover

performance of a wide variety of materials in this configuration has been characterized, and several theories have been developed to explain the observed behavior. [Det73, And75, Avd77b, Ber77, Avd78, Bra78, And80, Lat81, Pil83, Gra85]

In practice, one is much more likely to encounter a slightly more complicated case, in which the plane interface is inclined at an angle to the electrodes, as in Figure 1.1(b). Although the body of experimental knowledge is smaller in this case than for the previous case, it has been confirmed that this case exhibits superior breakdown strength. [Wat67, Haw68, Mil72] Although this case seems to be only a slight perturbation of the previous case, it is not obvious that the same mechanisms which contribute to flashover in the previous case apply here.

The case of an angled insulator in the presence of intense ultraviolet radiation (Figure 1.1(c)) has received little attention experimentally except from this author, and none theoretically until now. Perhaps this is because that often the problem of reduced breakdown strength could be cured by simply isolating the ultraviolet source from the surface of the insulator, as shown in Figure 1.2. Although this may be an acceptable solution, it is an unsatisfying one. Clearly, it adds complexity and places additional bounds on the pulsed-power system designer. What is less obvious is that in many applications, one pays a price in system performance by the addition of inductance in the convolute section.

Several reasons may be given for studying ultraviolet-induced flashover of insulators in vacuum:

- 1) Solving a problem without clearly understanding it is counter to the spirit of science.

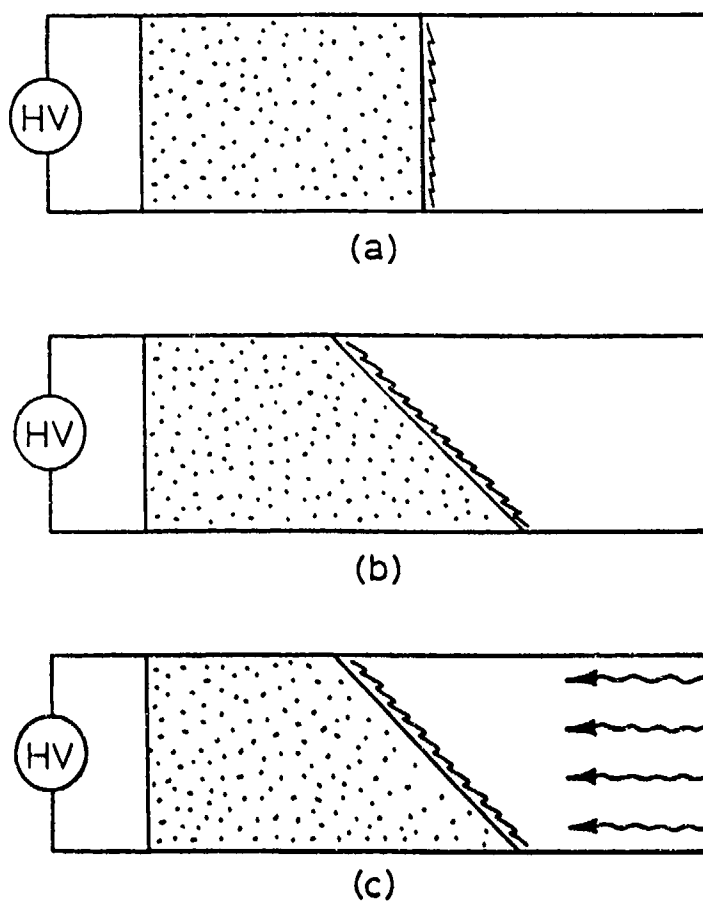
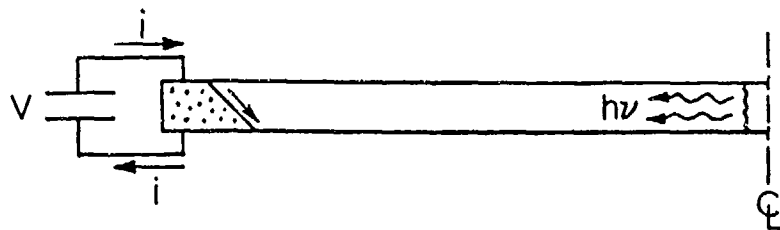
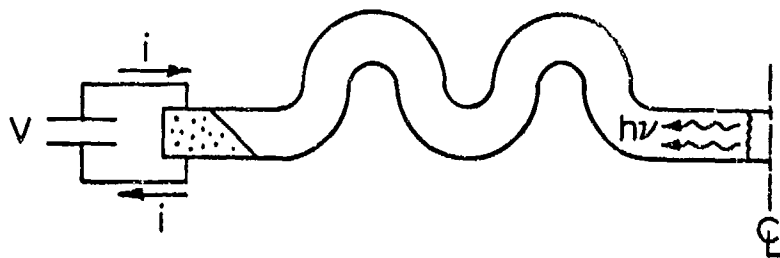


Figure 1.1. Examples of insulator flashover in various situations. a) The simplest case, a plane insulator/vacuum interface between plane parallel electrodes, with the interface normal to the electrodes. b) As in (a), except that the insulator/vacuum interface is at an angle to the electrode normal. c) As in (b), except that ultraviolet radiation is incident on the insulator surface.



(a)



(b)

Figure 1.2. Solving the problem of ultraviolet-induced insulator flashover by isolating the insulator surface from the ultraviolet source. The straight transmission line (a) is replaced by a convoluted transmission line (b).

- 2) The topic becomes more relevant as more large pulsed-power devices are built, and as one considers fielding pulsed-power systems in space.
- 3) Without an understanding of the process of ultraviolet-induced insulator flashover, it is impossible to exploit the effect to advantage in other applications. Such applications conceivably include switching, plasma processing, and the design of flashboard ion sources, excimer lasers, and other devices.
- 4) Understanding flashover behavior under ultraviolet illumination may aid in an understanding of the flashover process in general.
- 5) The processes involved in ultraviolet-induced insulator flashover may be applicable to other severe environments.

While any of these reasons would justify studying the process of ultraviolet-induced insulator flashover, together they make the study compelling.

1.2. Approach

Given that there is no theoretical base from which to approach the particular problem of ultraviolet-induced flashover of vacuum insulators, this work takes the following approach: Take a number of samples of insulating materials and catalogue as many properties of these materials as may be relevant. (Some properties may be available in the literature, while other properties may need to be determined in the course of the experiment.) Determine the flashover behavior of each of these materials under ultraviolet illumination in vacuum, diagnosing the phenomenon as completely as possible. Look for correlations between material properties and flashover behavior. Arrive at a theory which explains these correlations in as simple a way as possible.

The materials to be studied should be diverse enough to allow correlations over a reasonable range of properties, yet not so disparate as to have nothing in common. The materials chosen for this work are all polymers, and the basis of that choice was twofold: 1) Polymers exhibit both significant similarities and differences, and so are an optimum group to choose according to the previous criterion. 2) Because of their mechanical properties, polymers are the insulating material of choice in most large pulsed-power systems, where the effect of ultraviolet is most significant.

Clearly, any experiment must limit the portion of parameter space which it examines. The choices made in limiting the scope of the present experiment were based on the current state of understanding of insulator flashover in vacuum. These choices may be justified after a brief review of vacuum insulator behavior in the absence of ultraviolet radiation.

CHAPTER 2

A REVIEW OF UNILLUMINATED INSULATOR FLASHOVER BEHAVIOR

As a basis for understanding the flashover performance of vacuum insulators under ultraviolet illumination, it is helpful to understand their flashover performance in the unilluminated case. Although such behavior has been well-characterized and parameterized, the theoretical understanding of the process is not yet mature.

2.1. Empirical Results

Much of the work in the area of insulator flashover in vacuum has gone into determining which parameters are important in predicting flashover behavior, and which may be neglected.

Flashover behavior is particularly insensitive to two variables, background pressure and electrode material. Although most vacuum insulator flashover experiments are conducted in modest to high vacuum (10^{-7} – 10^{-4} Torr), it has been shown that flashover behavior does not vary significantly for pressures $\leq 10^{-2}$ Torr. [Haw68] Therefore almost any experiment which one is likely to encounter in the literature is well within the allowable vacuum regime. Likewise, the electrode material appears to have minimal, if any, effects on flashover behavior, [Gle51b, Pil85a] so that the choice of electrode material is largely a matter of convenience.

The time history of the voltage pulse can affect flashover behavior to some degree. In particular, flashover strength—the voltage at which flashover occurs for a given configuration—tends to be higher for pulses of nanosecond duration than for microsecond duration. [Wat67, Mil72, Bra78] For pulselengths longer than microsecond duration, however, flashover performance shows little variation. [Pil84, Pil85a] Besides the shape of the applied voltage pulse, conditioning effects are commonly observed. Flashover strength tends to increase as an insulator is exposed to high voltage, whether in the form of increasing DC voltage or repetitive pulses.

The insulator material, on the other hand, has a major effect on flashover behavior. [Gle51b, Bor58, Wat67, Haw68, Mil72, Jac83, Pil82, Pil85a] A wide variety of insulating materials have been tested in vacuum, including polymers, glasses, metal oxides, and combinations of these. In identical geometries, flashover strength can vary by an order of magnitude among a group of different materials. Significant work has gone into coating and otherwise modifying insulator surfaces to improve flashover performance. [Cro74, Sud76, Mil78, Mil80, Jac83, Mil85, Pil85b] Thin coatings of conducting and semi-conducting materials on the insulator surface can increase flashover strength significantly.

The insulator geometry is the other major parameter, besides the insulator material, which most effects flashover performance in vacuum. [Bor58, Sha65, Wat67, Haw68, Mil72, Avd77a, Tho80, Pil84] A large number of complicated geometries have been tried, concentrating especially on modifying the geometry of the triple points where insulator, electrodes, and vacuum meet, but none have exhibited significant increases in performance over the plane dielectric/vacuum interface of optimal design. [Sha65]

The performance of the plane interface is, however, a strong function of the angle of the interface. By convention, the angle θ of the interface is the acute angle between the interface and the normal to the electrode surfaces, so that $-90^\circ < \theta < +90^\circ$. The sign convention is determined by the nominal trajectory of electrons in the interelectrode region. If electrons tend to be accelerated away from the insulator surface, then the insulator angle is positive; otherwise, it is negative. The angle convention is illustrated in Figure 2.1.

The flashover strength of several insulating materials versus angle of the insulator is shown in Figure 2.2. This behavior is typical of almost all insulating materials. Flashover strength is minimum for $\theta = 0^\circ$, and has a local maximum at $\theta = \pm 45^\circ$. Typically, the maximum at $\theta = 45^\circ$ is greater than that at $\theta = -45^\circ$, hence, conventional design practice calls for an insulator at $+45^\circ$. An insulator installed at -45° would be an unconventional configuration.

The behavior of flashover strength with angle has generally been explained by considering the electric field configuration in the interelectrode region. [Wat67, Bra78, Tho80, Pil84] Because of the presence of the dielectric, the electric field is modified so that it may be enhanced in some regions and reduced in others. The field enhancement depends, of course, on the insulator geometry, but it also depends on whether or not the surface of the insulator has acquired a charge.

2.2. Theory of Surface Charging of Vacuum Insulators

It has long been known that, under certain conditions of high-voltage stress, the surface of a vacuum insulator may acquire a charge. [Boe63, DeT72, DeT73, Bra74, Bra75, And79] The reason for this charging of the surface lies in the secondary electron emission characteristics of the surface. If an electron of energy

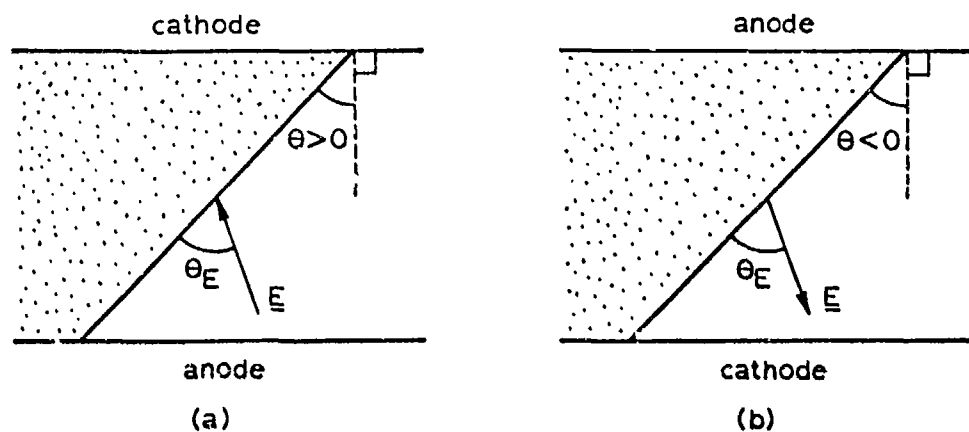


Figure 2.1. The angle convention in insulator flashover. a) Positive angle, in which an electrons are accelerated away from the insulator surface. This is the conventional configuration. b) Negative angle, in which electrons are accelerated into the insulator surface. This is the unconventional configuration.

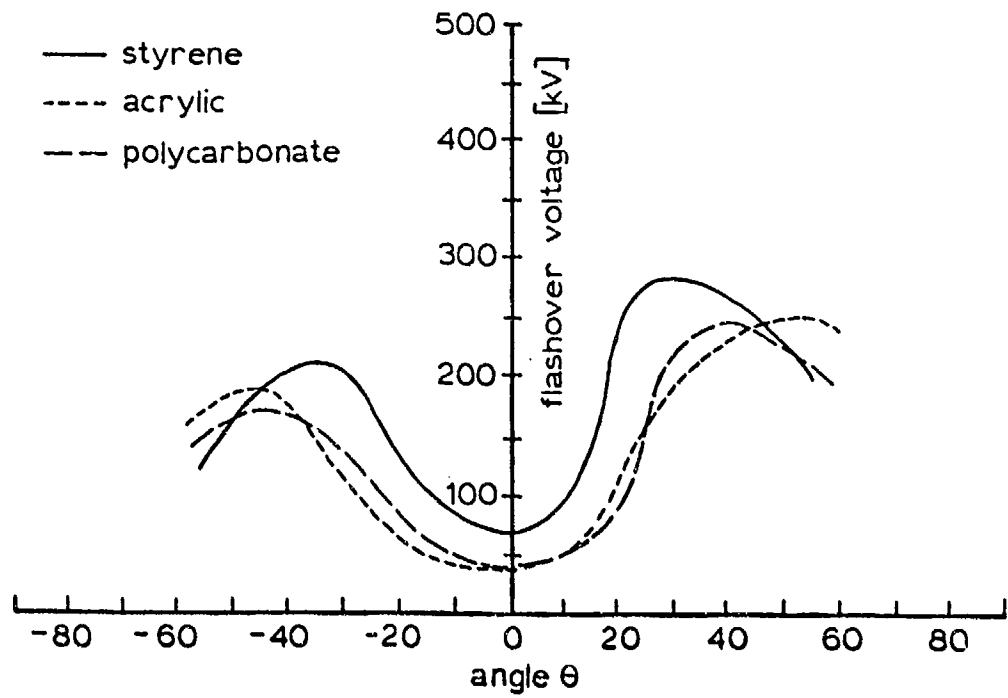


Figure 2.2. Flashover strength of several materials without ultraviolet illumination versus angle of the insulator (from Milton [Mil'72]).

\mathcal{E}_i strikes the surface of an insulator, on the average δ electrons will re-emerge from the surface; δ is the secondary electron emission coefficient and is a strong function of \mathcal{E}_i . In general, δ is zero at zero incident energy, as well as at multi-kilovolt energies when the incident (primary) electrons are quite penetrating. At moderate energies, δ has a single maximum.

Burke [Bur80] has shown that for polymers, the secondary electron emission coefficient versus incident energy follows a universal curve (shown in Figure 2.3). The formula is semi-empirical, based on the one-dimensional power law theory of secondary electron emission, [Dio73] and is given by [Bur80]

$$\delta = 3.41 K \left[\frac{1 - \exp(-5.45 \mathcal{E}_i^{1.725}/K)}{5.45 \mathcal{E}_i^{0.725}} \right] \quad (2.1)$$

where the constant K varies with the material, and \mathcal{E}_i is in keV. The maximum yield is $\delta_m = 9.5 \mathcal{E}_i[\text{keV}]$ and occurs at $\mathcal{E}_m[\text{keV}] = (K/12.09)^{0.580}$. (Dionne [Dio75] has a more precise three-dimensional treatment of the calculation of these quantities, but the difference between the one-dimensional and the three-dimensional models is only a few percent, at least for polymers.) The constant K is a function of the composition of the insulator and for certain polymers, specifically those containing hydrogen, carbon, nitrogen, and oxygen, is given by

$$K = 10.64 (N/M) - 3.15 \quad (2.2)$$

where (N/M) is the ratio of the valence electrons to the gram molecular weight on the unit polymer chain. For hydrogen, carbon, nitrogen, and oxygen, respectively, $N = 1, 4, 5, 6$, so that for many polymers the secondary electron emission properties can be readily determined from the composition of the insulator. Burke also gives data for materials (notably teflon) for which Equation (2.2) does not apply.

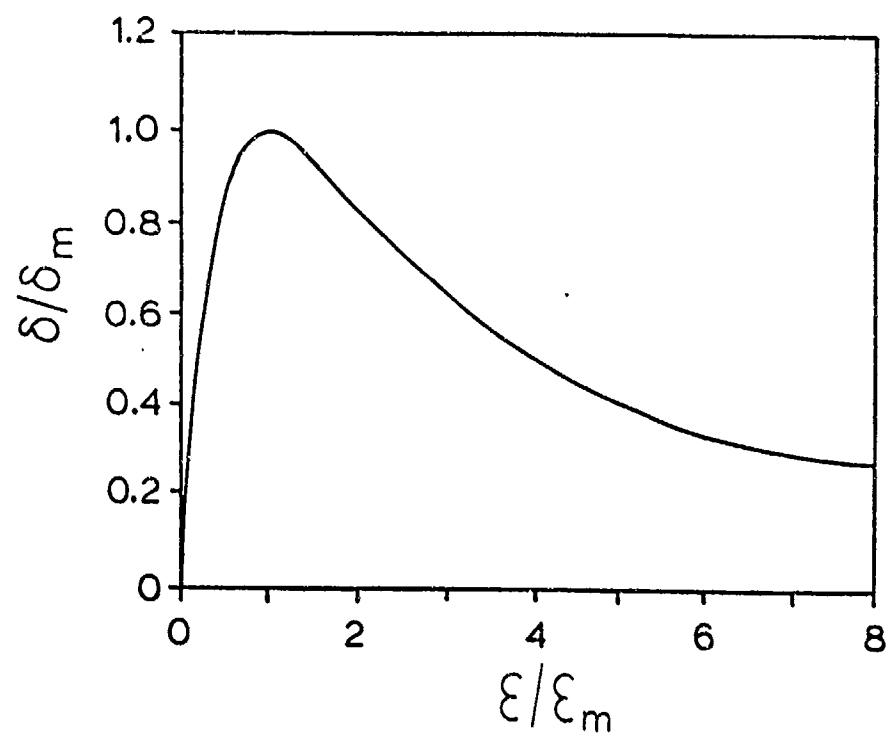


Figure 2.3. Universal secondary electron emission coefficient curve for polymers (from Burke [Bur80]).

For most materials, $\delta_m > 1$. Therefore, there are two "crossover energies," \mathcal{E}_1 and \mathcal{E}_2 , where $\delta = 1$. By convention $\mathcal{E}_2 > \mathcal{E}_1$. Because the slope of the secondary electron emission curve through \mathcal{E}_1 is positive, this quantity plays a major role in determining how the insulator charges. An equilibrium is established when the local electric field on the insulator surface is such that an electron emitted from the surface returns to the surface with energy \mathcal{E}_1 .

Consider the situation illustrated in Figure 2.4. Assume that electrons which leave the insulator surfaces return with $\mathcal{E}_i \approx \mathcal{E}_1$. If $\mathcal{E}_i > \mathcal{E}_1$, then $\delta > 1$. More negative charge leaves the insulator surface with the secondary electrons than arrives with the primaries, on the average, so that the surface acquires a positive charge. The perpendicular electric field increases, so that subsequently electrons are attracted back to the insulator sooner. Because of this, their pathlength in the field is shorter, and they are accelerated to lower energy; that is, their impact energy \mathcal{E}_i is reduced. The surface will continue to acquire charge until $\mathcal{E}_i = \mathcal{E}_1$. By a similar argument, one can readily see that if $\mathcal{E}_i < \mathcal{E}_1$ initially, then \mathcal{E}_i will increase until $\mathcal{E}_i = \mathcal{E}_1$. When this condition is met, the charge on the insulator surface does not change, regardless of the electron current on the surface. A stable charge distribution exists.

The requirement that $\mathcal{E}_i = \mathcal{E}_1$ implies a condition on the electric field. Following DeTourel, [DeT73] consider an electron which is emitted normal to the surface with energy \mathcal{E}_s . The highest point in its trajectory, h , will be reached when its perpendicular kinetic energy is zero, or when

$$h = \frac{\mathcal{E}_s}{eE_{\perp}} \quad (2.3)$$

The electron will return to the insulator surface in time t given by

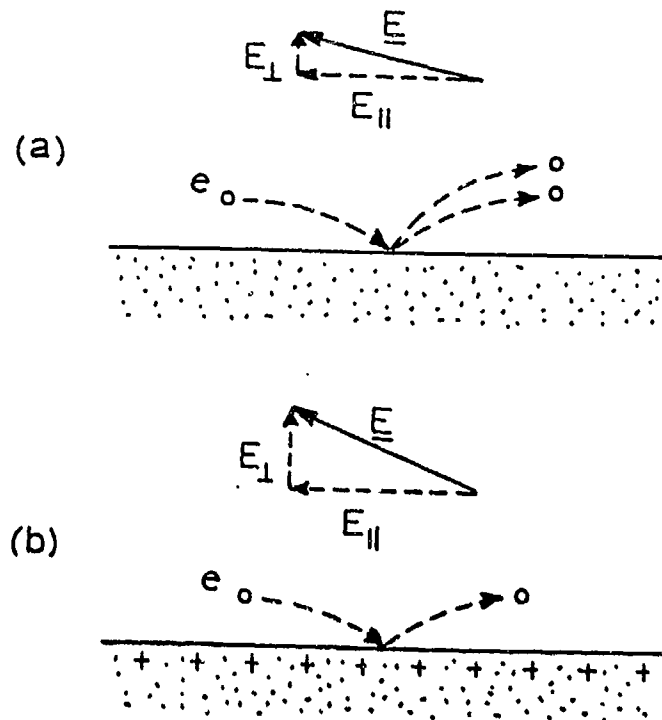


Figure 2.4. Insulator surface charging. a) Uncharged insulator surface.
b) Equilibrium surface charge distribution.

$$t = \frac{2^{3/2}(m_e \mathcal{E}_s)^{1/2}}{eE_{\perp}} \quad (2.4)$$

during this time, it will be accelerated parallel to the insulator over a distance

$$r = \frac{4\mathcal{E}_s E_{\parallel}}{eE_{\perp}^2} \quad (2.5)$$

It will gain energy $\Delta\mathcal{E}$ in the parallel field, given by

$$\Delta\mathcal{E} = eE_{\parallel}r = \frac{4\mathcal{E}_s E_{\parallel}}{E_{\perp}} \quad (2.6)$$

Therefore its impact energy will be

$$\mathcal{E}_i = \mathcal{E}_s [1 + 4(E_{\parallel}/E_{\perp})^2] \quad (2.7)$$

If instead of being emitted normal to the insulator surface, the electron is emitted in an arbitrary direction, $\mathcal{E}_{s\perp} = \mathcal{E}_s \cos^2 \phi$, where ϕ is the angle between the electron trajectory and the normal to the insulator surface. Replacing \mathcal{E}_s with $\mathcal{E}_{s\perp}$ in the previous analysis and averaging over all emission angles,

$$\mathcal{E}_i = \mathcal{E}_s [1 + 2(E_{\parallel}/E_{\perp})^2] \quad (2.8)$$

Or, solving for E_{\perp}/E_{\parallel} ,

$$\frac{E_{\perp}}{E_{\parallel}} = \left[\frac{1}{2} \left(\frac{\mathcal{E}_i}{\mathcal{E}_s} - 1 \right) \right]^{-1/2} \quad (2.9)$$

Since the charge distribution is stable when $\mathcal{E}_i = \mathcal{E}_1$, replacing the former with the latter in Equation (2.9) gives the electric field configuration at equilibrium. But E_{\perp}/E_{\parallel} is nothing other than the tangent of the angle between the electric field and the surface. At equilibrium, this is the critical angle θ_c , given by

$$\theta_c = \tan^{-1} \left[\frac{1}{2} \left(\frac{\epsilon_1}{\epsilon_s} - 1 \right) \right]^{-1/2} \quad (2.9)$$

where it is clear from this formula that θ_c depends only on material properties and not on the magnitude of the applied electric field. Note that since we have assumed that the electric field accelerates electrons into the insulator surface, by convention θ_c is negative. We have used the example of a positively charged insulator, but this is not necessarily the case. In general, if θ_{E0} is the angle of the applied electric field in the absence of surface charge, then the surface will acquire a positive surface charge for $\theta_{E0} > \theta_c$, and a negative surface charge for $\theta_{E0} < \theta_c$.

2.3. Theory of Flashover of Vacuum Insulators

It is generally recognized that the flashover process involves a complicated, and as yet ill-defined, chain of events prior to the collapse of impedance across the insulator. [Avd77, Ber77, And80, Gra85] It is unfortunate that the theoretical treatments of flashover almost invariably model the insulator at zero angle, because it makes for a more tractable problem, while highly angled insulators are almost invariably employed in practice, because of their superior performance. It is not obvious that the models of flashover developed to explain behavior for insulators at $\theta = 0^\circ$ are valid at $\theta = \pm 45^\circ$. [Ber77, Tho80] Nevertheless, theory provides some insight into the problem.

The theories which have been developed to date concentrate on the effect of the pre-breakdown current on the insulator surface. Prior to breakdown, a current may be observed flowing across the insulator surface of a high-voltage insulator. [Sud77] As the previous section implies, once an equilibrium charge distribution is established on the insulator surface, virtually any amount of

current can flow across the insulator surface, carried by the electrons which are "hopping" across the surface, without affecting the charge distribution on the surface. The current will be limited only by the supply of primary electrons (usually assumed to be the cathode triple point) unless the current becomes so large that the space-charge effects in the electron sheath become prominent.

Because the electrons "hop" across the insulator surface, although one may measure a current across the surface, the effect is that of an electron flux into the surface. [And80] This flux can desorb neutral gas from the insulator surface. [Bug68, Avd77b, Avd79, And80] Originally, it was proposed that this flux heated the surface and caused desorbed gasses to be released, much as one bakes out a high vacuum system; however, this was shown to be an insufficient mechanism to explain the flashover of materials (principally ceramics) with high thermal conductivity. [And80] Rather, an electron-stimulated-desorption mechanism has been proposed. [Avd77b, Avd79, And80] Once a layer of gas is established above the insulator surface, the theory of avalanche breakdown in gases applies—ionization of the neutral gas by the electrons in the current sheath leads to a runaway increase in current, and the impedance of the "vacuum" gap collapses. The electron-stimulated-desorption model of insulator flashover is currently the best model available to describe the process. It is still essentially a qualitative model.

2.4. Parameters of the Present Experiment

The parameters of the present experiment were chosen based on the current understanding of insulator flashover just outlined and on the practice of the pulsed-power community. The plane insulator/vacuum interface was investigated exclusively, since it is almost exclusively the geometry applied in practice and in

theory. Large insulator angles were selected, again because it is these geometries which are found in practice, and because the body of knowledge about such insulators leaves room for original investigation. DC voltage was used, rather than attempting to field a more complicated pulsed system, assuming that the results would be applicable at least down to the level of microsecond pulses. Only one electrode material was used (except for the spectroscopic studies), assuming that flashover is as insensitive to electrode material under ultraviolet illumination as without it. No special attempt at extreme vacuum conditions were made. In short, while this experiment does not rigorously prove that those parameters which have little effect on unilluminated insulators have a similarly small effect on illuminated ones, areas of research which held little promise for interesting results were deferred to some later time.

While the choice of the materials tested was limited to polymers for the reasons noted in the introduction, specific polymers were chosen for which the chemical composition could readily be found in the literature, excluding those available only as proprietary formulas. This, in turn, allowed for such quantities as the secondary electron emission coefficient to be calculated and for other data to be found in the literature. The polymers chosen were: polyethylene, polystyrene, acrylic (polymethylmethacrylate, specifically Lucite), nylon-6 (polycaprolactam), acetal (specifically Delrin), teflon (polytetrafluoroethylene), and PVC (polyvinylchloride). The chemical formulas for these materials is illustrated in Figure 2.5. [Kir85, Flo69] A brief listing of the properties of these materials appears in Table 2.1.

Table 2.1. Properties of Insulating Materials

Material	Formula ⁽¹⁾	K ⁽²⁾	ϵ_r ⁽³⁾
polyethylene	C ₂ H ₄	1.37	2.36
polystyrene	C ₈ H ₈	0.907	2.55
acrylic	C ₄ H ₈ O ₂	1.115	3.12
nylon-6	C ₆ H ₁₁ NO	1.148	4.0
acetal	C ₂ H ₄ O ₂	1.106	3.7
teflon	C ₂ F ₄	1.564	2.1
PVC	C ₂ H ₃ Cl	1.006 ⁽⁴⁾	4.55

(1) [Flo69, Kir85]

(2) [Bur80]

(3) [Lyn75, Wea85]

(4) [Bur80] (Estimated from Burke's data.)

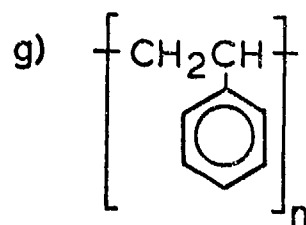
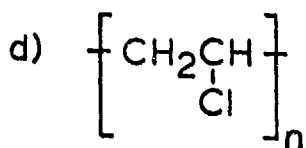
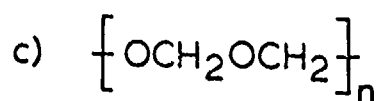
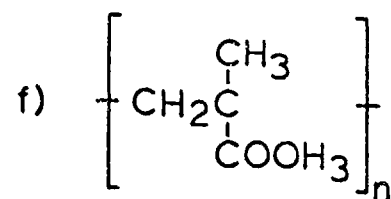
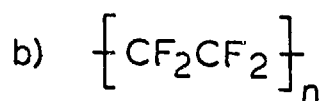
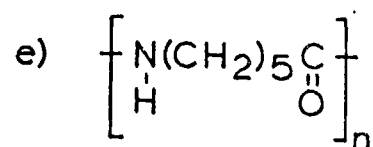
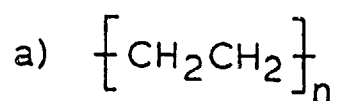


Figure 2.5. Chemical formulas for the materials used in this experiment.
 a) Polyethylene. b) Teflon. c) Acetal. d) PVC. e) Nylon-6.
 f) Acrylic. g) Polystyrene.

CHAPTER 3

EXPERIMENTAL CONFIGURATION

The apparatus for this experiment consisted of a source of ultraviolet illumination, a test chamber in which the insulator samples were located, and its associated diagnostics. The diagnostics used may be broadly divided into electrical and optical diagnostics. The experimental configuration is illustrated in Figure 3.1.

3.1. Ultraviolet Illumination Source

The ultraviolet source was an excimer laser (Lumonics TE-292), optimized for KrF at a wavelength of 248 nm, and operable at other wavelengths using different gas mixtures (ArF at 193 nm, and XeF at 350 nm). The maximum energy available in a 60 ns pulse was 1.0 J over a 2.0 x 2.5 cm aperture. The beam profile was compressed with single plano-convex quartz lens and apertured to control the area of illumination on the surface of the sample. Typically, the insulator sample was illuminated from the anode triple point to the cathode triple point, but since the sample was mounted beyond the focal point of the lens and the laser light was diverging as it entered the interelectrode region, the electrode surfaces themselves remained unilluminated. Figure 3.2 illustrates the variation in pulse energy, measured with a carbon block calorimeter, versus shot number for a single gas fill of the laser. A quick initial rise was noted over approximately the first ten shots. During this time, the spatial uniformity of the beam also

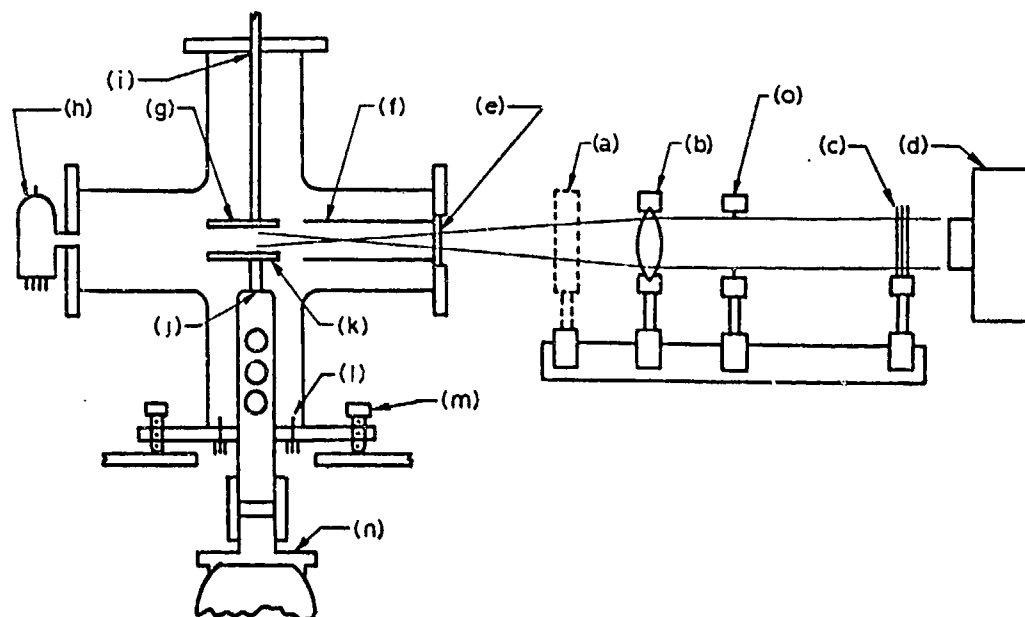


Figure 3.1. Experimental configuration. a) Carbon block calorimeter. b) Quartz converging lens. c) Attenuators. d) Excimer laser. e) Quartz window. f) Optional Collimator. g) Top electrode. h) Vacuum gauge. i) Slip seal. j) Screw-thread adjustment. k) Bottom electrode. l) BNC feed-through. m) Adjustable feet. n) Turbomolecular pump. o) Variable aperture.

improved as the lasing chamber was conditioned. Following this, the energy per pulse decreased, probably due to impurities building up in the laser. [Kea83] This decrease was monotonic and hence was predictable if the laser energy were monitored periodically. The shot-to-shot variation between pulses was $\pm 7\%$. Spatial uniformity of the beam deteriorated after approximately 200 shots. At this time, the gas fill needed to be replaced with a fresh mixture.

The temporal shape of the laser pulse was monitored with an ultraviolet-sensitive p-i-n diode. If the diode were placed anywhere near the test chamber, the laser intensity even in the wings of the beam was sufficient to saturate the output and severely distort the pulse shape. Therefore the diode was placed near the screen room and the effect on the relative timing of the signal was accounted for. The temporal shape of the pulse was constant for all shots, since it depended on the discharge circuit used to pump the laser. The pulse shape is shown in Figure 3.3. It is singly-peaked, but is not symmetrical. The full width of the laser pulse was $\tau = 60$ ns, while the width at half maximum was $\tau_{FWHM} = 24$ ns. The peak intensity occurred at $t_p = 18$ ns. The integral of the pulse shape is also shown in Figure 3.3.

Control of the fluence (that is, the integrated intensity or energy per unit area) illuminating the sample was achieved by attenuating the laser beam with thin sheets of polyethylene inserted into the beam path. Figure 3.4 shows that the transmission versus the number of sheets varied exponentially as the number of sheets, as one would expect. Each sheet had a transmission of about 0.5. A thinner "half sheet" with a transmission of about 0.75 was used for finer tuning of the pulse energy.

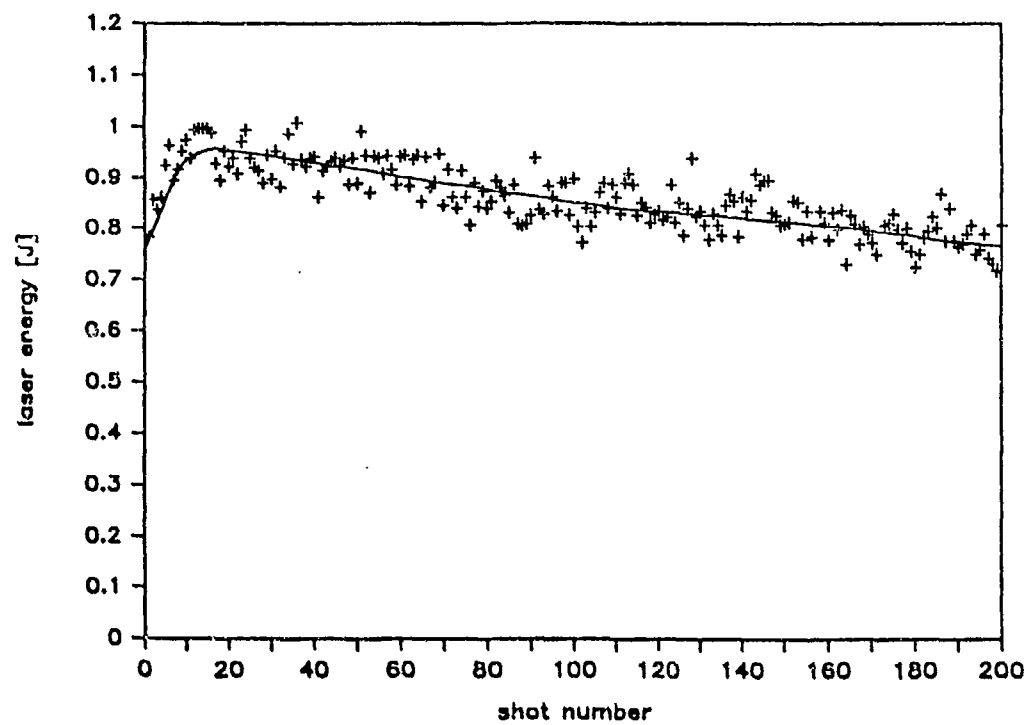


Figure 3.2. Variation of energy in the excimer laser pulse versus shot number.

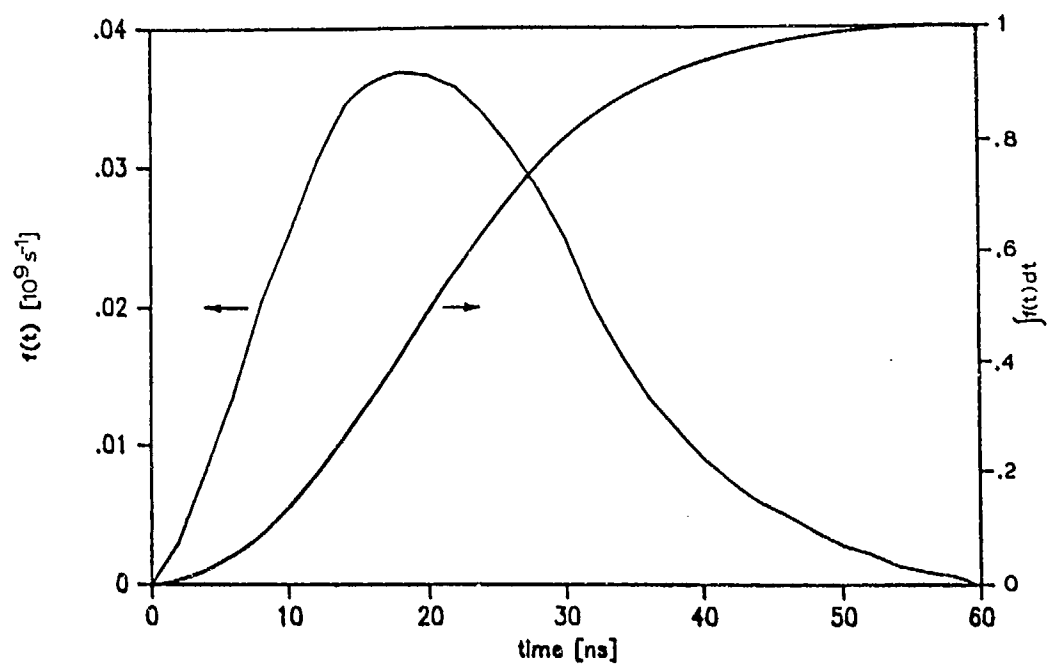


Figure 3.3. Normalized laser pulse shape $f(t)$ and its integral, which were the same for all shots.

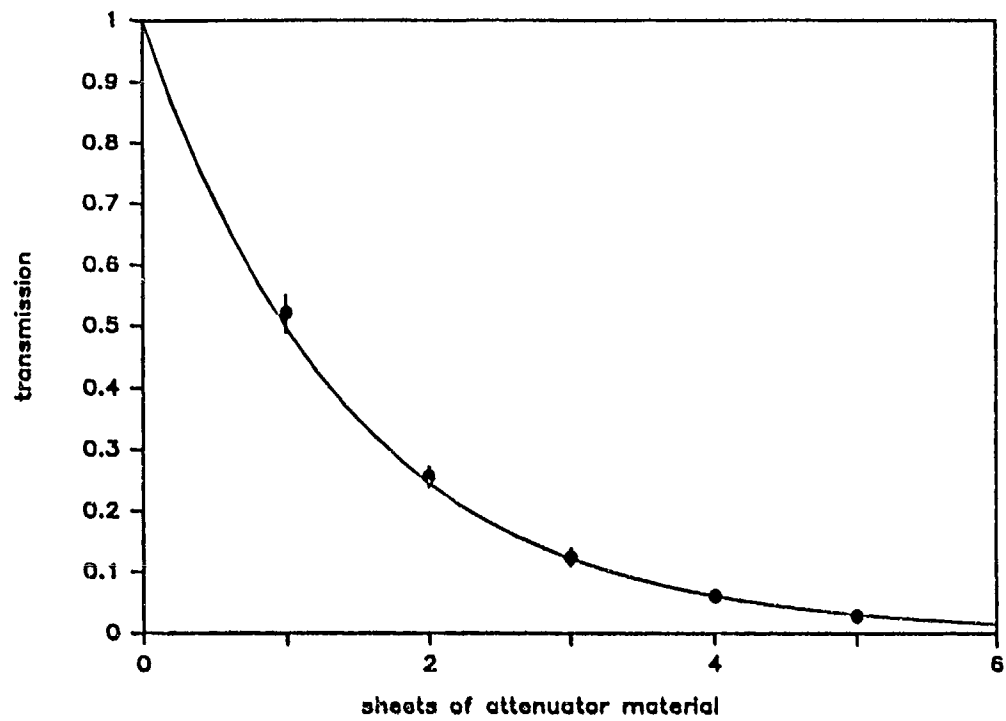


Figure 3.4. Transmission of the excimer laser beam versus number of sheets of plastic attenuators.

3.2. Test Chamber

3.2.1. Vacuum System Design

The test chamber was designed to allow the cleanest vacuum and the easiest diagnostic access possible. The chamber consisted of a 10.2 cm I.D. (4 in) pyrex cross with two 5.1 cm (2 in) pyrex arms perpendicular to the cross. Each arm was sealed with a metal or a glass port and a flat rubber gasket. A clean vacuum was important, since preliminary results indicated that impurities on the insulator surface or at the triple points could significantly alter flashover performance. [Enl87a]

The bottom port provided a mechanical base for the chamber, a support for the lower electrode, and a connection to the pumping unit. A turbomolecular pump was used to eliminate the effects of oil backstreaming into the system. The pump was connected to the vacuum chamber by a 5.1 cm (2 in) metal tube which extended inside the chamber. The chamber was evacuated through twelve 1.9 cm (0.75 in) holes in the side of this tube, while the top of the tube was capped to support the lower electrode. The metal tube was broken between the chamber and the pump by a short section of rubber vacuum hose, which isolated the electronics of the pump controls from the high voltage in the chamber and provided some flexibility in positioning of the chamber as well.

Four bolts outboard on the bottom port served as adjustable feet for the chamber. This facilitated aligning the electrodes parallel to the incident laser beam. The feet rested on a non-conducting wooden base on a stand over the pumping unit, so that a single ground current path could be maintained if desired. Once aligned, the base of the chamber was clamped to the wooden base with a pair of metal bars which were isolated from ground by a wooden clamp.

The system was readily evacuated to $\leq 1 \times 10^{-5}$ Torr in one to two hours. Vacuum flashover phenomena typically show no variation with pressure below 1×10^{-2} Torr, [Haw68] so that this level of vacuum was sufficient for the experiment. Also, over one to two hours time, the outgassing rate from polymers is typically reduced by an order of magnitude from its initial value, so that spurious results resulting from initial outgassing were eliminated.

A quartz window, 0.32 cm thick, allowed the ultraviolet light to enter the front of the chamber. The attenuation of the window to the laser light was too small to be measured accurately since it was on the order of the shot-to-shot variations in the beam. Rather, from manufacturer's data, the window transmission was estimated to be 0.985 (corresponding to 4% loss at each face and 1.5% loss in the bulk).

Vacuum gauges (thermocouple and ionization gauges) monitored the chamber through ports in the back. To avoid spurious effects, the filament of the ion gauge was turned off during all measurements of flashover.

The top of the chamber admitted the high voltage lead through a slip seal. The high voltage lead itself was a 0.32 cm (0.125 in) metal rod sealed inside a 0.64 cm (0.25 in) acrylic tube. The rod was mated to the top electrode after the high voltage lead was placed through the slip seal. A crown glass port on one side allows the sample to be viewed edge-on across the entire width of the side arm. A pipe-threaded hole in the port on the opposite arm allow a variety of devices to be attached to the chamber, including a small window (to admit a He-Ne laser beam) or a leak valve.

3.2.2. Electrode Configurations

The electrodes were two D-shaped pieces of 0.64 cm (0.25 in) brass. They were polished with 1.0 micron polishing compound. The position of the lower electrode could be adjusted by a threaded connection to the cap of the vacuum outlet. The slip seal through which the upper electrode was connected to the high-voltage supply allowed the insulator sample to be wedged tightly between the two electrodes without the use of additional clamps. High voltage was maintained across the electrodes by a small (250 pF) capacitor isolated from the power supply by a large (100 M Ω) resistor. A maximum voltage of 25 kV could be obtained from the high voltage supply (Sorensen model 1030-20), so that < 80 mJ of electrical energy was stored on the capacitor. With a sample made from 0.64 cm stock, this corresponded to a maximum electric field of 39 kV/cm. Samples machined to half this thickness allowed fields of up to 78 kV/cm. These values are significantly below the DC flashover strength of most angled insulators. Since the experiment was concerned only with flashover initiation, the electrical energy was purposely kept low to eliminate damage to the insulator surface after the discharge was established. The output of the high-voltage power supply was calibrated using a Tektronix 100x attenuating probe. The input voltage to the power supply's transformer was assumed to be constant within a few percent.

In order to minimize edge effects, the effect of the position of the insulator sample relative to the edge of the electrodes on the local electric field at the insulator surface was modelled with the Poisson-solving computer code LAPLACE. [LAP86] Figure 3.5 shows the equipotentials calculated for an insulator at 45° to the electrode surface near to and far from the edge of the electrodes. By comparing the equipotential contours, one sees that the electric field at the

surface of the insulator is the same for both cases: in other words, an insulator inset from the edge of the electrodes by approximately its own thickness is a good approximation to the case of infinite plane-parallel electrodes.

The electrodes could also be configured as a charged-particle collector for the study of ultraviolet effects on insulator surfaces apart from flashover. A small voltage between the electrodes (300 V) accelerates charged particles away from the surface from the insulator. The signal S is then related to the charge collected Q simply by [Kno79]

$$S = \frac{Q}{C} \quad (3.1)$$

where C is the capacitance of the collector plus additional parallel capacitance. The two electrode configurations are illustrated in Figure 3.6.

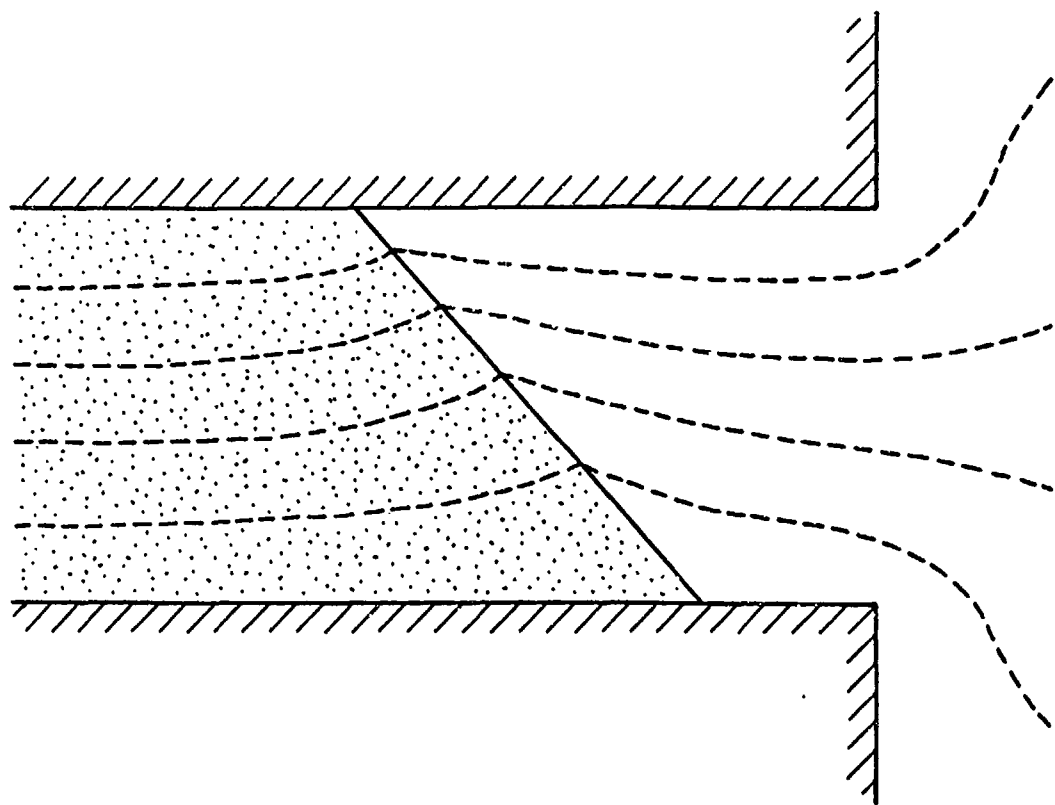
3.3. Electrical Diagnostics

The voltage across the electrodes and the current across the interelectrode gap were continuously monitored, using a capacitive V -dot probe and a Rogowski coil, respectively. Both of these diagnostics required a high-speed passive integration network, because of the extremely rapid changes in voltage and current associated with the flashover event.

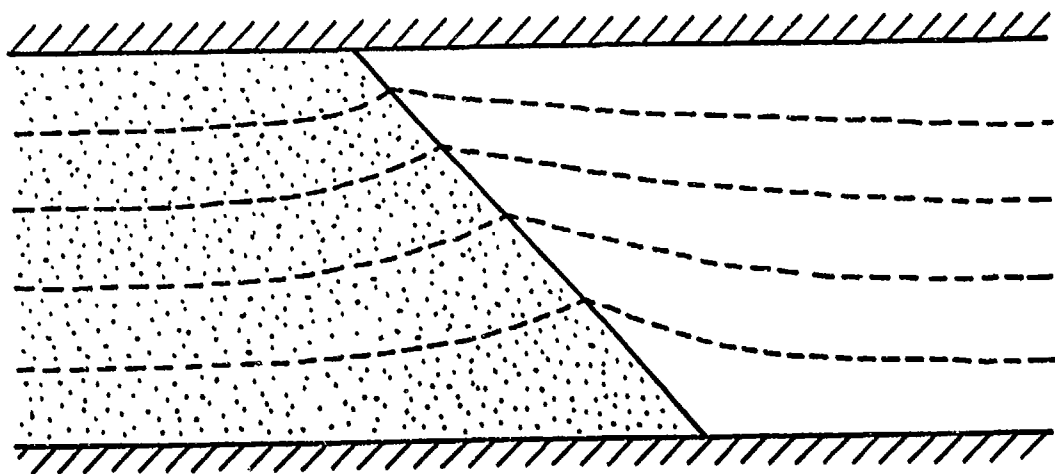
3.3.1. Rogowski Coil

The Rogowski coil is a common diagnostic for the measurement of pulsed currents. [Nas79, Pel80] In this work, it is necessary to understand its theory of operation in order to insure that the coil which was used was appropriately designed for high-speed operation.

The Rogowski coil, in its simplest form, is a solenoidally-wound loop of wire, closed on itself to form a torus, with a load resistor bridging the ends of the loop.



(a)



(b)

Figure 3.5. Equipotential contours for an insulator near to (a) and far from (b) the edge of the electrodes, demonstrating that edge effects may be neglected if an insulator is inset from the edge of the electrodes by approximately its thickness.

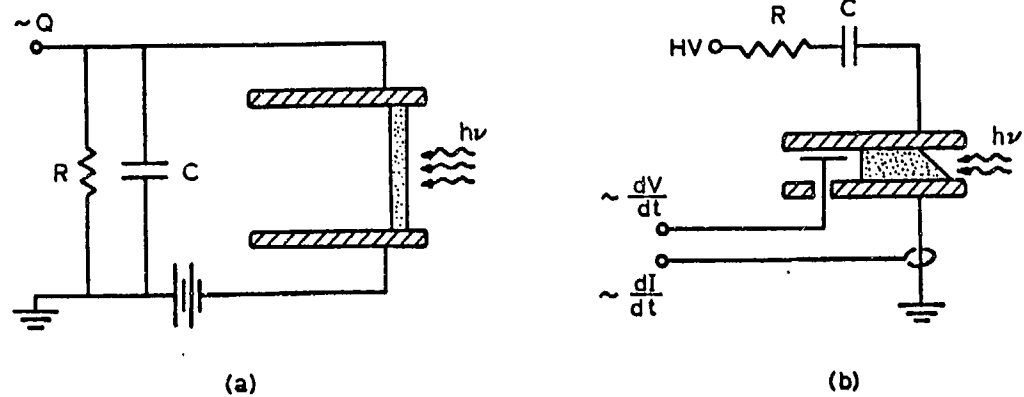


Figure 3.6. Electrode configurations. a) Charged particle collector. b) Typical configuration, including voltage and current monitors.

The particular coil used in this experiment consisted of ten turns around a plastic form with a rectangular cross-section. The physical layout of the coil and a schematic of the circuit to which it was attached is illustrated in Figure 3.7.

A time-varying axial current I passing within the circumference of a Rogowski coil has associated with it a time-varying magnetic field \mathbf{B} in the azimuthal direction, where from Maxwell's equations

$$\oint \mathbf{B} \cdot d\mathbf{l} = \mu_0 I \quad (3.2)$$

independent of the current distribution, where l is the circumference. A magnetic flux Φ_i links the i th turn of the coil, and the change in this magnetic flux induces a current in that turn. Because the turns are laid out along the circumference of the coil, summing the contribution of each turn Φ_i is analogous to performing the integral in equation (3.2), and

$$\Phi_t = \sum_i \Phi_i \propto I \quad (3.3)$$

where Φ_t is the total flux linking the Rogowski coil. If a return loop is included along the circumference of the coil, then the net area of the coil perpendicular to the axis is zero and the effect of the finite pitch of the coil is negated. Hence, the coil is sensitive only to currents which pass through its circumference, since the line integral of equation (3.2) is zero for currents outside the closed path.

Consider a Rogowski coil of inductance L with a load resistance R , as shown in Figure 3.7(b). As indicated in the figure, for the Rowgowski coil in the experiment, R is the 50Ω terminated signal cable. The equation for the voltage around the loop is

$$V_{\text{loop}} = \frac{d\Phi_t}{dt} = I_c R + L \frac{dI_c}{dt} \quad (3.4)$$

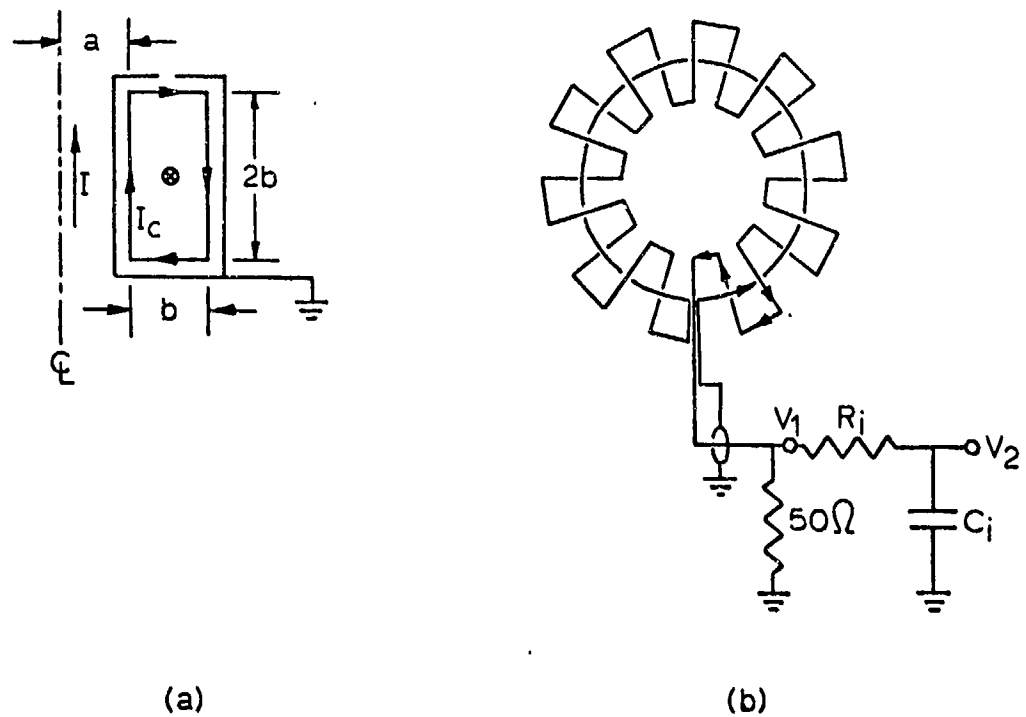


Figure 3.7. Rogowski coil used in the experiment. a) cross-section of the coil, including electrostatic shield. b) Top view of the coil, including terminating resistor and passive integrating circuit.

where I_c is the current in the Rogowski coil. This may be rewritten

$$\frac{1}{L} \frac{d\Phi_t}{dt} = \frac{I_c}{(L/R)} + \frac{dI_c}{dt} \quad (3.5)$$

If the response time of the coil L/R is small compared to the timescale over which the current changes, then $(dI_c/dt) \ll I_c/(L/R)$ and the last term in Equation (3.5) may be neglected. The voltage V_1 across the load resistor is then given by

$$V_1 = I_c R = \frac{d\Phi_t}{dt} \quad (3.6)$$

Since $\Phi \propto I$, this voltage is proportional to dI/dt , the time rate of change of the current through the coil, and may be integrated with the passive integration network shown in the figure to yield a voltage V_2 which is proportional to the current through the coil. In performing this analysis, the implicit assumption is that the resistance of the integrator $R_i \gg R$, so that the integrator does not load the coil. Similarly, $R_s \gg R_i$, where R_s is the input impedance of the oscilloscope, typically $1 \text{ M}\Omega$.

The trade-off in designing a Rogowski coil is one of sensitivity for speed. As the number or the area of the turns increases, the sensitivity of the coil increases, but its inductance does as well, so that the response time L/R increases. If L/R is comparable to the pulsewidth, then Equation (3.6) is no longer true and the relationship between V_2 and I is no longer linear. If L/R is very much larger than the pulsewidth, then the coil is "self-integrating"; that is, V_1 is proportional to I and an integrating network is unnecessary. While this may seem a simplification, it implies that L is inconveniently large or R is inconveniently small.

For the coil used in this experiment, the inductance may be calculated from the familiar formula for a solenoid

$$L = \frac{\mu_0 N^2 A}{l} \quad (3.7)$$

where N is the number of turns, A is the area of each turn, and l is the length of the solenoid (here, the circumference of the coil). For the geometry shown in the figure, this is equivalent to

$$L = \frac{\mu_0 N^2 b^2}{\pi[a + (b/2)]} \quad (3.8)$$

and using $N = 10$, $a = 0.9$ cm, and $b = 1.0$ cm, one may calculate $L = 290$ nH, or $L/R = 5.8$ ns for a 50Ω load. Since the pulsewidth of the pre-breakdown current pulse was on the order of $\tau_{\text{pre}} I = 20$ ns, the Rogowski coil was fast enough to yield an output which, when integrated, is linearly proportional to I . The degree of non-linearity depends on the particular shape of the current pulse,[Pel80] but is on the order of $\exp[-\tau_{\text{pre}}/(L/R)] = 0.03$; in other words, the coil was accurate to within a few percent.

The time constant of the passive integrator used with the Rogowski coil was $R_i C_i = 0.82 \mu\text{s}$. The combination of Rogowski coil and integrator was calibrated *in situ* versus a Pearson current monitor, the sensitivity of which was known. The results of the calibration are shown in Figure 3.8. The results were fitted by least squares to a straight line, and the sensitivity of the combination was determined to be 0.055 V/A.

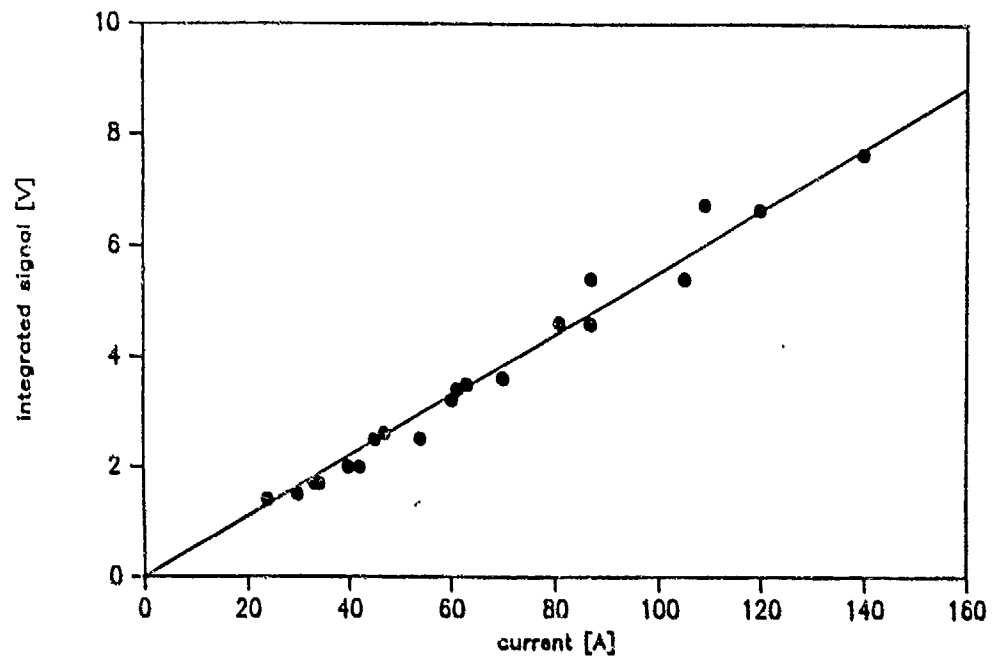


Figure 3.8. Calibration of the Rogowski coil used in the experiment.
Sensitivity 0.055 V/A.

3.3.2 Capacitive V-dot Probe

The capacitive V-dot probe is a convenient way to measure pulsed voltages. [Ekd80] It is particularly well suited to high-voltage circuits, since it does not load the circuit under observation.

The probe used in this experiment consisted simply of a small metal disk separated from the high-voltage electrode by an insulating spacer. The physical configuration of the probe is shown in Figure 3.9(a). The disk had an area of 2.0 cm^2 and was separated from the high voltage electrode by 0.16 cm of acrylic. The spacer also isolated the disk from the ground electrode, and its exterior was angled to resist flashover across its outside surface. The disk was connected to the inner conductor of a 50Ω transmission line.

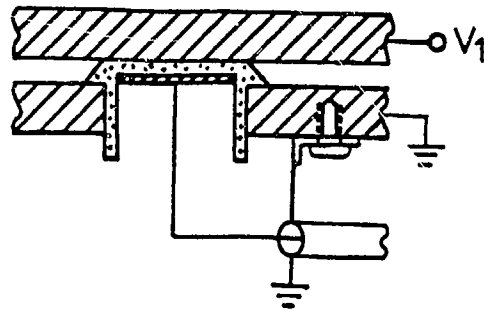
The equivalent circuit is shown in Figure 3.9(b), including the passive integrating network. The capacitance C_1 is the capacitance of the probe itself. The capacitance C_2 is the stray capacitance to ground. The resistance R is simply the 50Ω impedance of the terminated cable. If the time constant $RC = R(C_1 + C_2)$ is small, then the capacitors are effectively discharged, and the equation for the current I_p in the first portion of the circuit is

$$\frac{dV_1}{dt} = \frac{I_p}{C_1} + R \frac{dI_p}{dt} \quad (3.9)$$

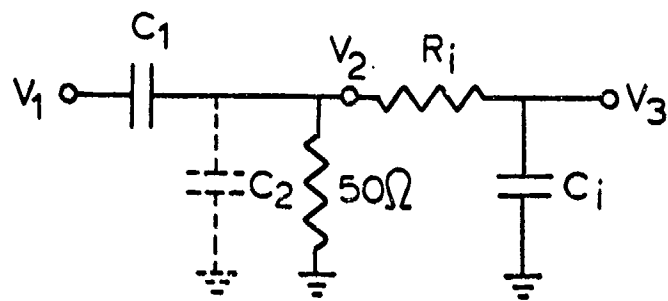
which may be rewritten

$$\frac{1}{R} \frac{dV_1}{dt} = \frac{I_p}{RC_1} + \frac{dI_p}{dt} \quad (3.10)$$

If the time constant RC_1 is short compared to the timescale over which the signal changes, then $dI_p/dt \ll I_p/RC_1$, and the last term in Equation (3.10) may be neglected. The voltage V_2 across the load resistor is then given by



(a)



(b)

Figure 3.9. Capacitive V-dot probe used in the experiment. a) Physical implementation. b) Equivalent circuit, including terminating resistor and passive integrating network.

$$V_2 = I_p R \approx RC_1 \frac{dV_1}{dt} \quad (3.11)$$

This voltage may be integrated with the passive integration network shown in the figure to yield a voltage V_3 which is proportional to the voltage V_1 on the high-voltage electrode.

One may readily design a V-dot probe which is quite fast. If RC is comparable to the pulsewidth of the voltage pulse, then Equation (3.10) is no longer valid and the relationship between V_3 and V_1 is no longer linear. If RC is very much larger than the pulsewidth, then the capacitors remain charged, and the result is a capacitive divider. The capacitance of the probe in this experiment may be calculated from the formula for a parallel plate capacitor,

$$C_1 = \frac{\epsilon_r \epsilon_0 A}{d} \quad (3.12)$$

where A is the area of the plates and d is the separation, while ϵ_r is the relative dielectric constant of the intervening material. Using $A = 2.0$ cm, $d = 0.16$ cm, and $\epsilon_r = 3.12$, one may calculate $C_1 = 3.5$ pF, so that $RC_1 = 0.18$ ns. Similarly, the stray capacitance in the connection to the transmission line may be calculated from the formula for a coaxial capacitor,

$$C_2 = \frac{2\pi\epsilon_0 l}{\ln(b/a)} \quad (3.13)$$

where l is the length of the capacitor and (b/a) is the ratio of the diameters of the inner and outer conductors. Using $l = 0.64$ cm and $(b/a) = 4.3$, one may calculate $C_2 = 0.083$ pF, which is negligible. The V-dot probe was fast enough to track the voltage collapse associated with the flashover event with negligible distortion.

The time constant of the passive integrator used with the V-dot probe was $4.7 \mu\text{s}$. The combination of the probe and the integrator was calibrated by charging the high-voltage electrode to a known voltage, and then shorting the electrodes by initiating a flashover event, so that the magnitude of the voltage change was equal to the charge voltage. The results of the calibration are shown in Figure 3.10. The results were fitted by least squares to a straight line, and the sensitivity of the combination was found to be 0.046 V/kV .

3.3.3. Passive Integrator

Both of the previous diagnostics depended on the use of a passive integrator. The schematic of the passive integrator is well known, and has been identified in Figure 3.7, for example. The analysis is straightforward. The equation for the second loop in the circuit is

$$\frac{dV_1}{dt} = R_1 \frac{dI_1}{dt} + \frac{I_1}{C_1} \quad (3.14)$$

which may be rewritten

$$\frac{1}{R} \frac{dV_1}{dt} = \frac{I_1}{R_1 C_1} + \frac{dI_1}{dt} \quad (3.15)$$

If $R_1 C_1$ is large, then $dI_1/dt \ll I_1/R_1 C_1$ and neglecting the last term in Equation (3.15),

$$I_1 = \frac{V_1}{R_1} \quad (3.16)$$

The voltage on the capacitor C_1 is just $V_2 = Q/C_1$, but this is

$$V_2 = \frac{1}{C} \int_0^t I_1 dt = \frac{1}{R_1 C_1} \int_0^t V_1 dt \quad (3.17)$$

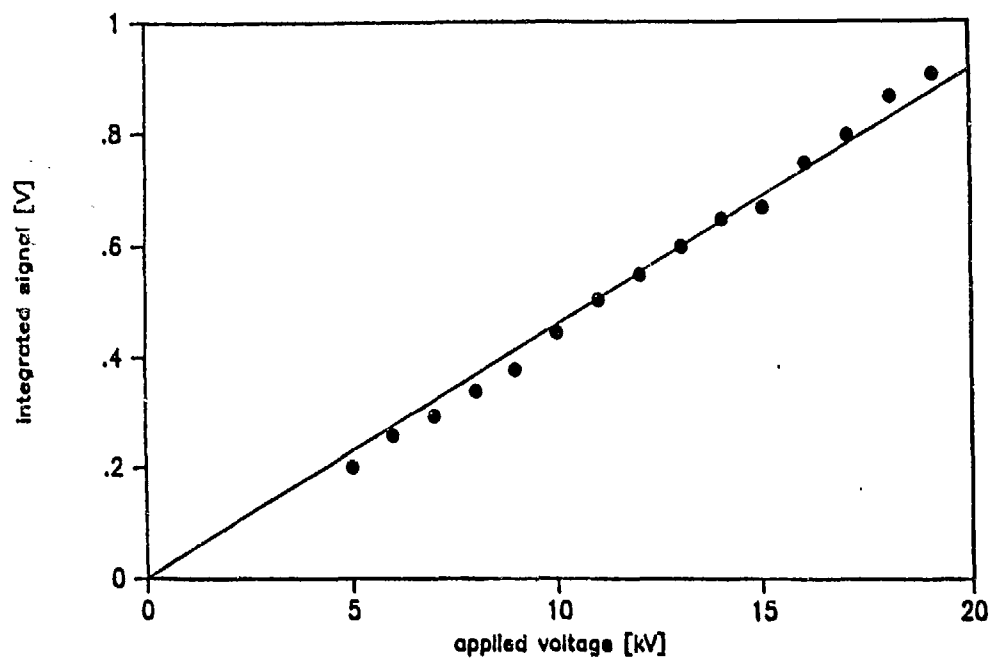


Figure 3.10. Calibration of the capacitive V-dot probe used in the experiment. Sensitivity 0.046 V/kV.

Therefore, the circuit behaves as an integrator for short pulses. Since the shortest time constant was $R_i C_i = 0.82 \mu\text{s}$, while the timescale for prebreakdown activity was $\tau_{\text{pre}} = 20 \text{ ns}$, the condition $R_i C_i \gg \tau_{\text{pre}}$ was adequately met. Since the longer the time constant, the smaller the signal, there is a trade-off between fidelity and signal.

Because the rapid risetime of the signals at the onset of flashover contained significant high-frequency components, it was necessary to package the integrators carefully in order to minimize inductance and the associated high-frequency LRC ringing. The integrators were built using a feed-through capacitor. The design of the high-speed integrators is shown in Figure 3.11. The internal components were assembled, and then the outer ground shield was attached in two pieces. The integrators faithfully integrated signals with a 1 ns risetime without exhibiting the ringing behavior which was observed with integrators built in a more traditional manner.

3.4. Optical Diagnostics

Optical diagnostics of the flashover event included simple photography of the flashover event, time-resolved spectroscopy of the flashover plasma, and probing of the interelectrode region with laser light.

3.4.1. Laser Deflection Technique

Investigation of the time-evolution of the products of the interaction of the ultraviolet source the insulator surface required a fast, sensitive probe. A probe which could discriminate between charged and neutral interaction products was very desirable.

The common technique of pulsed laser schlieren photography [Hud65] is inadequate to diagnose the temporal evolution of such products in a single shot.

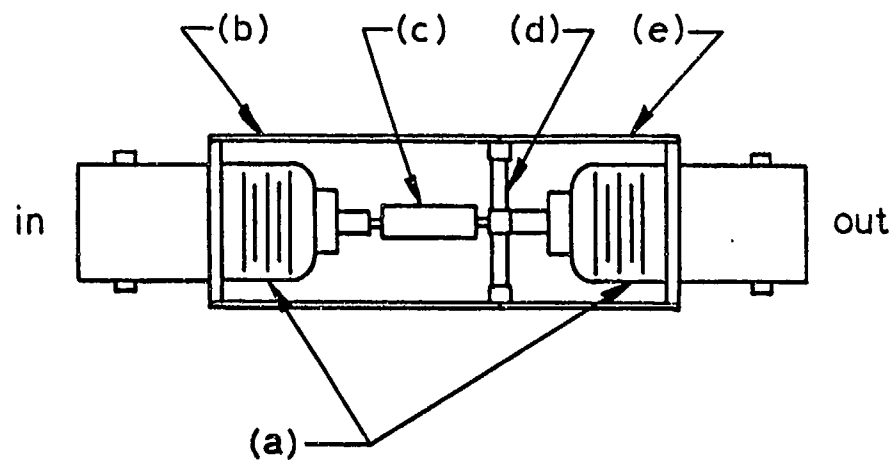


Figure 3.11. High-speed passive integrator used to integrate Rogowski coil and capacitive V-dot probe signals without introducing ringing.
a) BNC feed-through connectors. b) Copper foil outer conductor.
c) Resistor. d) Coaxial capacitor. e) Copper foil outer conductor.

Although fast (20 ns) "shuttering times" can be obtained by employing a Q-switched ruby laser, many identical shots are required, varying the timing of the probe laser, to observe the products evolve in time. In many cases, difficulties arise because the products may contain multiple components, since the presence of a plasma is a negative perturbation in the index of refraction while the presence of neutral particles is a positive perturbation. If a pinhole is used as a spatial filter in a schlieren system, the technique can simultaneously detect both plasmas and neutrals, but cannot distinguish between them. If a knife-edge is used as a spatial filter, the technique can distinguish between the two but cannot detect them simultaneously. Further, it is difficult to obtain quantitative results from schlieren photography. Applying the technique of holographic interferometry eliminates these difficulties, but at the expense of a large increase in cost and complexity, since not only are the laser optics required to make the hologram more complex, but the hologram must be reconstructed in order to interpret the results.

Diagnosing density by measuring the deflection of a laser beam [Gre82, Enl87c] is an analogous technique to schlieren photography, in that both techniques are sensitive to index of refraction gradients. The technique has been successfully applied to a number of fields; the chief impediment to its application to transient plasmas has been one of speed. For this experiment, a laser deflection system capable of detecting deflections of $0.5 \mu\text{rad}$ on a timescale of 20 ns was developed. Hence, its speed is comparable to Q-switched ruby laser schlieren, while its sensitivity is over two orders of magnitude greater. It is inherently quantitative, while at the same time being much simpler and less expensive to implement than a ruby laser and associated optics.

Figure 3.12 illustrates the laser deflection technique. A 5 mW He-Ne probe laser (Jodon Laser model HN-2SHP) is deflected by index of refraction gradients as it passes through the material in the vicinity of the insulator surface. The angular deflection is given by [Gre82]

$$\delta\phi = \frac{1}{\tilde{n}_0} \left| \int_{\text{path}} ds \nabla_{\perp} \tilde{n} \right| = \frac{D \left| \langle \nabla_{\perp} \tilde{n} \rangle \right|}{\tilde{n}_0} \quad (3.18)$$

where \tilde{n} is the index of refraction, \tilde{n}_0 is the unperturbed index of refraction (approximately equal to 1), $\nabla_{\perp} \tilde{n}$ is the gradient in the index of refraction perpendicular to the path of the beam, D is the thickness of the perturbed region, and $\langle \rangle$ indicates a line average taken over the path of the probe laser in the perturbed region. Since deflections are small, this average is taken over the straight-line unperturbed path. The deflection of the beam is detected by a position sensor, specifically a quadrant detector (Silicon Detector Corporation model SD-380-23-21-051), chosen for its fast response time. The sensor and its associated electronics are located a distance L from the region to be probed. Although the design of the detector circuit is inherently noise-resistant, a He-Ne laser line filter placed in front of the position sensor maximizes detector sensitivity by eliminating background light. The output of the detector is proportional to the deflection, $V(t) = C\delta\phi(t)$, where the constant C is readily calibrated.

For plasmas, the change in index of refraction $\delta\tilde{n}$ is proportional to the electron density n_e , and is given by [Hud65]

$$\delta\tilde{n} = - \left(\frac{e^2}{2\pi m f^2} \right) n_e = -K_p n_e \quad (3.19)$$

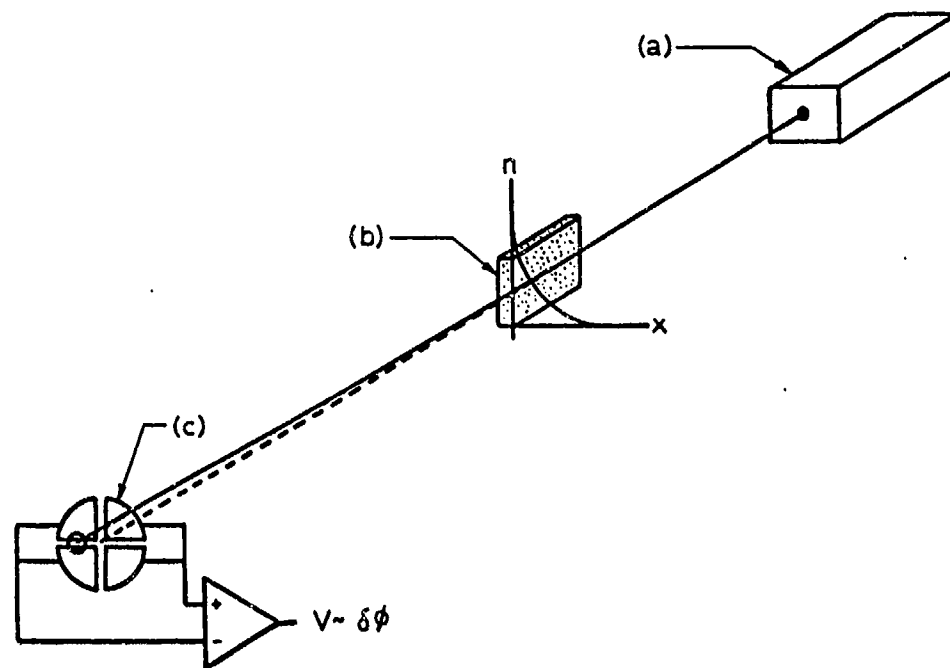


Figure 3.12. The laser deflection technique applied to detecting neutral emission from the insulator surface. a) He-Ne probe laser. b) Insulator surface, from which neutral particles are emitted. c) Position sensor.

where e is the electron charge, m is the electron mass, and f is the laser frequency, so that $K_p = 1.79 \times 10^{-22} \text{ cm}^3$ for He-Ne laser light. For neutral particles, δn is proportional to the neutral density n_n , and is given by [Loc68]

$$\delta n = \left(\frac{\tilde{n}_o - 1}{n_o} \right) n_n = K_n n_n \quad (3.20)$$

At STP, the neutral density $n_o = 2.6868 \times 10^{19} \text{ cm}^{-3}$ and $(\tilde{n}_o - 1) = 2.76 \times 10^{-4}$ for He-Ne laser light, so that $K_n = 1.0272 \times 10^{-23} \text{ cm}^3$.

The key to the performance of this system is the detector circuit, [Enl87c] shown in Figure 3.13. The quadrant detector is essentially four photodiodes on one substrate. Each pair of anodes on either side of the vertical midplane are connected, so that the detector is sensitive only to horizontal deflections of the probe laser. A bias voltage of 30 V applied to the common connection reduces the output capacitance, and hence the response time, of the detector. Voltage is developed across a 270 Ω resistor on each side. This resistance value optimizes the gain-bandwidth product of the system. The signal from each side is buffered and passed on to a 15x-gain differential amplifier. Since a differential configuration is used, the detector is insensitive to common-mode noise such as variations in probe laser power when the laser is centered on the detector. The amplifier is capable of driving a 50 Ω load to approximately + 1 V. A high-pass filter eliminates the effects of mechanical vibrations ($< 20 \text{ Hz}$) from the output.

The sensitivity of the system is a function of laser power and spot size. It generally increases as the moment arm L ; however, for large L the effect of beam divergence is large and the advantage of the long arm diminishes. For the laser employed, $L \simeq 3 \text{ m}$ appears to be optimum, yielding $dV/d\phi = 4.2 \text{ mV}/\mu\text{rad}$. Since the output noise level is approximately 2 mV, the resolution of the system is

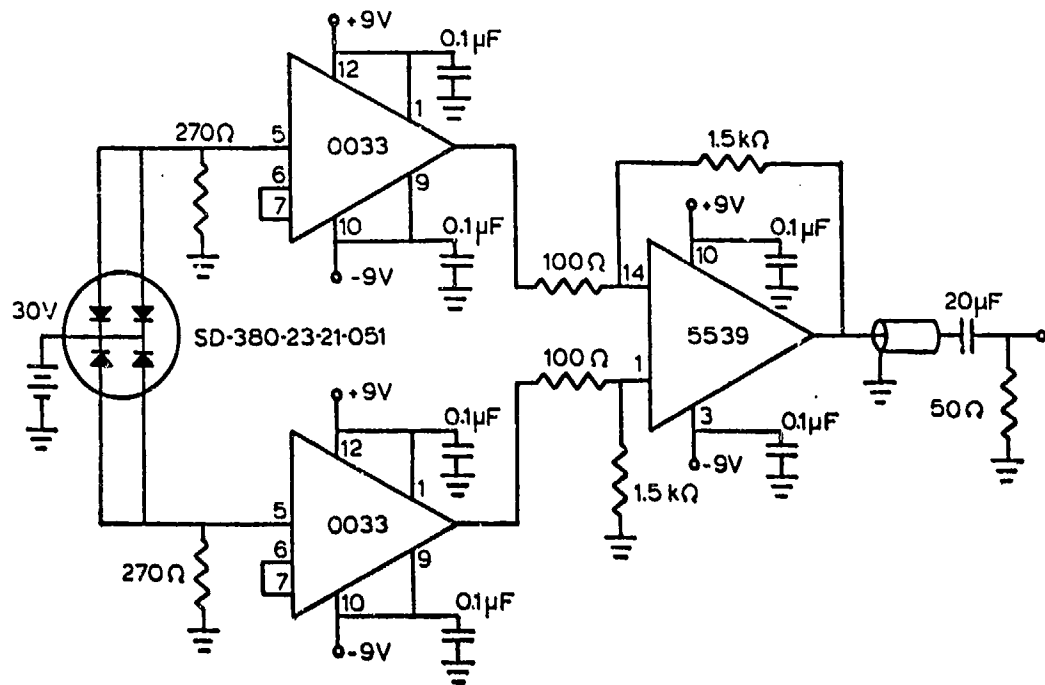


Figure 3.13. Position sensor circuit, including quadrant detector, differential stage, amplifying stage, and high-pass filter.

approximately $0.5 \mu\text{rad}$. For comparison, consider a typical schlieren system with a 500 mm focal length lens and a $100 \mu\text{m}$ pinhole. If the minimum detectable deflection is equivalent to a one f-stop change in density on the film, then the resolution of this schlieren system is approximately $100 \mu\text{rad}$. Therefore, the laser deflection technique offers higher resolution than the schlieren technique by over two orders of magnitude.

The time-response of the system was tested by masking one side of the detector at a time and using the detector to view a highly attenuated ruby laser pulse, comparing the output to that of a fast (2 ns risetime) p-i-n diode. The results are shown in Figure 3.14. From the formula for the addition of risetimes,

$$\tau_{\text{net}} = \left(\sum_n \tau_n^2 \right)^{1/2} = (\tau_{\text{laser}}^2 + \tau_{\text{circuit}}^2)^{1/2} \quad (3.21)$$

the response time of the circuit itself was approximately 20 ns. Differences in light path lengths to the detectors, cable lengths from the detectors to the oscilloscope, and relative timing between the oscilloscope channels accounted for less than 1 ns in the timing difference between the signals. A fixed circuit delay of approximately 30 ns is therefore apparent.

Since the laser deflection technique yields information about density gradients, one may either probe the region under observation at a number of positions over a number of shots and integrate dn/dx over space to obtain the density distribution, or make an assumption about the spatial distribution and obtain density information on a single shot. [Enl85]

Assume that neutral particles emitted from the insulator surface have a Maxwellian velocity distribution,

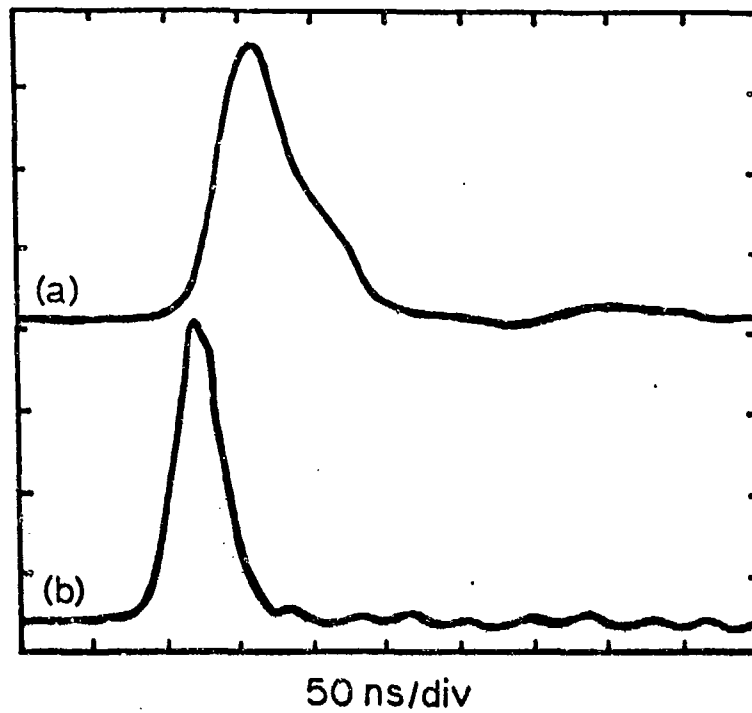


Figure 3.14. Comparing the output of one side of the position sensor (a) with that of a fast p-i-n diode (b) yields a circuit risetime of approximately 20 ns for the position sensor.

$$f(v) = \left(\frac{2m}{\pi kT}\right)^{1/2} \exp(-mv^2/2kT) \quad (3.22)$$

If the particles expand freely along x , then the number of particles per unit area between x and $x+dx$ at time t is just the number of particles with velocity between v and $v+dv$, where $v = x/t$. Thus, the particle density for the j th species, n_j , is (using $dv = dx/t$)

$$n_j(x,t) = \frac{N}{At} \left(\frac{2m}{\pi kT}\right)^{1/2} \exp(-mx^2/2kTt^2) \quad (3.23)$$

and the density gradient is

$$\frac{dn_j(x,t)}{dx} = -\frac{N}{A} \left(\frac{2}{\pi}\right)^{1/2} \left(\frac{m}{kT}\right)^{3/2} \frac{x}{t^3} \exp(-mx^2/2kTt^2) \quad (3.24)$$

At any point $x > 0$, the density gradient will peak for some time $t_p(x)$ which is the solution to

$$\frac{d}{dt} \left(\frac{dn_j}{dx} \right) = 0 \quad (3.25)$$

Thus,

$$t_p(x) = x \left(\frac{m}{3kT} \right)^{1/2} \quad (3.26)$$

If the position of the probe laser beam is x_b , then

$$\left(\frac{3kT}{m} \right)^{1/2} = \frac{x_b}{t_p} \quad (3.27)$$

and the peak density gradient seen by the beam is

$$\left(\frac{dn_j}{dx} \right)_{\max} = -\frac{3N}{A} \left(\frac{6}{\pi} \right)^{1/2} \frac{1}{x_b^2} \exp(-3/2) \quad (3.28)$$

so that the neutral emission in terms of the peak density gradient at the position of the probe laser is

$$\frac{N}{A} = 1.08 x_b^2 \left| \frac{dN_j}{dx} \right|_{\max} \quad (3.29)$$

But this is just

$$\begin{aligned} \frac{N}{A} &= 1.08 x_b^2 \left| \left(\frac{d\tilde{n}}{dx} \right)_{\max} \frac{dn_j}{d\tilde{n}} \right| \\ &= 1.08 x_b^2 \left| \left(\frac{\delta\phi}{D} \right)_{\max} \frac{1}{K_j} \right| \end{aligned} \quad (3.30)$$

Thus, given the position of the probe laser, the length of the laser path through the perturbed region, and the constant of proportionality between the change in the index of refraction and the density, the particle emission per unit area could be determined. Also, since neutral particles and plasma deflect the beam in different directions, the type of particle emission could be identified. Since the minimum detectable deflection is $\delta\phi = 0.5 \mu\text{rad}$, for $x_b = 1 \text{ mm}$ and $D = 1 \text{ cm}$, this corresponds to a minimum detectable neutral particle emission per unit surface area of $N/A = 5 \times 10^{14} \text{ cm}^{-2}$.

3.4.2. Spectroscopic Diagnostics

A 1-m spectrometer (Acton Research Corporation VM-510) and an intensified optical multichannel analyzer (OMA)(Tracor-Northern 6100 series, including a 6130-1 pulse driver) were used to take time-resolved emission spectra of the flashover plasma. Although the light emitted from the plasma occurred after the initiation of flashover, the temporal evolution of the spectroscopic line emission of the plasma enabled some inferences to be drawn about the initiation process.

The experimental configuration is illustrated in Figure 3.15. A single plano-convex lens collimated the light from the flashover plasma at its focal point. A turning mirror directed the collimated light onto another plano-convex lens, which focussed the light onto the entrance slit of the spectrometer.

The light was detected by the array of 1024 photodiodes which comprise the OMA. The photodiodes were back-biased except during the time that a 180 V gating pulse was applied, so that the spectrometer could be electronically shuttered. The shortest gate pulse available was approximately 100 ns.

The dispersion of the spectrometer, with a 600 line/mm grating installed, allowed approximately 40 nm of the spectrum to be sampled at any time. Therefore, the resolution of the detector was on the order of 0.04 nm, the width of one channel. Because of the low intensity of the flashover plasma light source, however, a wide input slit width (typically 50 μm) was employed, so that the instrument resolution of the system was approximately an order of magnitude greater than the detector resolution.

The region of the spectrum which could be sampled was limited by the cutoff of the glass optics at short wavelengths, and by the fall off in the efficiency of the grating at long wavelengths. Typically, spectra were taken over a range of 340–600 nm, although few interesting features appeared at the extreme long wavelength end of this range.

3.4.3. Open-shutter Photography

A 4" x 5" still camera was used to photograph the discharge in the visible region. The camera was used in the open shutter mode; that is, the room was darkened and the shutter remained open during the discharge. Thus, no time resolved information could be obtained; however, some features could be discerned.

Polaroid Type 55 positive-negative film ~~was used~~, since the resulting negative could be enlarged to reveal detail. In order to use such a slow film, it was necessary to open the aperture on the camera lens, which limited the useful depth-of-field.

3.5. Timing

The timing of the flashover event compared to the input ultraviolet illumination was a crucial measurement in interpreting this experiment. Care was taken to assure that the relative timing of the various diagnostics could be determined to within ± 2 ns. This involved more than insuring that all cable runs from the experiment to the screen room where the oscilloscopes were housed were of the same length, since the photodiode which monitored the laser output was located an appreciable distance from the interaction chamber.

The layout of the timing chain is shown in Figure 3.16. There was approximately a $7 \mu\text{s}$ delay from the time the laser received the trigger pulse until the time it fired, while the oscilloscopes typically covered only 200 ns. Therefore, the oscilloscope triggers were delayed.

The propagation speed along the RG-58 signal cables was measured, was found to conform to the manufacturer's specifications. In the cable, signals propagated with velocity $v = 0.66c$. Therefore, lengths of the cables were chosen so that the pathlength from the chamber to the screen room was the equivalent of 12.5 m of cable for both the electrical and the optical diagnostics. Equal lengths of cable were used inside the screen room as well.

A multi-channel triggering unit was developed, which provided two zero-delay and four delayed outputs (with two independent delay times). The schematic for this unit is shown in Figure 3.17. The outputs were 4 V amplitude

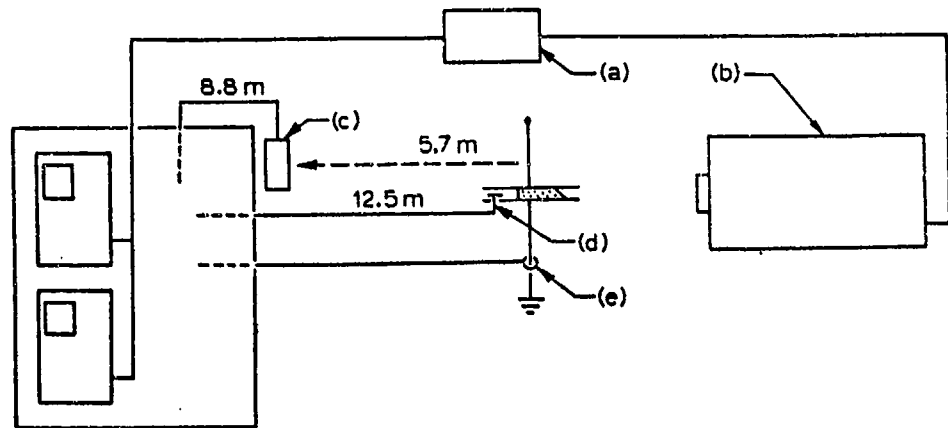


Figure 3.15. Timing chain. a) Trigger generator. b) Excimer laser.
 c) Ultraviolet-sensitive p-i-n diode. d) Capacitive V-dot probe.
 e) Rogowski coil.

and 100 ns wide square pulses into a 50 Ω load. The delay times could be varied over approximately 0-10 μ s. The advantage of multiple outputs was that one output could be used to trigger the oscilloscope(s) while an identical output was displayed on each oscilloscope channel, in order to calibrate the horizontal position of each channel versus the graticule.

CHAPTER 4

RESULTS AND ANALYSIS

4.1. Ultraviolet Effects on Polymers

Each insulator material used in this study was tested to determine its response to ultraviolet illumination under vacuum in the absence of electric field stress. Of particular emphasis was the emission of particles into the vacuum.

In order to interpret these results, it is useful to understand in general the effects of ionizing radiation on polymers. The chemical formulas for the materials under investigation have already been presented in Figure 2.5. Structurally, these monomers are linked into polymer chains which may be hundreds of monomers long. Under ionizing radiation, any of the following effects may occur: excitation, ionization, or scission (that is, breaking of chemical bonds). [Bov58, Nik63, Cha67] If scission occurs, then it is possible for the polymer to recombine in its original form, to stabilize as smaller molecules (degradation), or to branch or cross-link; in the last case, the resulting structure of the polymer is more complicated than a single linear chain. [Nik63, Cha67]

The parameters which determine which of these effects occur are the energy of the radiation involved and the timescale over which the interaction occurs. The common bonds in polymers are C-H, C-C, and C-O, with bond strengths of 4.28 eV, 3.44 eV, and 3.45 eV, respectively. [Ran67] Halogen bonds are somewhat stronger; C-F, for example, has a bond strength of approximately

5.7 eV. [Bov58] The ionization potential for typical polymers is approximately 9 eV. [Bov58, Win83] Cross-linking requires 20–30 eV in a single photon, because of the short lifetime of the intermediate products; in the usual scenario, radiation breaks a C–H bond on one polymer chain, while the resultant H radical breaks another C–H bond in another chain. The cross-link between the polymer chains occurs at the point of the broken C–H bonds. [Nik63, Cha67]

For this experiment, the incident ultraviolet photons have an energy of 5 eV, so that excitation or scission are possible given a single photon interaction. If the intermediate excited state is metastable, then multi-step ionization is possible. Recent studies of the process on ultraviolet ablation of polymers [Sut86, Sri87] point to the importance of a threshold in ultraviolet flux above which relaxation processes (recombination) are saturated and decomposition becomes significant.

Another effect which, although not strictly photochemical, must be considered, is induced outgassing from the insulator surface. Polymer surfaces readily absorb gas molecules [Gra85] which may be released if the surface is heated by ultraviolet radiation.

Two manifestations of the interaction of ultraviolet radiation with the surface of a polymer in vacuum—electron emission and neutral particle emission—were considered separately.

4.2. Electron Emission Measurements

Each insulator material was tested for its response to ultraviolet illumination without applied high voltage. Emission of electrons from the surface was measured by configuring the electrodes as a charged particle collector, as discussed in the previous chapter. It was necessary to apply a small electric field

to the sample to sweep the electrons into the anode; however, to avoid perturbing the measurement the smallest electric field sufficient to accomplish this was chosen. Figure 4.1 shows the emission signal versus applied voltage. The sharp knee and subsequent plateau in the curve indicates the point at which all charges emitted from the surface were collected. This corresponds to an electric field of approximately 50 V/cm. To insure that interaction with the background gas would not perturb the measurement, signal versus background pressure was measured, and is shown in Figure 4.2. Although the figure shows that the effect of background pressure is slight, all measurements were made at pressures $< 1 \times 10^{-4}$ Torr.

As shown in Figure 4.3, photoemission was higher for insulator samples which had not been previously exposed to ultraviolet illumination than for conditioned samples. This is probably due to removal of impurities, including desorbed gases, from the surface of the insulator. Exposure to ten pulses of 100 mJ/cm^2 fluence was sufficient to condition each of the materials considered, and all data shown in this work are for conditioned samples. The charge emitted from the insulator surface during laser illumination as a function of ultraviolet energy deposited is shown in Figure 4.4. Photoemission is highly non-linear in pulse energy; especially, below a certain threshold energy it is negligible. Photoemission is lowest for simple hydrocarbons, highest for polymers containing halogens, and somewhere between these bounds for more complex polymers.

As noted previously, the bandgap between the valence band and the vacuum level is, for most polymers, approximately 9 eV. [Bov58, Win83] The photon energy at KrF wavelength is 5 eV. Therefore, any photoionization must take place via a multiphoton interaction. All of the materials under consideration

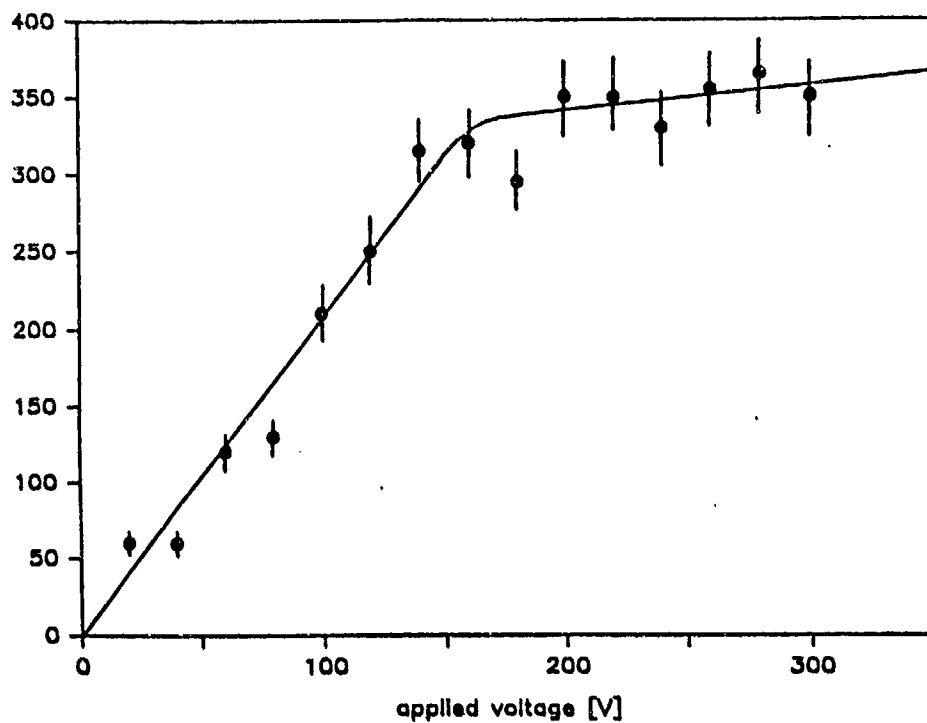


Figure 4.1. Electron emission signal versus voltage applied to the collecting plates. The knee in the curve corresponds to an electric field of approximately 50 V/cm.

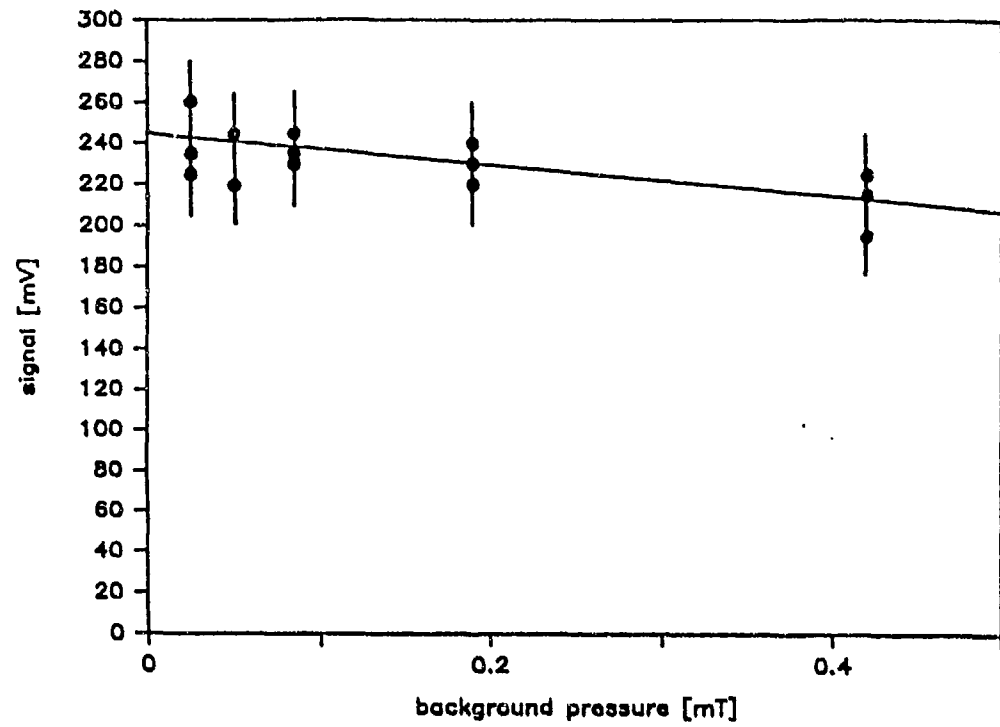


Figure 4.2. Electron emission signal versus background pressure in the chamber.

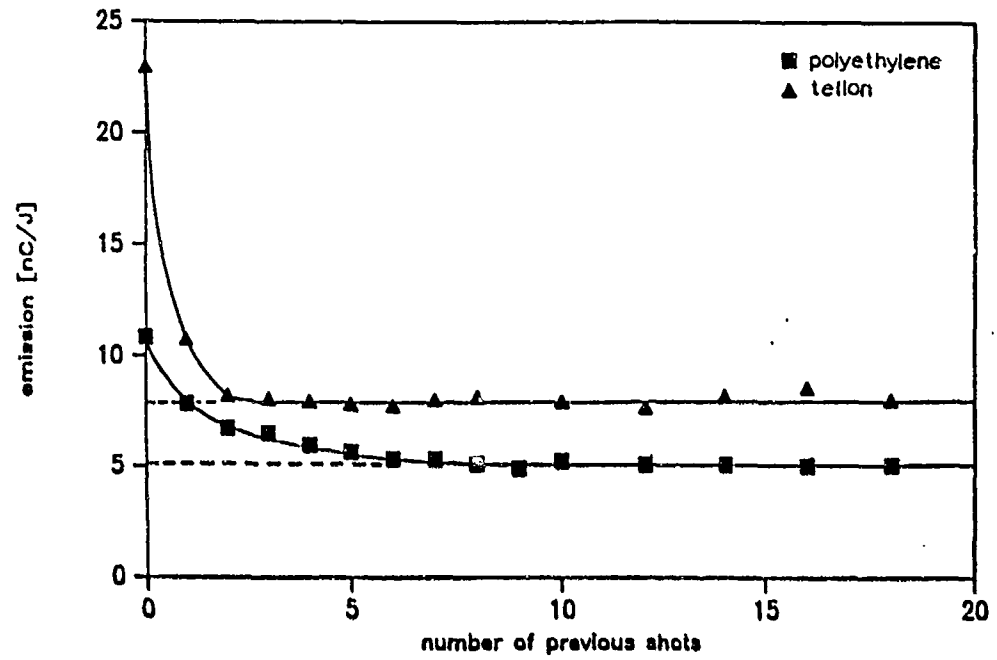


Figure 4.3. Electron emission from polyethylene and teflon, indicating the conditioning effects of repeated exposure to ultraviolet radiation.

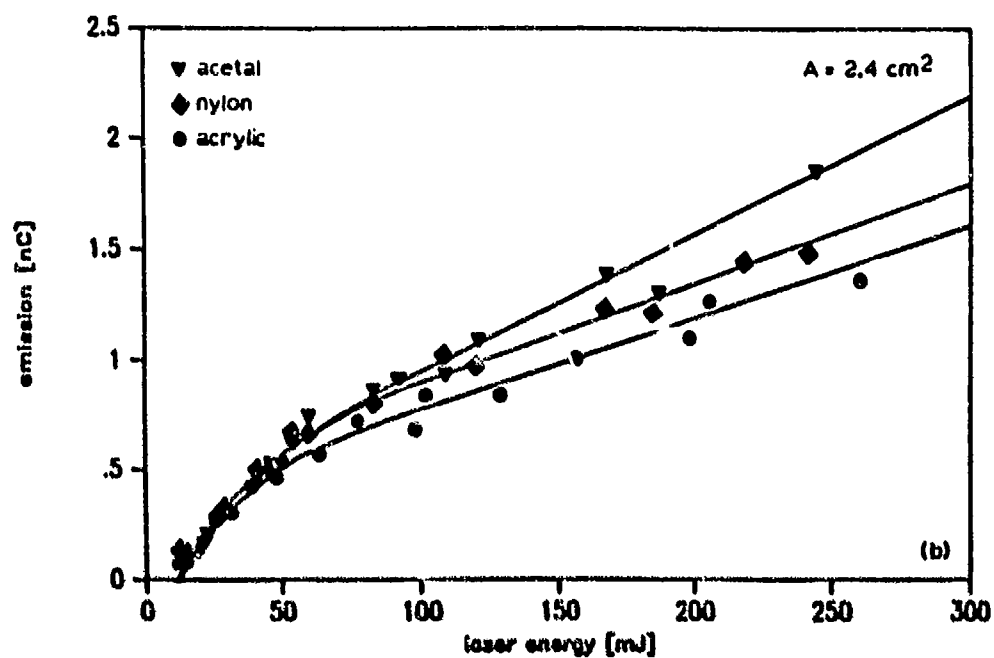
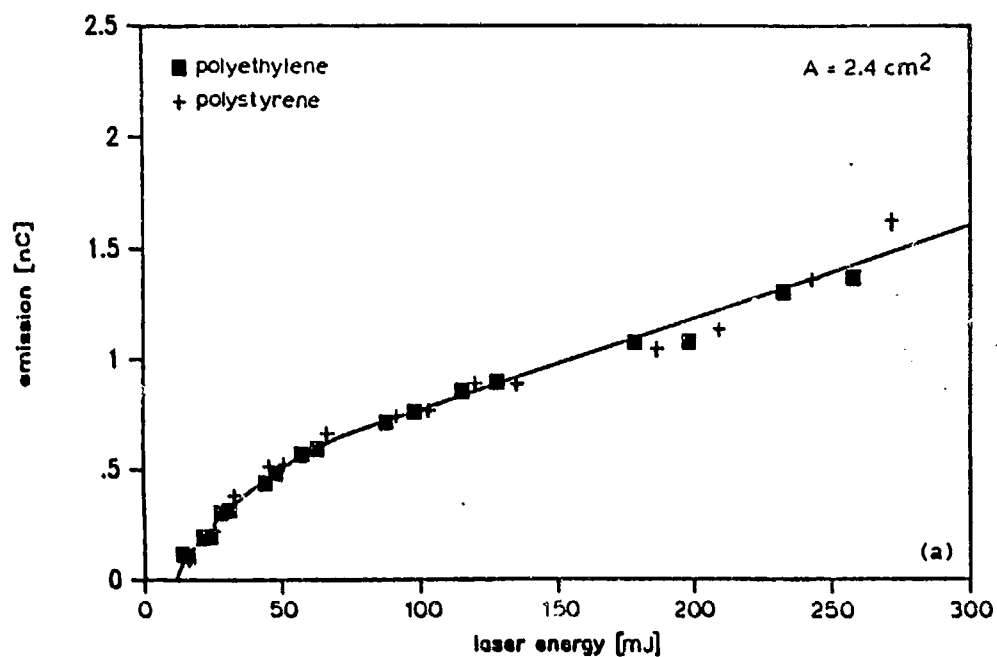


Figure 4.4. Electron emission from polymers under ultraviolet illumination.
 a) Polyethylene and polystyrene, which are simple hydrocarbons.
 b) Acetal, nylon, and acrylic, which are more complex polymers.
 c) Teflon and PVC, which are polymers containing halogens.

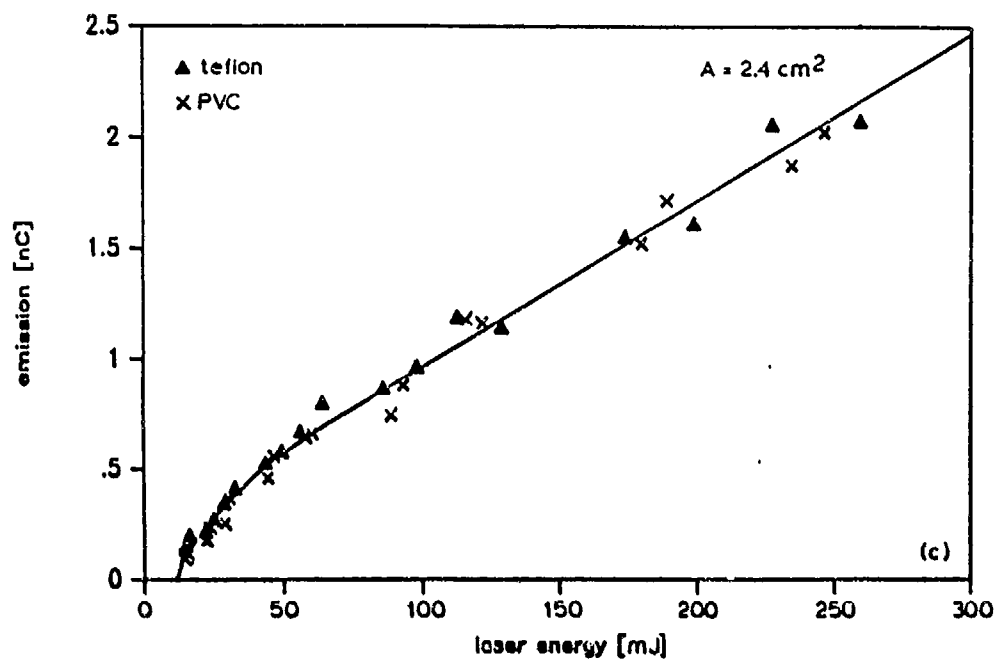


Figure 4.4. (continued).

fluoresce under KrF laser illumination; further, the fluorescence persists for several tens of nanoseconds after the end of the laser pulse. This implies that there are metastable states in the bandgap region which may be excited by the ultraviolet radiation and subsequently ionized. [Win83] A simple experiment was devised to test whether the lifetime of the intermediate state were sufficiently long to allow for a multi-step interaction. The experimental arrangement is illustrated in Figure 4.5. An acrylic sample (chosen because it was transparent to visible light) with a thickness of 0.64 cm was placed at a 45° angle to the incident ultraviolet laser beam. A p-i-n diode viewed the acrylic at an angle of 90° to the laser beam. The diode was shielded from the line of sight of the laser. The acrylic sample was opaque to the ultraviolet, and any stray visible light from the laser discharge would either pass through the acrylic or be reflected away from the photodiode at either the front or the back surface of the sample. Thus, the only light visible to the photodiode was that from the fluorescence of the acrylic under the influence of the ultraviolet radiation incident on its front face.

The pulse shape of the incident laser light $f(t)$ has already been described (see Figure 3.3 and Figure 4.6(a)) and has a pulsewidth τ . The greatest portion of the fluorescence (the prompt fluorescence) [Kno79] decays exponentially, $f'(t) = e^{-t/\tau_1}$, where τ_1 is the lifetime of the excited intermediate state or states (see Figure 4.6(b)). Thus, the pulse shape of the fluorescence induced by the ultraviolet laser pulse is a convolution of $f(t)$ and $f'(t)$, which is

$$f''(t) = \int_0^t dt' f(t') \tau_1^{-1} e^{-(t-t')/\tau_1} \quad (4.1)$$

In the limit of $\tau_1 \ll \tau$, $f(t) \simeq \delta(t)$ and $f''(t) \simeq f(t)$; that is, the fluorescence output pulsedshape will be the same as the laser input pulsedshape. Conversely, in the

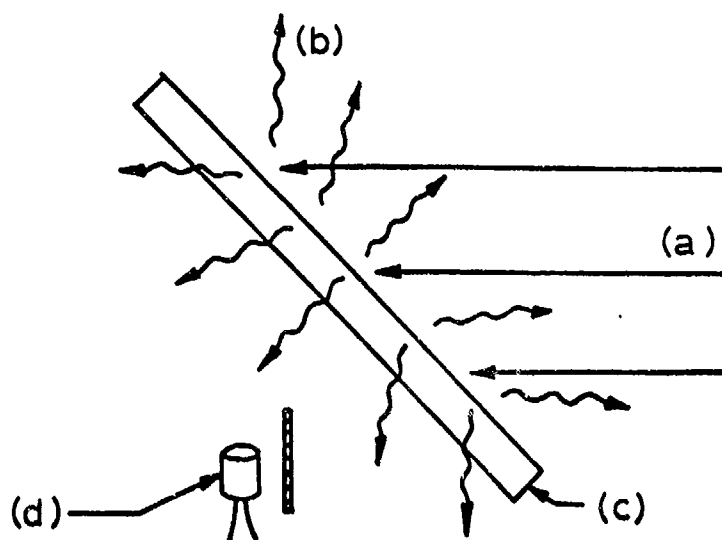


Figure 4.5. Experimental configuration for determining the lifetime of excited states in a polymer. a) Incident ultraviolet laser beam. b) Visible light (fluorescence). c) Acrylic sample. d) Photodiode.

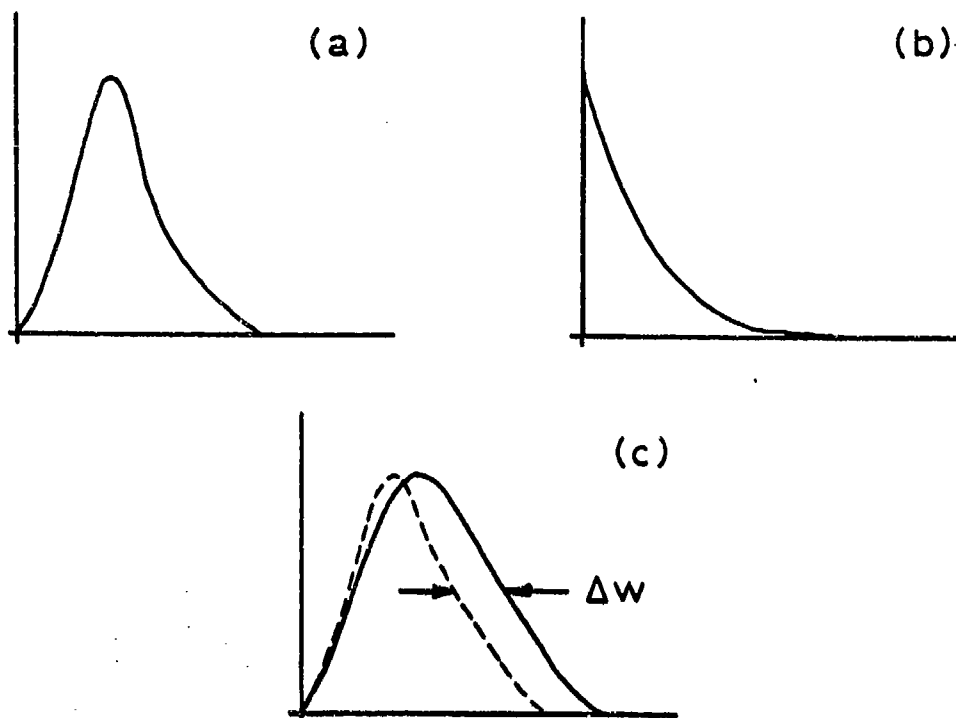


Figure 4.6. a) Input ultraviolet laser pulseshape. b) Decay of prompt fluorescence. c) Convolution of (a) and (b) indicating increased pulsewidth Δw .

limit of $\tau_i \gg \tau$, $f(t) \simeq \delta(t)$ and $f'(t) \simeq f(t)$; an exponential decay of the fluorescence will be observed. For intermediate values of τ_i , the fluorescence output pulsedshape will be similar to, but wider than, the input pulsewidth (see Figure 4.6(c)). Indeed, this is what was observed. By evaluating equation (4.1) numerically, the increase Δw in the FWHM due to the lifetime of the intermediate state is related to the lifetime of that state τ_i (for τ_i on the order of τ) by the linear relationship

$$\Delta w = 0.78\tau_i \quad (4.2)$$

Using this formula, a typical lifetime for the intermediate state was found to be $\tau_i = 13$ ns, which is a significant fraction of the pulsewidth of the laser. Therefore, multi-photon ionization is possible.

Figure 4.7 is the result of modelling the two-step ionization process with three coupled rate equations. Three populations are considered: n_0 , the ground state, n^* , the excited state, and n_i , the ionized state. The evolution of each of the populations is given by

$$dn_0/dt = -An_0 + Cn^* \quad (4.3)$$

$$dn^*/dt = An_0 - Bn^* - Cn^* \quad (4.4)$$

$$dn_i/dt = Bn^* \quad (4.5)$$

where A represents the ultraviolet flux times the excitation cross-section of the ground state, B represents the ultraviolet flux times the ionization cross-section of the excited state, and C represents the lifetime of the excited state. No pretense was made to solve for the actual quantities which the constants represent; rather, the units were normalized and the ratio A:B:C was varied to determine if any values of A, B, and C could yield a response similar to that which was observed.

Indeed, the result is similar to the experimental results in that: 1) at very low pulse energy, photoionization is negligible, since the probability of a photon's interaction with an excited electron is small, 2) at moderate pulse energy, photoionization increases rapidly as the intermediate state is populated, and 3) at high pulse energy, the increase in ionization with fluence is reduced as the process becomes saturated. Clearly, the results of the simple model do not match the experimental results exactly, but a real polymer is unlikely to be such a simple system. Comparing the major features supports the hypothesis that two-step photoionization is indeed the active process. Photoemission due to three or more photons can be discounted, because lower-energy visible light photons do not cause significant fluorescence, which implies that their energy is too low to excite the intermediate states.

4.3. Neutral Particle Emission Measurements

Neutral particle emission was similarly measured for each of the materials under consideration. The laser deflection technique previously described was used. Again, data are shown for conditioned samples. Neutral emission per unit area of the insulator surface as a function of fluence deposited is shown in Figure 4.8. The data are consistent with those found in the literature, [Sut86, Sri87] obtained from measuring the ablation of the insulator surface over many shots. Below a particular threshold fluence which varies with material (on the order of 100 mJ/cm^2) neutral particle emission is negligible.

The current state of understanding of ultraviolet ablation of polymers [Sut86] may be quickly summarized. Although ultraviolet radiation may break numerous chemical bonds in a polymer, relaxation processes quench, to a great extent, the formation of stable photofragments (decomposition) as long as the

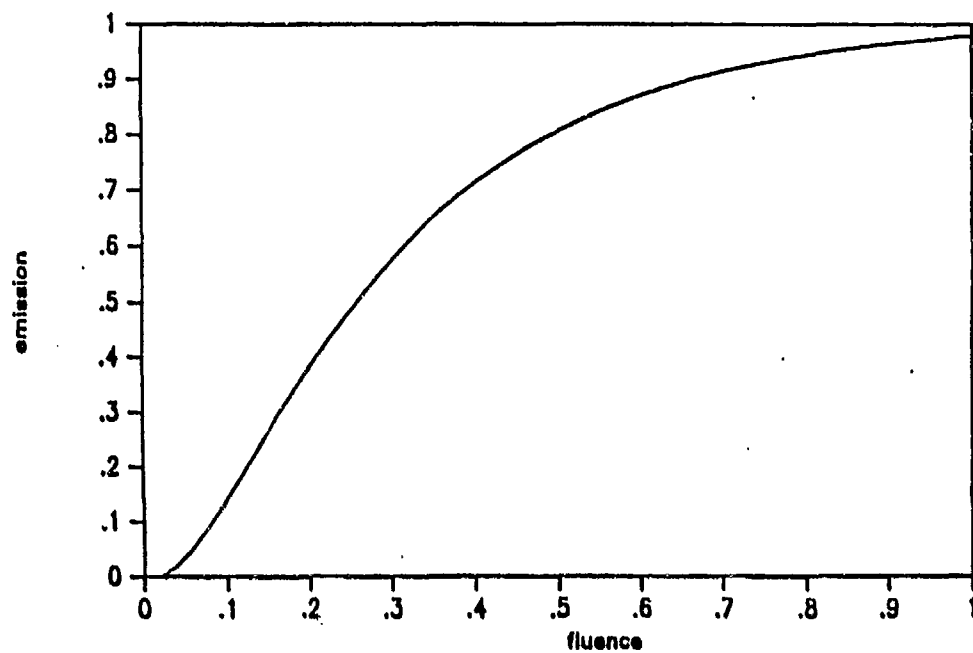


Figure 4.7. Results of a coupled rate equation model of two step photoionization.

ultraviolet flux is not too great. If, however, a certain critical flux (which varies with material and with the wavelength of the ultraviolet) is exceeded, then the relaxation processes become saturated and photofragments begin to form. Because the photofragments occupy more volume than the polymer chains from which they were formed, mechanical stress builds up in the material. Eventually, the photofragments are ejected; that is, ablation occurs. The critical flux is on the order of a few MW/cm^2 , [Sut86] which for a typical excimer laser pulse with a pulsewidth of several tens of ns is equivalent to a fluence on the order of $100 \text{ mJ}/\text{cm}^2$. If a shorter pulsewidth is used, then ablation will be observed at a lower fluence level. [Han88]

In studying flashover behavior under high voltage, the ultraviolet fluence was typically kept below this threshold value; thus, neutral particle effects do not play a significant role in the results presented, except perhaps at very low field stress (on the order of $10 \text{ kV}/\text{cm}$) where the fluence required to initiate flashover was larger.

4.4. Characterization of Induced Flashover

4.4.1. Observations

In order to characterize the flashover event, current and voltage in the interelectrode region were monitored as the ultraviolet illumination was applied. Typical data are shown in Figure 4.9. Although significant prebreakdown activity is evident, flashover is identified as the discontinuity in the voltage and current indicating the sudden collapse of the impedance in the gap. With time $t = 0$ taken as the start of the laser pulse, and with \mathcal{E} the laser pulse energy, the time t_f at which flashover occurs was noted. The laser beam was attenuated, reducing \mathcal{E} ,

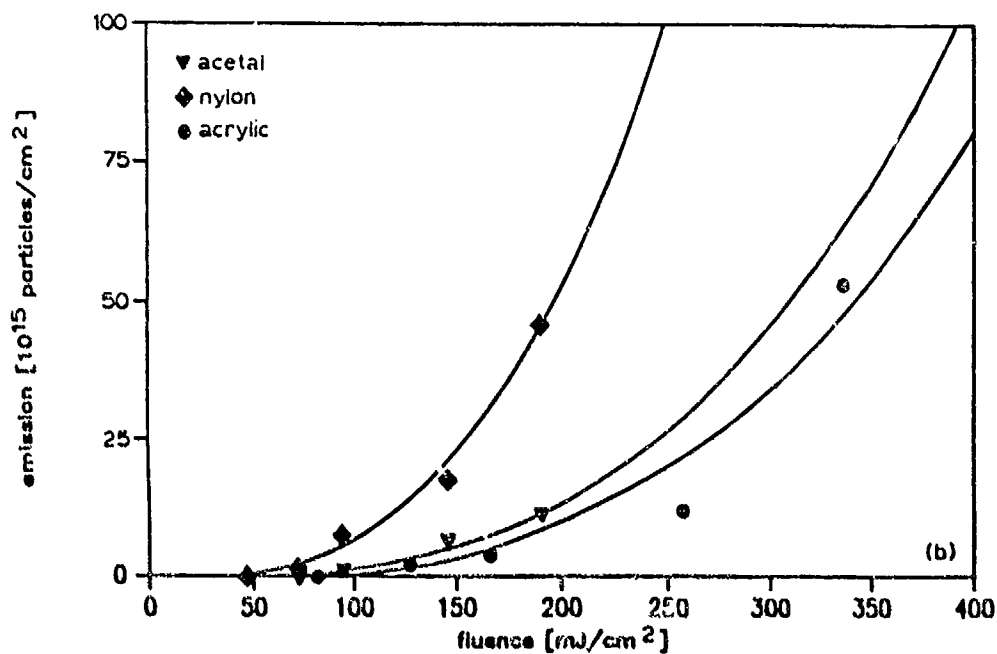
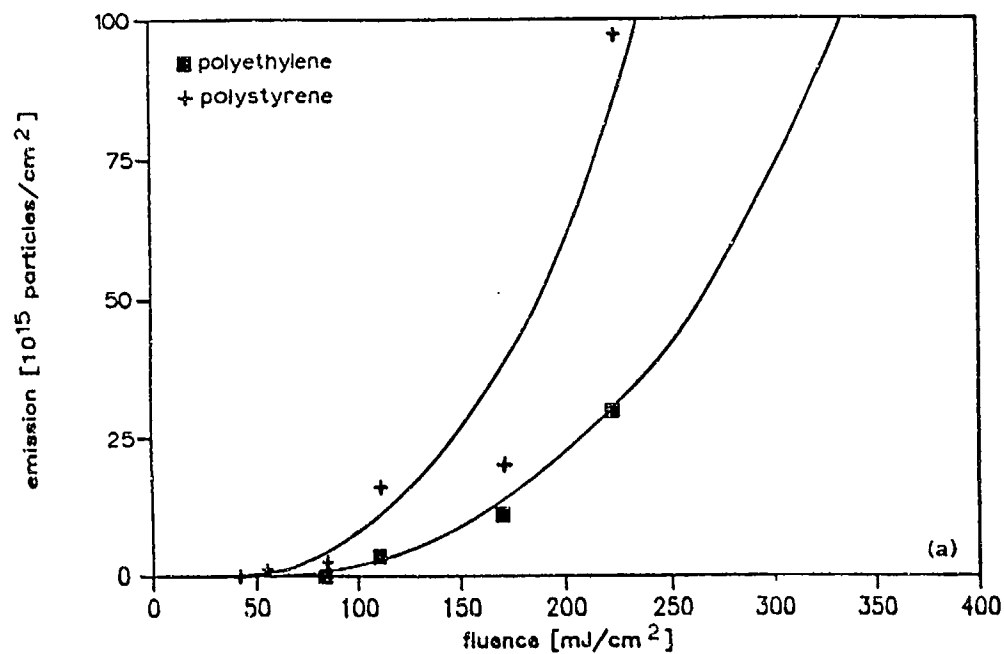


Figure 4.8. Neutral emission from polymers under ultraviolet illumination.
 a) Polyethylene and polystyrene. b) Acetal, nylon-6, and acrylic.
 c) Teflon and PVC.

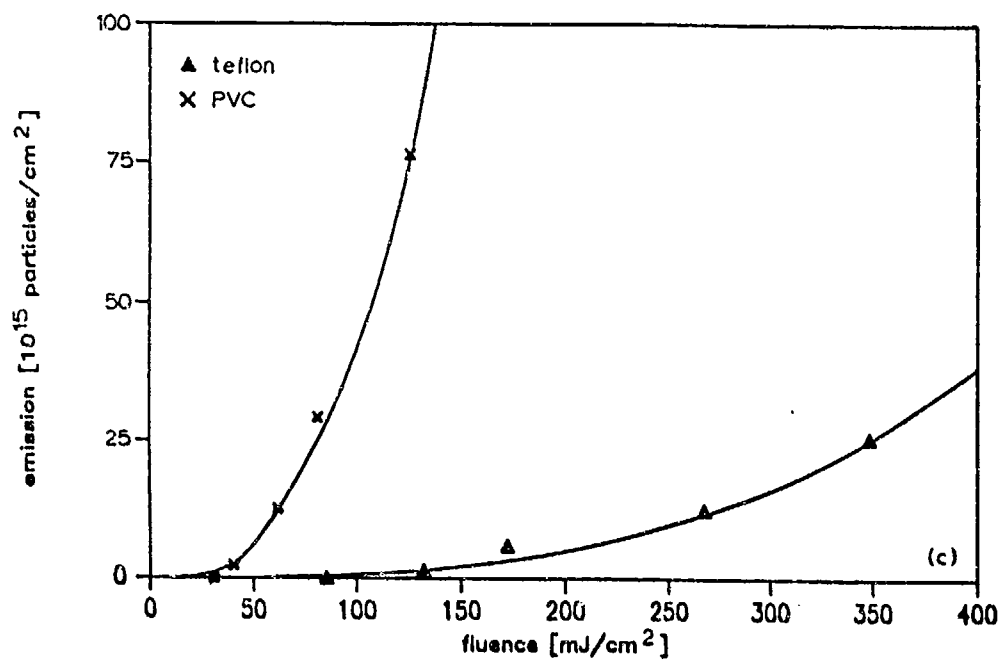


Figure 4.8. (continued).

and again t_f was noted. As more attenuation was added, t_f increases until flashover was no longer observed ($t_f = \infty$).

The prebreakdown current $i(t)$ was found to be nearly proportional to the illumination intensity $I(t)$, and the flashover event may be roughly characterized according to the prebreakdown current behavior, as 1) strongly induced flashover, in which illumination intensity and prebreakdown current increase continuously until flashover occurs, 2) weakly induced flashover, in which $I(t)$ and $i(t)$ reach a maximum and are actually decreasing at the time of flashover, or 3) stable, in which no flashover is observed, even though $i(t)$ is not zero during the illumination pulse.

No correlation of the time of the flashover event with either the instantaneous value of the illumination intensity or the prebreakdown current could be found. Depending on the pulse energy \mathcal{E} , flashover was observed with equal regularity on the rising as well as the falling edge of the illumination pulse, even late in time when the illumination was significantly less than its peak value. Flashover occurring after the illumination ceased entirely, however ($t_f > \tau$), was rare, observed in fewer than one percent of the flashover events.

This simple observation leads to the conclusion that it is ultraviolet fluence, rather than power density, which governs the initiation of flashover. If there were a critical power density required to initiate flashover, then that power density would be achieved, if at all, on the rising edge of the illumination pulse, and flashover would either be observed on the rising edge of the pulse, or not at all. Since flashover is indeed observed even late on the falling edge of the pulse, fluence, rather than power density, must be the determining quantity. One may attempt to account for flashover late in time by postulating some formative time-

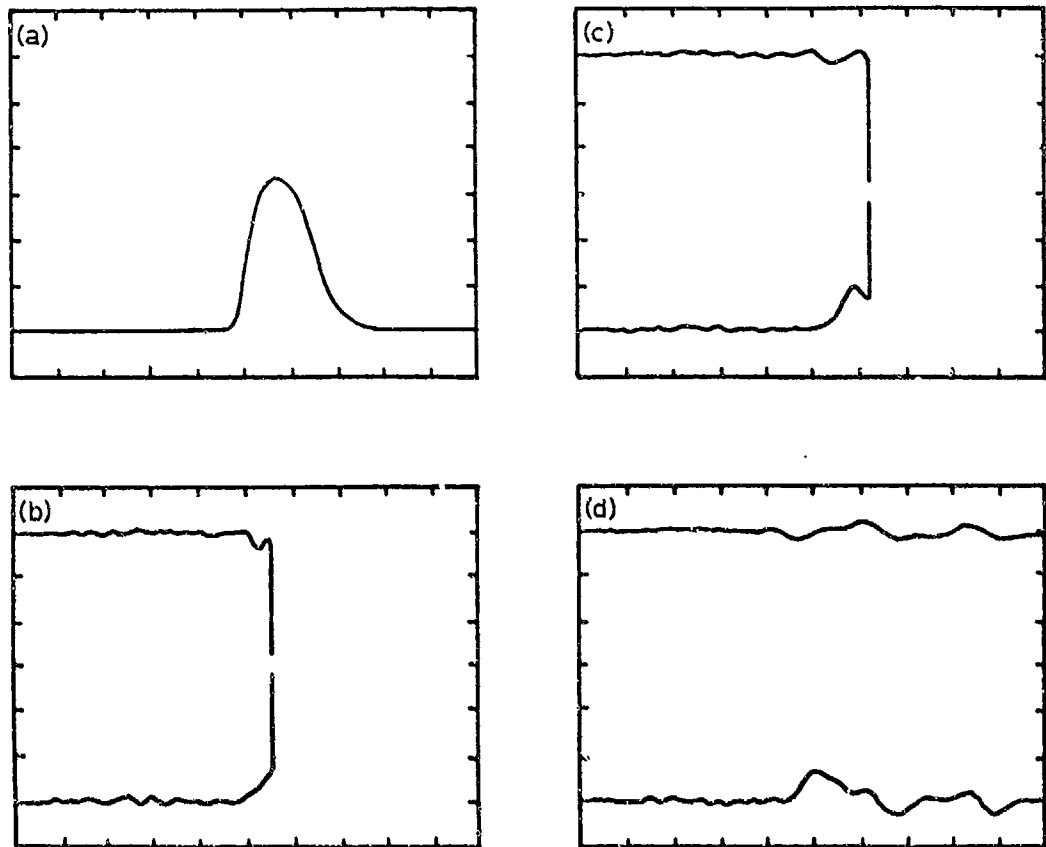


Figure 4.9. Typical data from ultraviolet-induced insulator flashover. a) Incident laser pulse. b-d) Voltage (top) and current (bottom) in the interelectrode region. Shots (b) through (d) are in order of decreasing laser pulse energy.

lag; however, since the falling edge is longer than the rising edge, that proposition leads to the absurd conclusion that flashover observed on the rising edge was initiated before illumination began, and hence may be discounted.

Emission spectroscopy of the flashover plasma was performed for the particular configuration illustrated in Figure 4.10. An aluminum cover plate was set in place around the inside and front surfaces of the top electrode, while the brass bottom electrode was unmodified. The insulator material was teflon, chosen because of its particular chemical formula, $(C_2F_4)_n$. This arrangement allowed the source of the constituents of the flashover plasma to be identified by identifying spectral lines—Al from the top electrode, Cu and Zn from the bottom electrode, and C and F from the insulator. Presumably any other spectral lines, such as N, O, and H, would come from desorbed gasses on the surfaces exposed to the vacuum.

For this particular portion of the experiment, the capacitance of the discharge circuit was increased to 1500 pF to provide a brighter light source by increasing the energy available to the discharge plasma. Still, large slit widths on the input of the spectrometer ($50\text{ }\mu\text{m}$) and long time gates were required to achieve acceptable signal to noise ratios. With the larger capacitance, the circuit had a ringing period of approximately 280 ns. The shortest gate used was 140 ns wide, covering $0 < t < 140\text{ ns}$, the first current maximum. Later in time, longer gates were used to compensate for the exponentially decaying power input into the plasma.

It is instructive to compare the spectra taken at early time ($0 < t < 140\text{ ns}$) with those taken late in time ($420 < t < 840\text{ ns}$) for both the

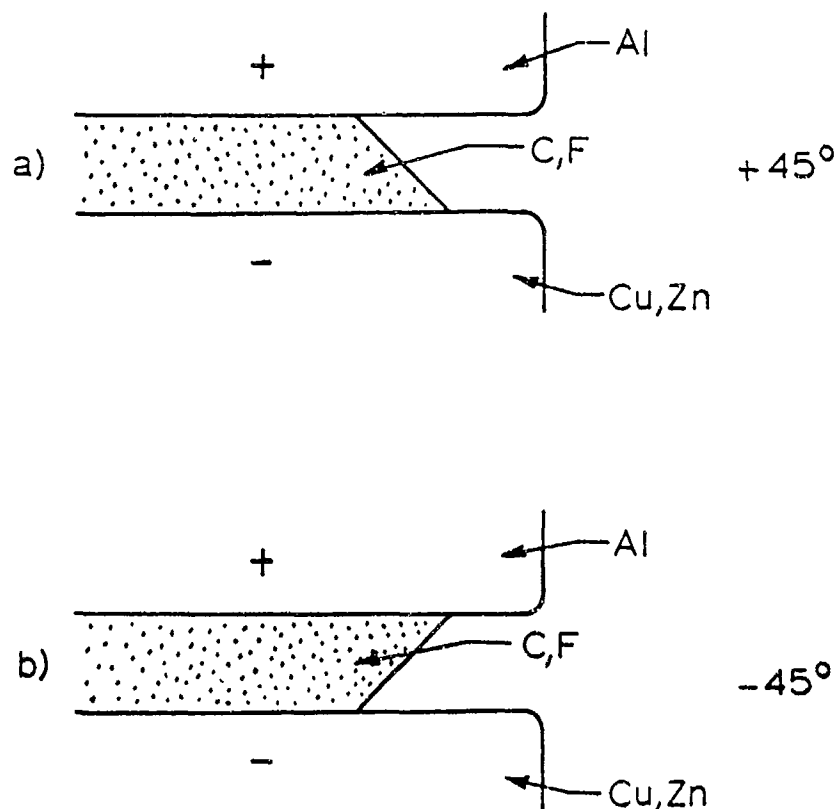


Figure 4.10. Experimental configuration for emission spectroscopy, indicating the composition of each component. a) $+45^\circ$ (conventional) configuration. b) -45° (unconventional) configuration.

+45° (conventional) and the -45° (unconventional) configurations. The results are tabulated in Table 4.1 and illustrated in Figure 4.11.

The spectra for both polarities early in time are very similar, containing strong C and F components and minimal metal lines. The insulator itself is the source of material for the plasma. Late in time, the spectra are quite different. In both polarities, metal lines dominate, including the higher excited states Cu II, Al II, and Al III. In the conventional configuration, however, Al dominates, while in the unconventional configuration Cu dominates and a Zn component appears for the first time. Referring to Figure 4.10, this means that late in time, material from the electrode at the narrow end of the insulator enters the plasma.

The explanation for the spectra may be found by examining the burn patterns left on the electrodes after the discharge. Typical burn patterns are illustrated in Figure 4.12. At the wide end of the insulator, damage is limited essentially to the triple point. It appears that the current density was uniformly distributed across the illuminated portion of the insulator, while no evidence of significant current density exists outside the illuminated region. The burn patterns on the narrow end of the insulator have a different character. Although another uniform region of damage (somewhat more diffuse) may be seen near the triple point, numerous distinct spots are visible a significant distance away from the insulator. The appearance is similar to the burn patterns found in a high-pressure discharge, [Gil83] and implies that current filaments have formed.

Thus, interpreting the spectral data in the light of the observations, the following scenario is likely—flashover initially occurs near the insulator surface, uniformly across the illuminated region. Most of the flashover plasma early in time consists of electrically ablated insulator material. Once the discharge is

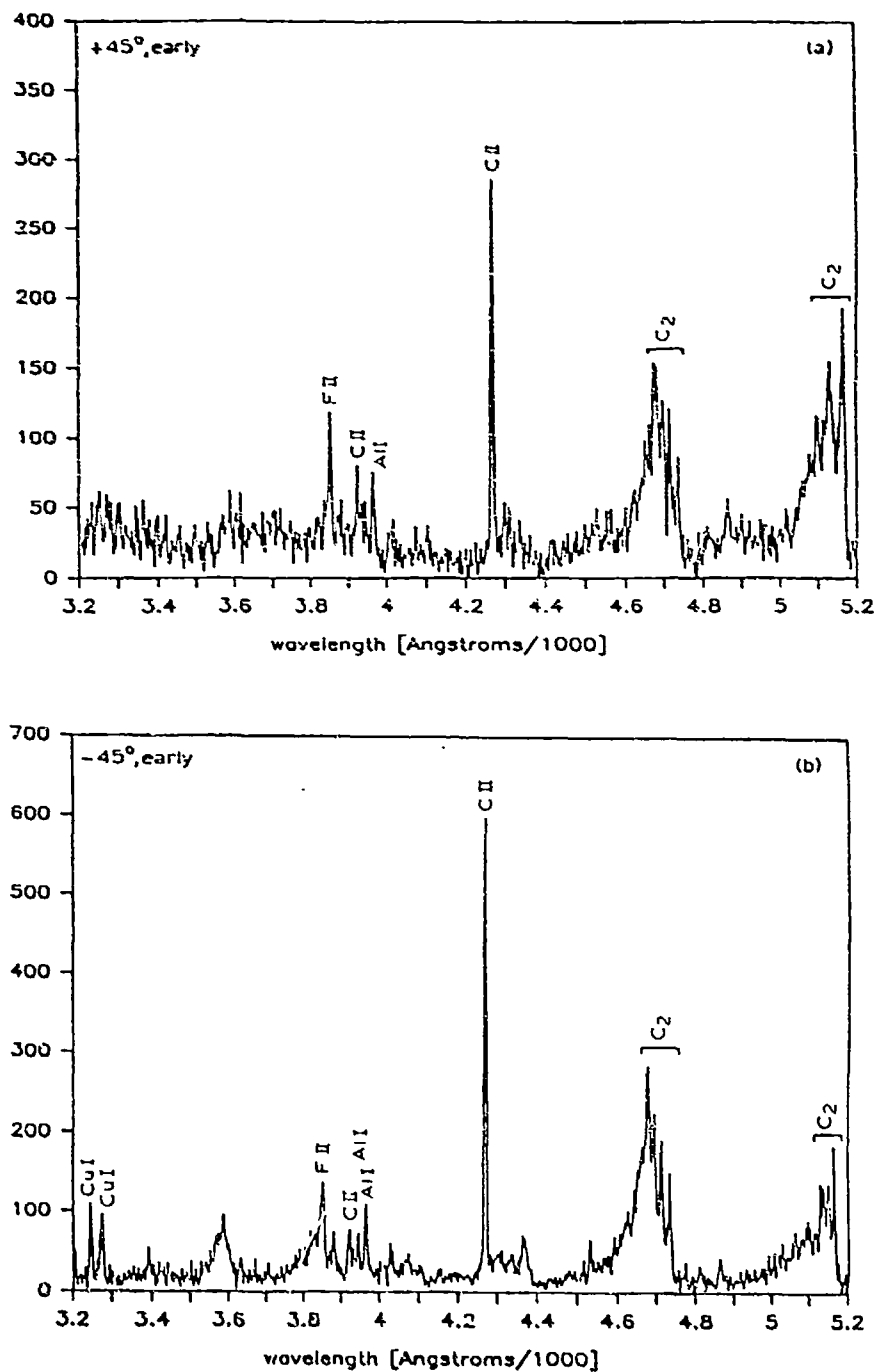


Figure 4.11. Emission spectra of flashover plasmas with an aluminum anode, a brass cathode, and a teflon insulator. a) +45° (conventional) configuration, early time. b) -45° (unconventional) configuration, early time. c) +45° (conventional) configuration, late time. d) -45° (unconventional) configuration, late time.

Table 4.1. Spectral Lines in Flashover Plasmas

-45°		+45°		Identity
Early	Late	Early	Late	[Pea41, Rea80]
3247.2	3248.9	Cu I, 3247.54
3276.9	3274.9	Cu I, 3273.96
.....	3301.4	Cu II, 3300.881, 3301.229
.....	3344.5	Zn I, 3345.02
.....	3587.5	Unknown
.....	3618.6	Unknown
.....	3659.3	Al II, 3654.98, 3655.0
.....	3708.5	Unknown
.....	3718.6	Unknown
3848.8	3853.8	F II, 3501.39-3505.63
.....	3878.5	Unknown
3920.8	3922.9	C II, 3918.98
3944.8	3943.2	3944.8	A II, 3944.006
3963.9	3963.9	3961.9	3963.1	A II, 3961.520
.....	4151.3	Al III, 4149.92, 4150.17
4269.1	4265.9	4267.9	C II, 4267.00, 4267.27
.....	4309.0	4307.9	CH, 4312.5
4367.6	4368.8	Unknown
.....	4483.1	Al III, 4479.89, 4479.97
.....	4513.5	Al III, 4512.56
.....	4529.5	Al III, 4529.19

- 45°		+ 45°		Identity
Early	Late	Early	Late	[Pea41, Rea80]
.....	4611.0	Unknown
4676.0	4680.1	4677.6	4677.1	C ₂ Swan 4684.8
4693.1	4696.8	4698.6	C ₂ Swan 4697.6
4711.9	4715.1	4712.7	4713.5	C ₂ Swan 4715.2
4735.0	4736.3	4735.0	4735.5	C ₂ Swan 4737.1
.....	4862.5	Unknown
.....	5097.0	C ₂ Swan 5097.7
.....	5131.4	5130.2	5130.6	C ₂ Swan 5129.3
5163.9	5165.1	5164.7	5165.9	C ₂ Swan 5165.2

established, electromagnetic forces lift it off the insulator surface and cause the once-uniform discharge to filament. The discharge then exists between the triple point on the wide end of the insulator and the opposite electrode, and a significant fraction of the flashover plasma consists of ablated electrode material.

Consistent with these burn patterns, open-shutter photography of the flashover event revealed bright spots, probably indicative of explosive emission, at the wide end of the insulator. This behavior was noted regardless of polarity. Also, no plasma was observed in the narrow end; rather, the discharge lifted off

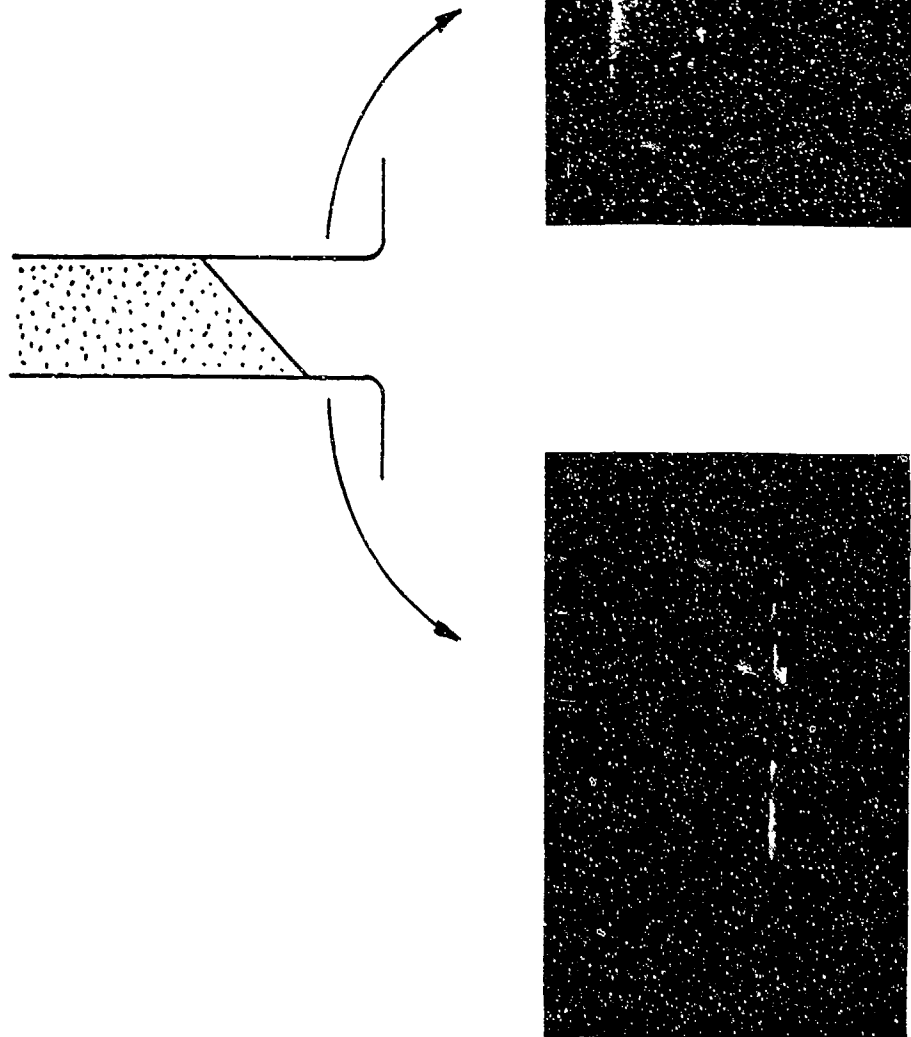


Figure 4.12. Burn patterns observed after ultraviolet induced flashover.

the surface before reaching the narrow end. Sample open-shutter photographs are shown in Figure 4.13.

4.4.2. Analysis

The normalized pulse shape $f(t)$ of the ultraviolet illumination and its integral, which are the same for all shots, have been presented previously. The pulse shape is normalized such that

$$\int_0^{\infty} f(t) dt = 1 \quad (4.6)$$

Thus, for any time t , the instantaneous illumination intensity, $I(t)$, can be expressed in terms of the pulse energy \mathcal{E} and the cross-sectional area A of the beam (see Figure 4.14), and is defined to be

$$I(t) = \frac{\mathcal{E}f(t)}{A} \quad (4.7)$$

while the fluence deposited at time t , $F(t)$, is

$$F(t) = \int_0^t I(t') dt' \quad (4.8)$$

From Equation (4.5), it follows that the total fluence is simply $F(\tau) = \mathcal{E}/A$. However, it is clear that any ultraviolet illumination of the surface *after* flashover occurs can have no effect on the process of flashover *initiation*. Therefore, it is the fluence deposited at the time of flashover $F(t_f)$ which is appropriate to consider in investigating the initiation process.

The results shown in Figure 4.15 are typical of the phenomenon of induced insulator flashover. As the total fluence $F(\tau)$ (or equivalently, the pulse energy \mathcal{E}) decreases, the time to flash t_f increases, as shown in Figure 4.15(a). However, it appears that there is a critical value of the fluence, F_c , which governs the initiation of flashover by ultraviolet illumination, irrespective of the illumination

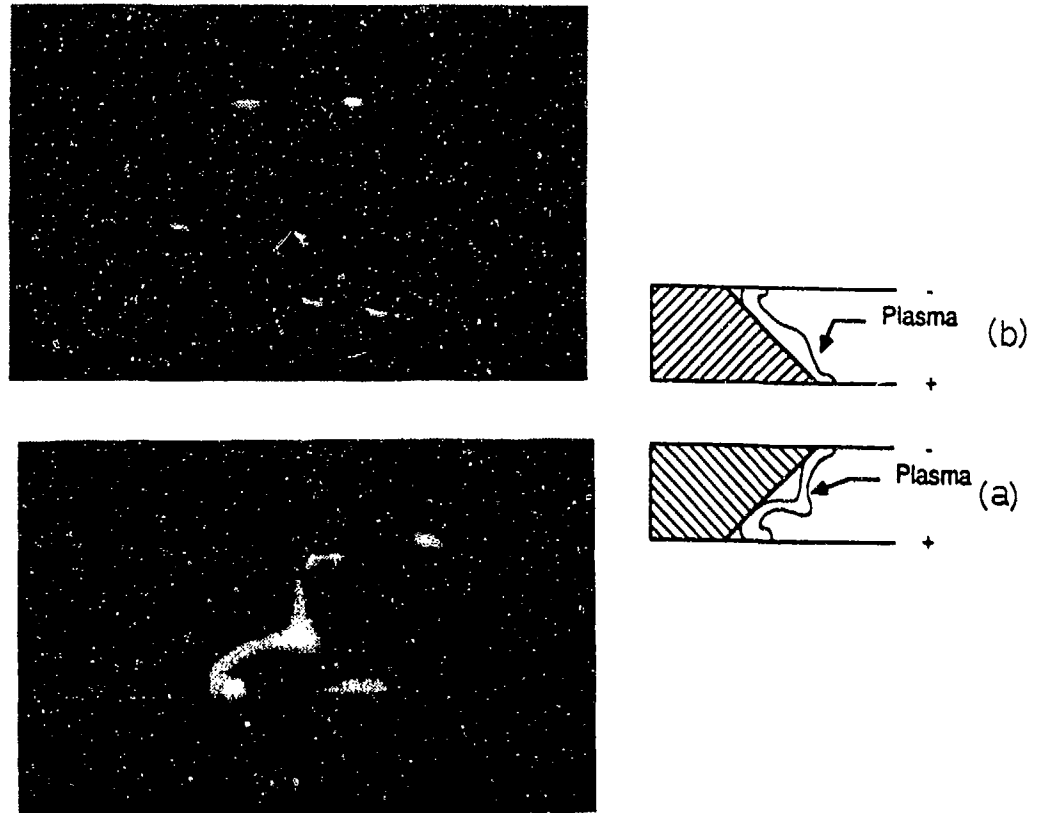


Figure 4.13. Open-shutter photographs of the flashover event.
a) Conventional configuration. b) Unconventional configuration.

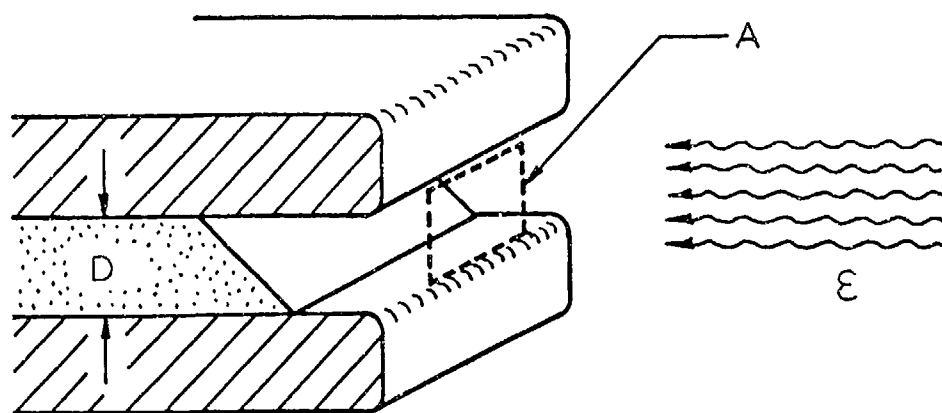


Figure 4.14. Geometry used in data analysis.

intensity. Specifically, if the total fluence $F(\tau) < F_c$, then flashover is not induced, although some current may be observed in the interelectrode region. If $F(\tau) > F_c$, then flashover is induced at a time t_f such that $F(t_f) = F_c$. This is illustrated in Figure 4.15(b), which shows that as the total fluence $F(\tau)$ is changed by nearly a factor of 10, by changing the pulse energy \mathcal{E} , the critical fluence at which flashover occurs remains essentially constant.

The critical fluence is, however, a strong function of the insulator geometry and the electric field stress. Insulator samples were tested over a range of electric field stress from 10 to 80 kV/cm in both conventional and unconventional configurations. The critical fluence is displayed in Figure 4.16 as a function of electric field stress for each of the insulator materials tested in both configurations. Only acetal exhibited such a low unilluminated flashover strength in the unconventional configuration that it could not be tested over the full voltage range. Several trends are evident: 1) the critical fluence decreases with increasing electric field stress for $E < 40$ kV/cm, 2) the critical fluence is approximately constant for $E > 40$ kV/cm, and 3) the unconventional configuration is more tolerant to ultraviolet radiation by nearly a factor of two in fluence, except for some materials at very low field stress and correspondingly high fluence.

4.4.3. Correlations

The critical fluence at high electric field stress (the constant portion of each of the curves in Figure 4.16) displays various degrees of correlation to the macroscopic and microscopic properties of the insulating materials. Neutral particle emission characteristics can be eliminated as a cause of ultraviolet induced insulator flashover at high field stress, since the fluence involved is too

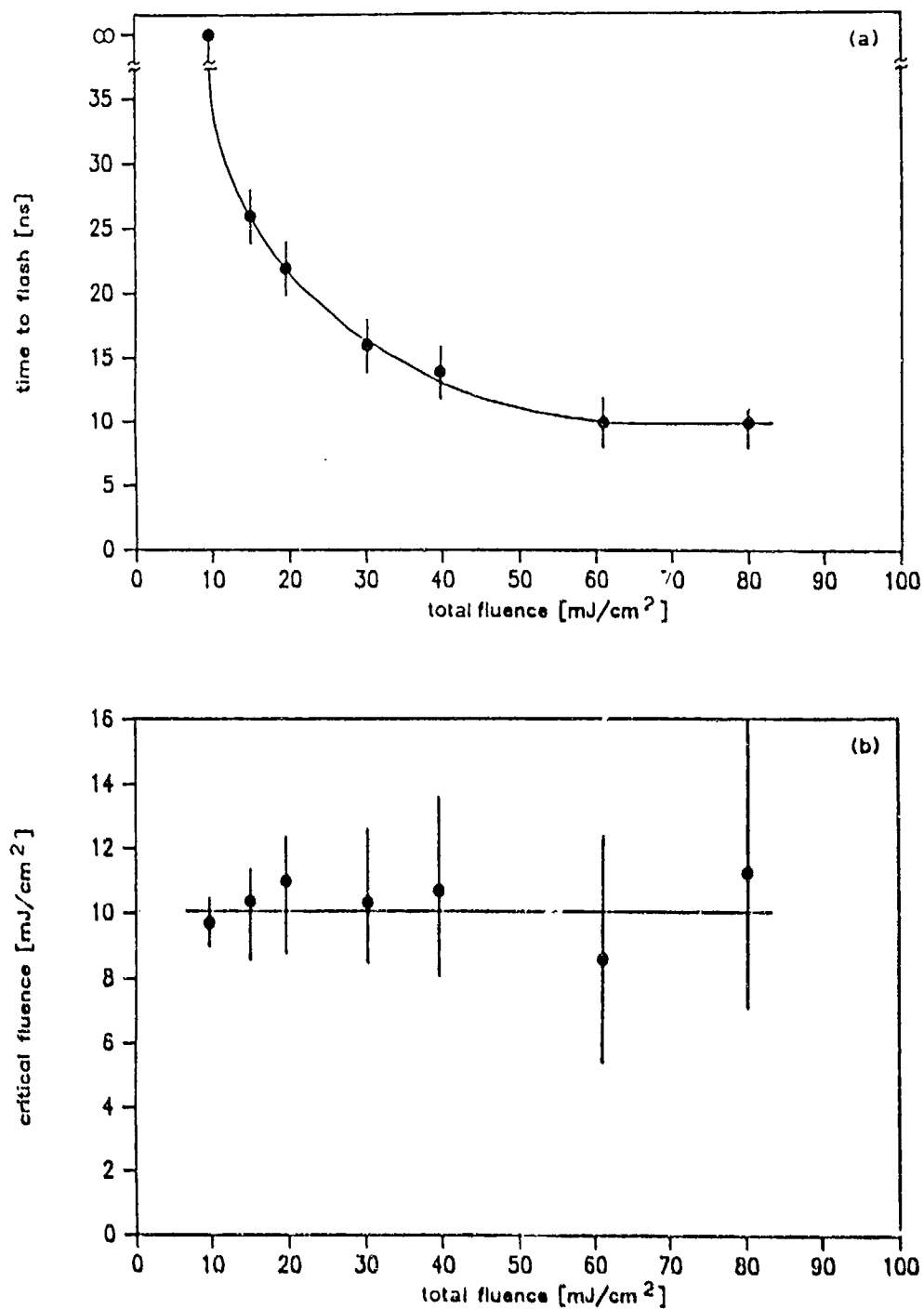


Figure 4.15. Typical insulator flashover behavior. a) Time to flash versus total fluence (laser pulse energy divided by illuminated area). b) Critical fluence (fluence at the time of flashover) versus total fluence.

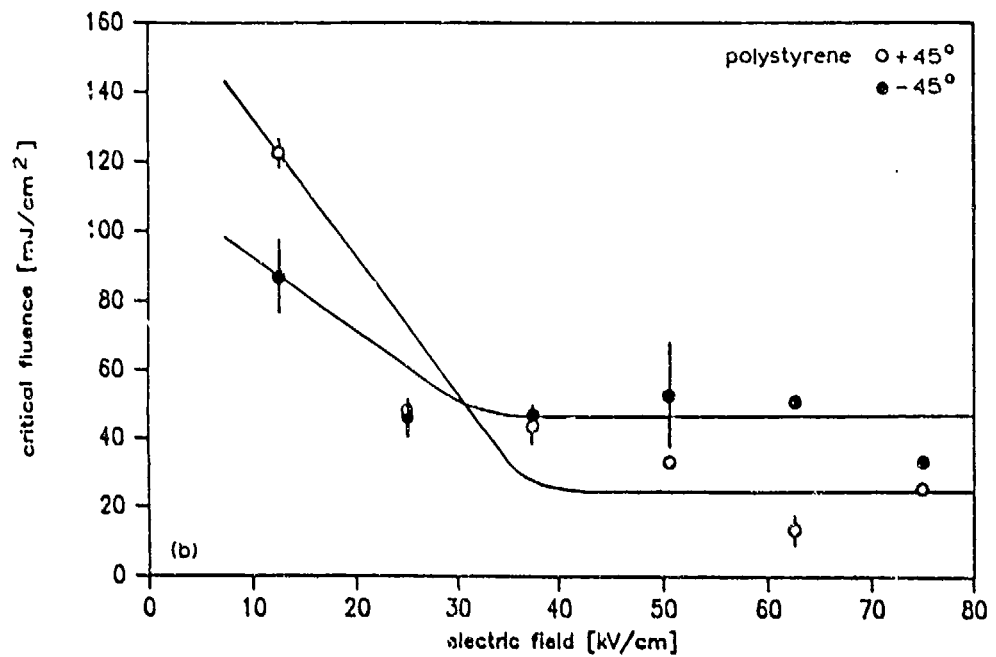
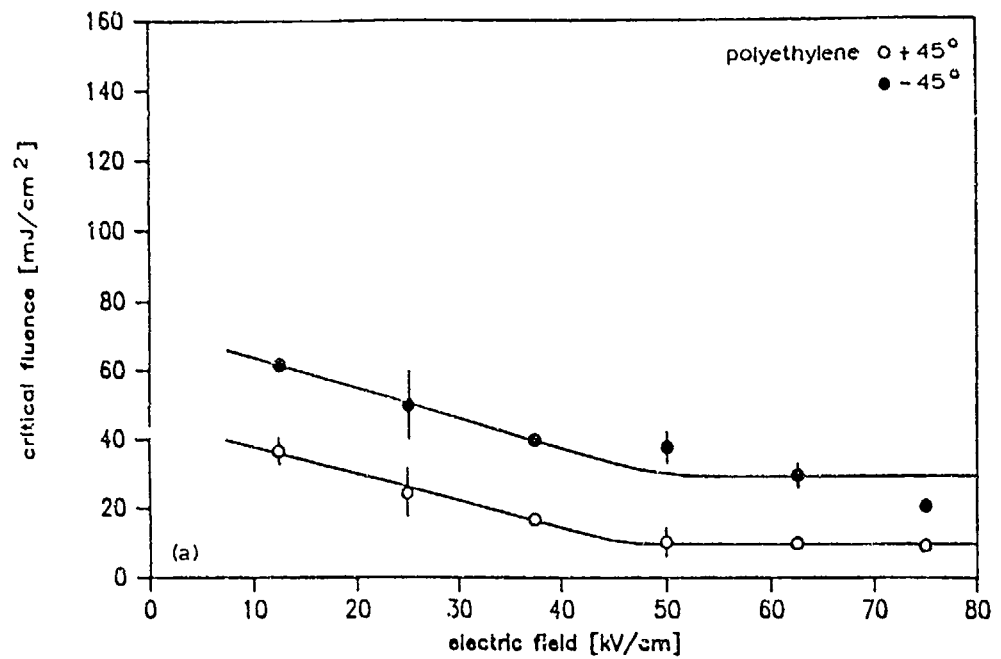


Figure 4.16. Critical fluence as a function of polarity and electric field stress for insulators angled at 45° . a) Polyethylene. b) Polystyrene. c) Acrylic. d) Nylon-6. e) Acetal. f) PVC. g) Teflon.

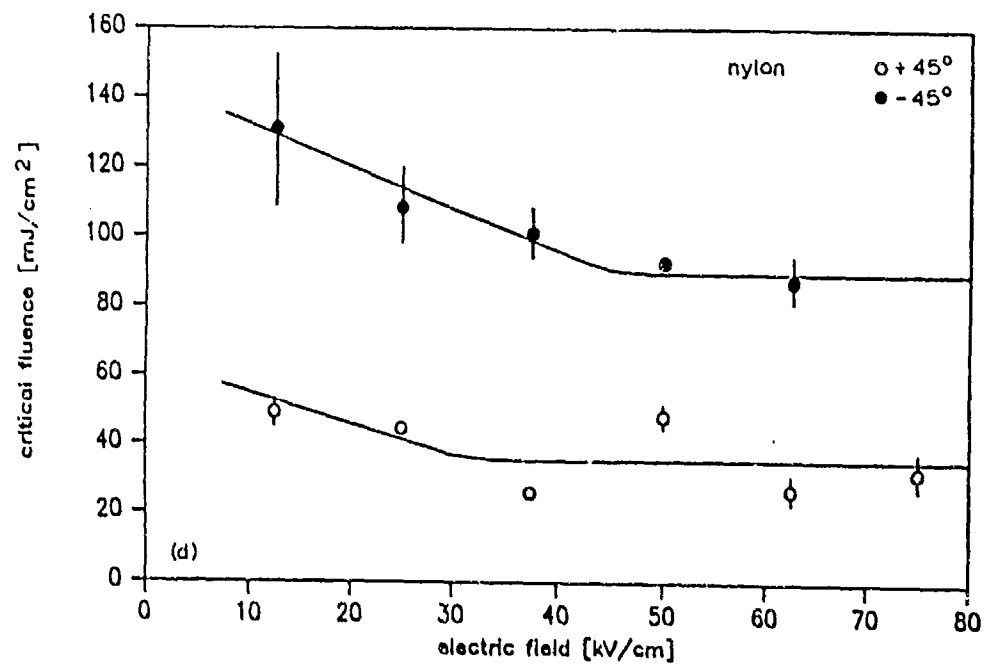
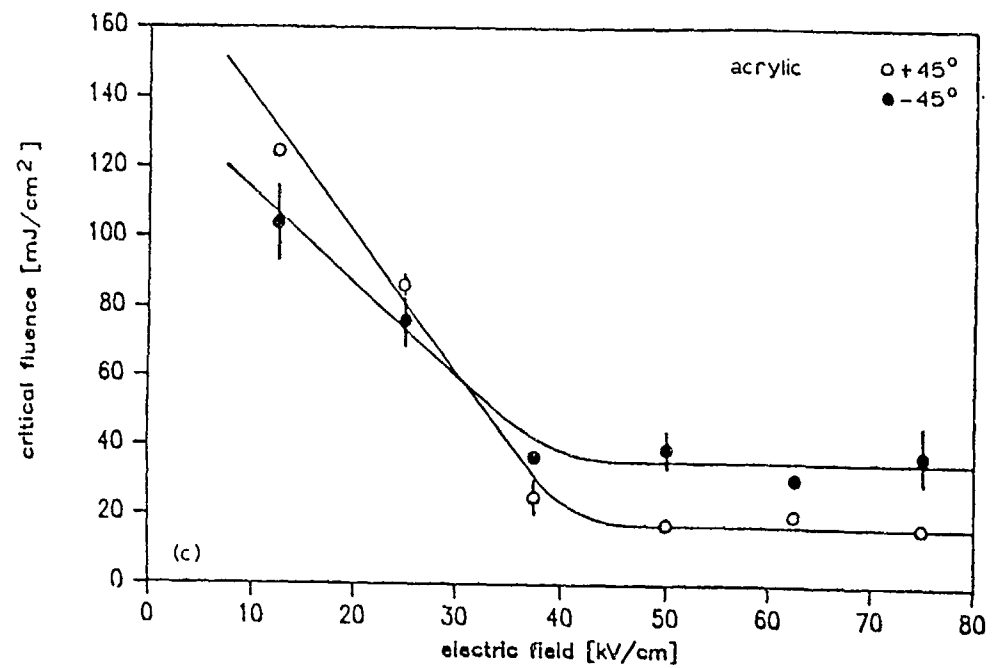


Figure 4.16. (continued).

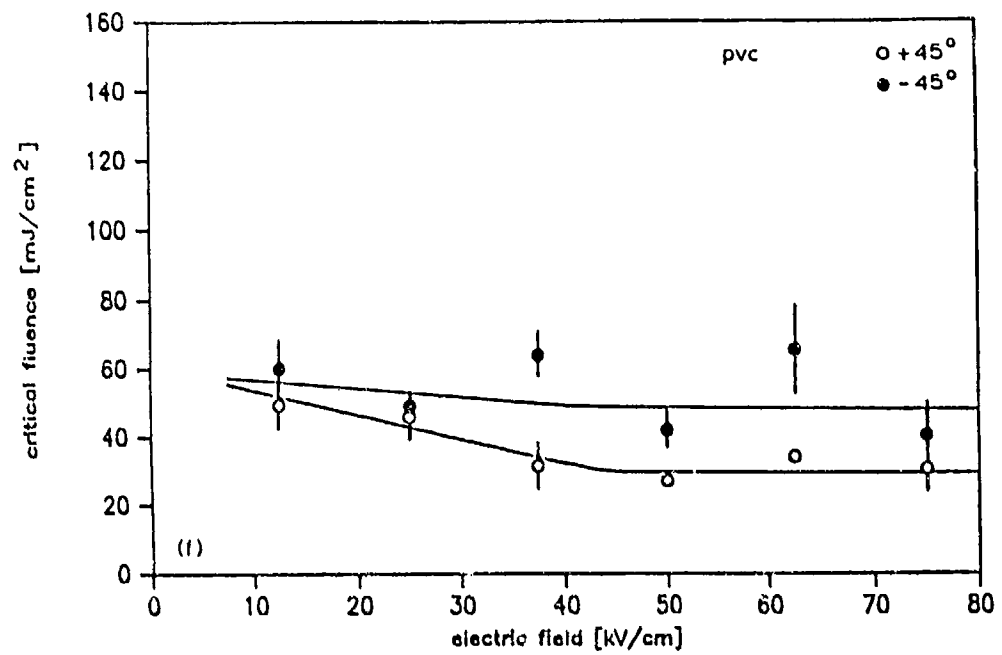
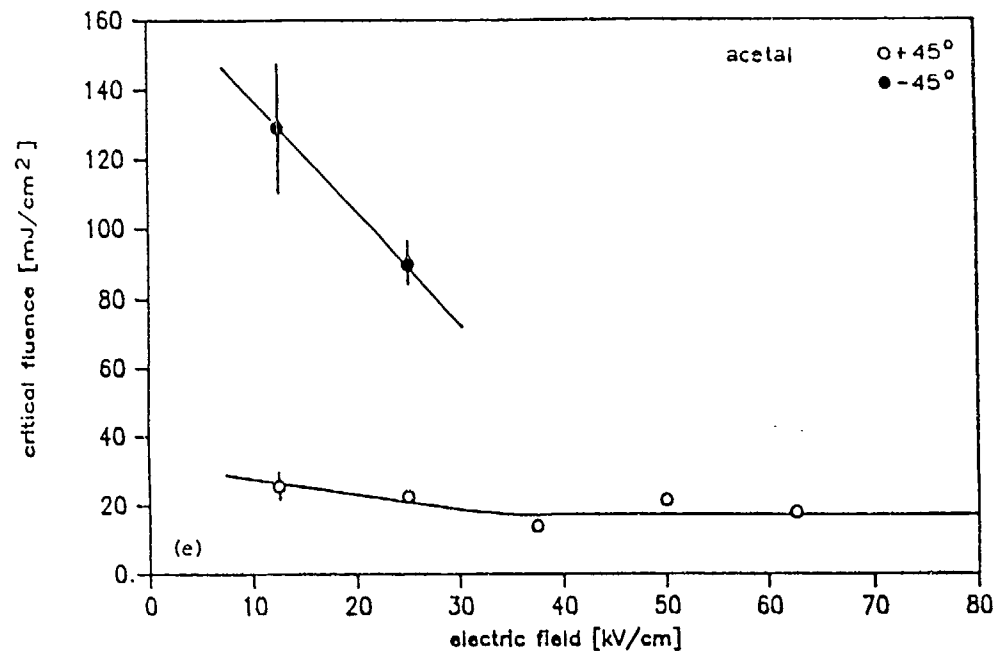


Figure 4.16. (continued).

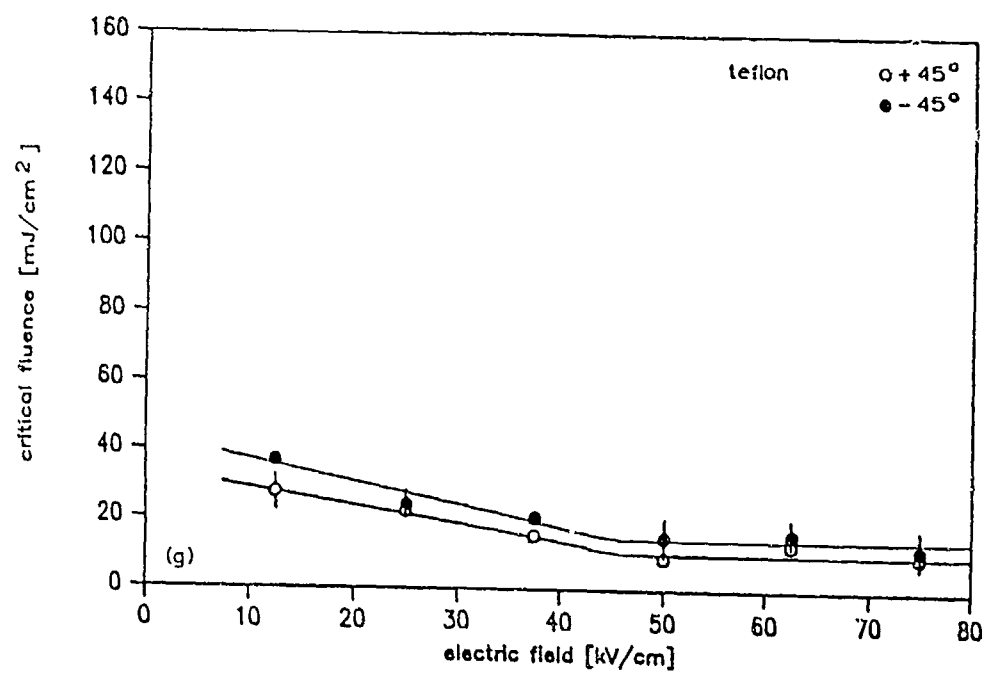


Figure 4.16. (continued).

low to produce significant neutral emission. Neutral emission may be a cause of the crossover in some of the curves in Figure 4.16 at high fluence.

The critical fluence is only weakly correlated to the electron photoemission, although to a slight degree the more readily a material emits photoelectrons, the less tolerant it is to ultraviolet radiation. The critical fluence exhibits a much greater correlation to secondary electron emission, as shown in Figure 4.17. Again, the more readily a material emits secondary electrons, the less tolerant it is to ultraviolet radiation. The critical fluence also shows a positive correlation to the dielectric constant of the material, as in Figure 4.18. The greater the dielectric constant, the more tolerant the material is to ultraviolet radiation. These correlations are summarized in Table 4.2. Overall, of the materials tested, nylon had the best performance (highest critical fluence in both polarities) because of its high dielectric constant and low secondary electron emission, whereas teflon had the worst performance because of its low dielectric constant and high secondary electron emission.

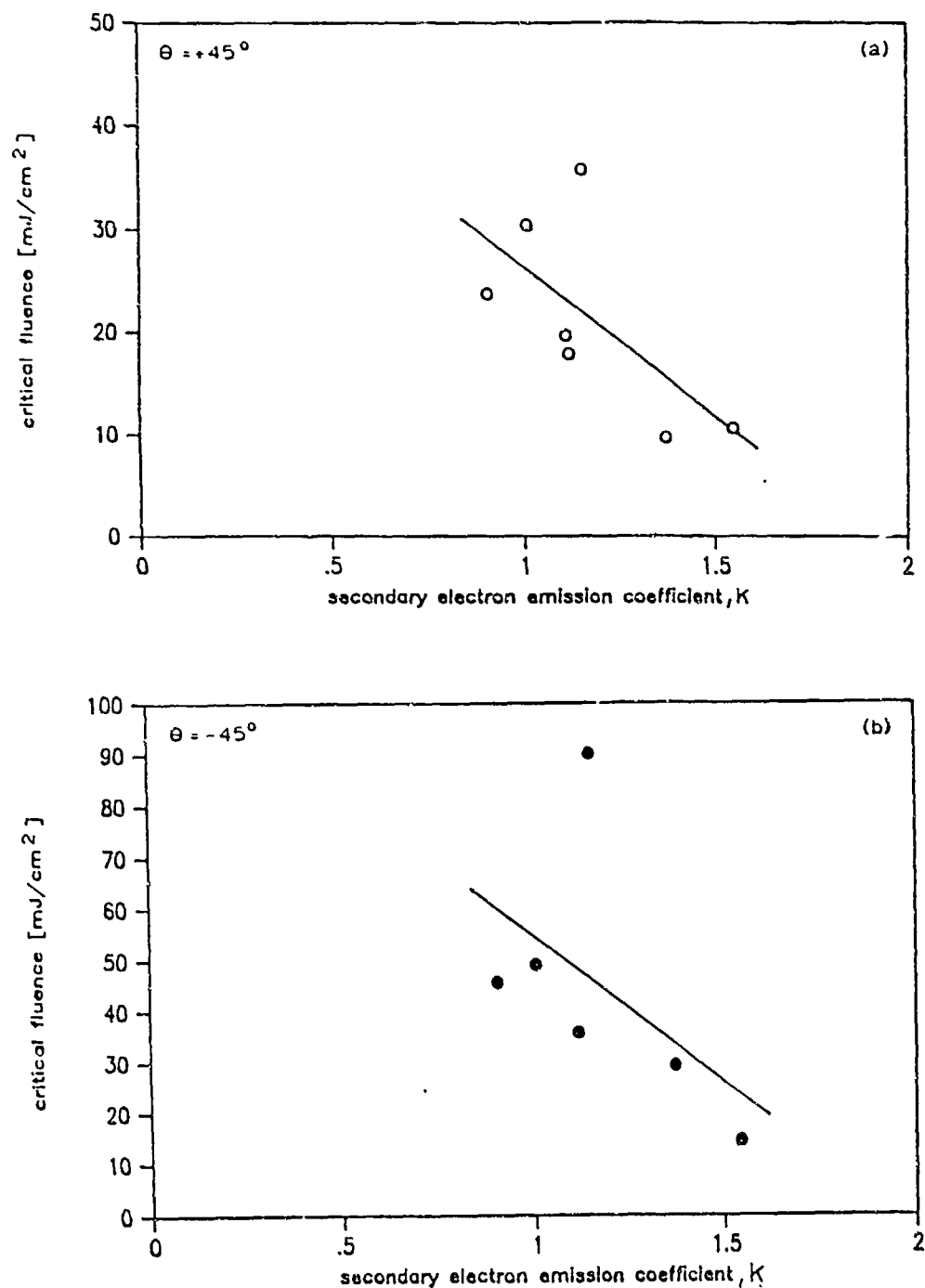


Figure 4.17. Critical fluence (for $E > 40$ kV/cm) versus secondary electron emission coefficient for the conventional (a) and the unconventional (b) configurations. Note the change in scale between the two graphs.

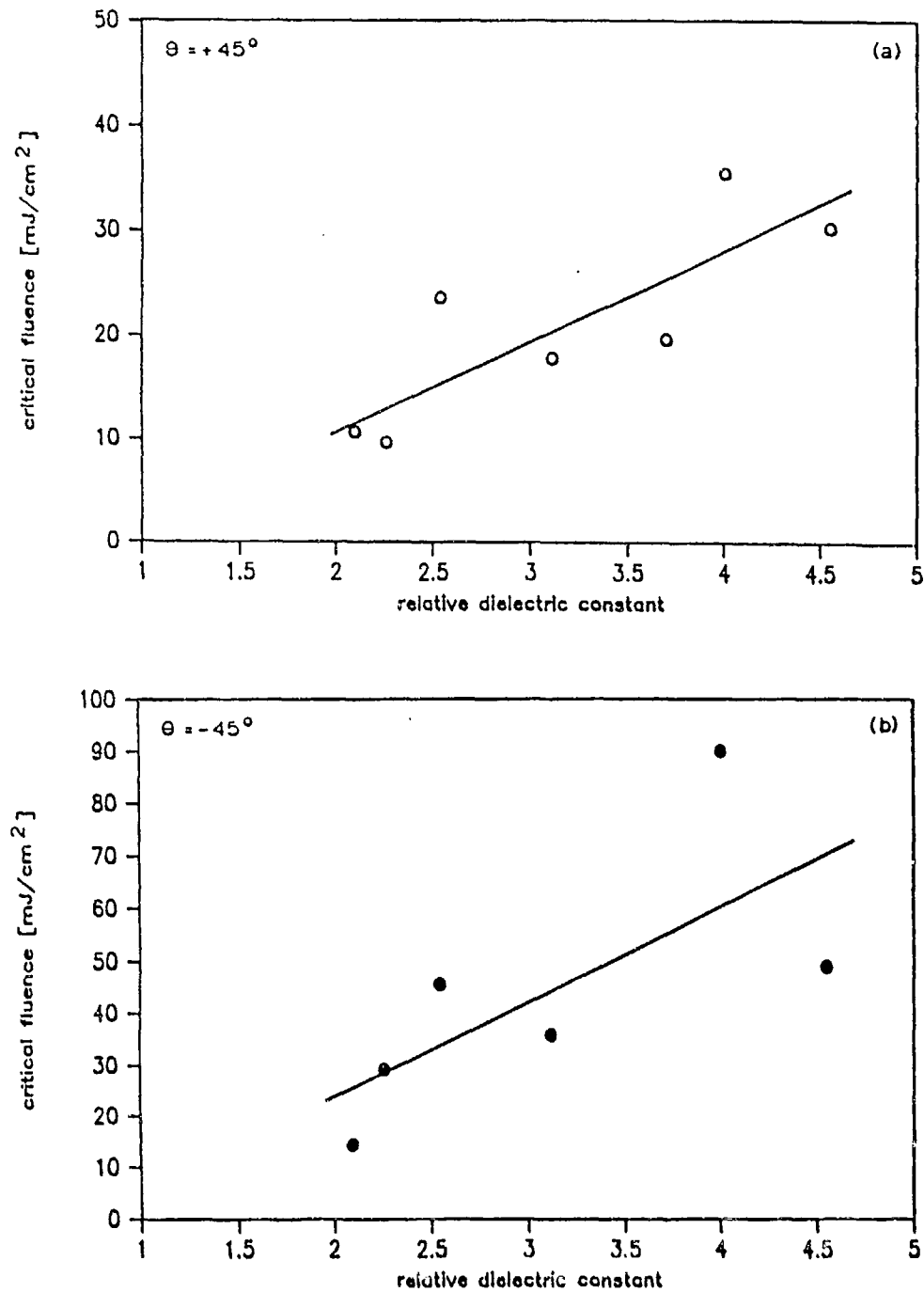


Figure 4.18. Critical fluence (for $E > 40 \text{ kV}/\text{cm}$) versus relative dielectric constant for the conventional (a) and the unconventional (b) configurations. Note the change in scale between the two graphs.

Table 4.2. Flashover Performance of Insulating Materials

Material	K	ϵ_r	$F_{c,+45^\circ}$ [mJ/cm ²]	$F_{c,-45^\circ}$ [mJ/cm ²]
polyethylene	1.37	2.36	9.6	29.3
polystyrene	0.907	2.55	23.7	45.7
acrylic	1.115	3.12	17.8	35.8
nylon-6	1.148	4.0	35.5	89.9
acetal	1.106	3.7	19.6
teflon	1.564	2.1	10.6	14.4
PVC	1.006	4.55	30.3	49.1

CHAPTER 5

THEORY OF INDUCED FLASHOVER

The observations and analysis of the phenomenon of ultraviolet-induced insulator flashover point to a particular mechanism of flashover initiation. To summarize the results, ultraviolet-induced flashover depends neither on the instantaneous value of the intensity of the ultraviolet illumination nor on the prebreakdown current, but rather on the time-integrated ultraviolet fluence on the insulator surface. The critical fluence required to initiate flashover is a function of the insulator material, and is less in the positive-angle (conventional) configuration than in the negative-angle (unconventional) configuration by approximately a factor of two. The critical fluence increases with increasing dielectric constant and decreases with increasing secondary (and to a slight degree, primary) electron emission.

The evidence indicates that the effect of the ultraviolet illumination is to prepare the dielectric/vacuum interface by causing the buildup of surface charge, making it more susceptible to flashover than the unilluminated, uncharged state. The flashover event itself is quite distinct from the prebreakdown phenomenon; the timescale of the former is on the order of 1 ns, while the timescale of the latter is tens of nanoseconds. If this disparity were due entirely to some formative time-lag, then one would expect to regularly see flashover occurring a significant time after the end of the illumination pulse. In fact, such events are rare. Also

consistent with this inference is the observation that fluence, independent of illumination intensity, is the quantity which determines flashover behavior.

The geometry-dependent behavior of the flashover strength of vacuum insulators without ultraviolet illumination has been reviewed, especially the data of Milton and Watson. [Wat67, Mil72] The theory of surface charging of vacuum insulators via secondary electron emission has also been reviewed. More recently, Brainard [Bra78] has analyzed Milton and Watson's data, and has determined that surface charging plays a significant role in the flashover process for $-30^\circ < \theta < 0^\circ$, but is negligible for $\theta = \pm 45^\circ$.

By a numerical solution to the Poisson equation (in this case, by applying the charge simulation technique outlined in Appendix A), it is straightforward to show that for an uncharged interface, the electric field is enhanced near the narrow end of the insulator, while if a sufficient surface charge is present, the electric field is enhanced near the wide end of the insulator. This effect is illustrated in Figure 5.1, with the critical angle taken to be $\theta_c = 30^\circ$. This value of the critical angle has been found to be typical for insulators. [Boe63, Bra78] The magnitude of the enhancement of the total and parallel electric fields are shown in Figures 5.2 and 5.3 respectively. Here ζ is the coordinate along the insulator surface from the narrow end to the wide end, while L is the length of the insulator interface. Although the gross effect is the same for the case of a conventionally-angled insulator which has acquired positive charge as for an unconventionally-angled insulator which acquires a negative charge, the situation is not entirely symmetrical. Applying the condition that $\theta_E = \theta_c$ everywhere on the insulator surface, with surface charge present, the field enhancement near the wide end is much greater for the conventional than for the unconventional

configuration. This is readily explained, since in the unconventional configuration, neglecting surface charge, the uncharged electric field angle is much nearer the critical angle.

If, however, surface charging is to occur via secondary electron emission, there must be a source of primary electrons. For $\theta \simeq 0^\circ$, the cathode triple point is a ready source of primary electrons. As Figure 5.4(a,c) shows, however, the cathode triple point is a poor source of primary electrons for large values of θ . For $\theta = +45^\circ$, electrons miss the insulator surface entirely. For $\theta = -45^\circ$, since $\delta < 1$ over the insulator surface and the path length along the insulator of the electron trajectories is small (a few μm), [Ber77] charging cannot propagate from the cathode triple point. It is not surprising, then, that insulators at large angles, whether positive or negative, do not charge under an applied electric field alone. [Bra78] Ultraviolet illumination, however, provides a source of electrons which is distributed over the insulator surface, as in Figure 5.4(b,d). Therefore, for insulators which are highly angled, it is possible for the electric field configuration in the interelectrode region to be significantly modified under ultraviolet illumination, due to charging of the insulator surface.

The magnitude of the surface charge required to significantly affect the interelectrode electric field varies with the dielectric constant of the insulating material. Figure 5.5 shows the dependence of the electric field angle θ_E on the surface charge density, as determined from a numerical solution to the Poisson equation (in this case, using the code LAPLACE [LAP86], described further in Appendix B). The results presented are for uniform positive surface charge on a positively-angled insulator; the results are analogous for negative surface charge on a negatively-angled insulator with the sign of θ_E reversed. The surface charge

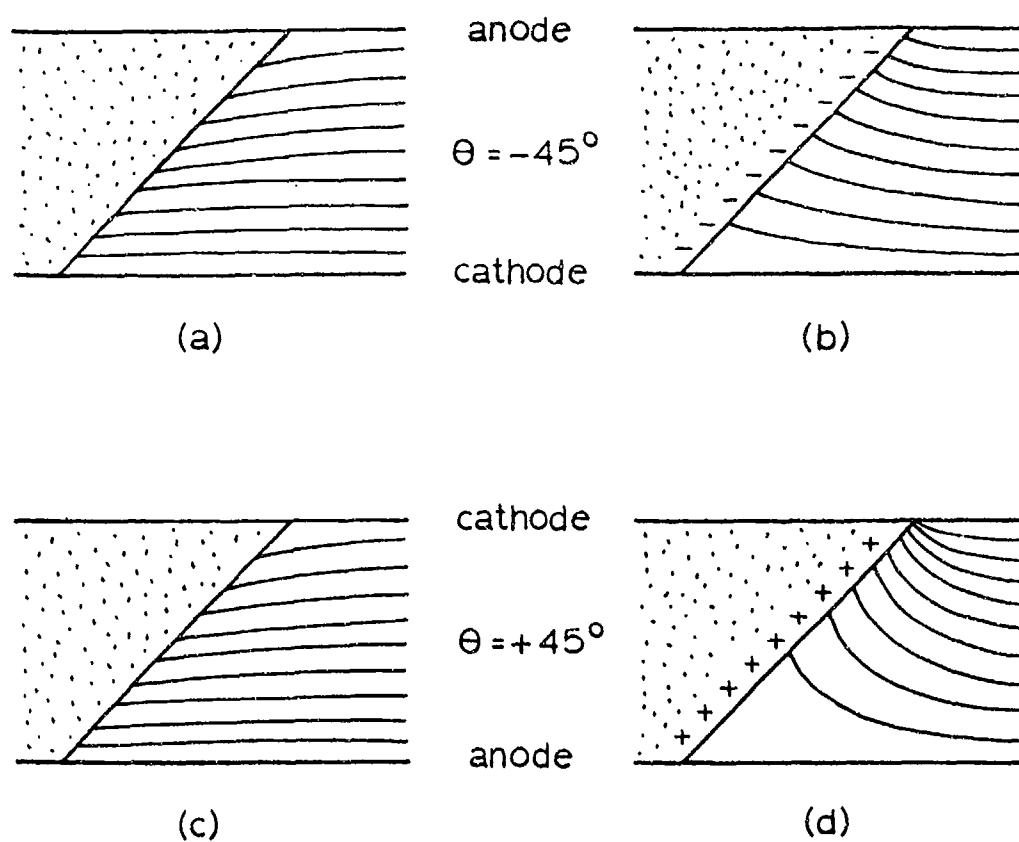


Figure 5.1. Equipotential contours near the interface of a dielectric and vacuum. a and c) Uncharged surface. b and d) Charged surface.

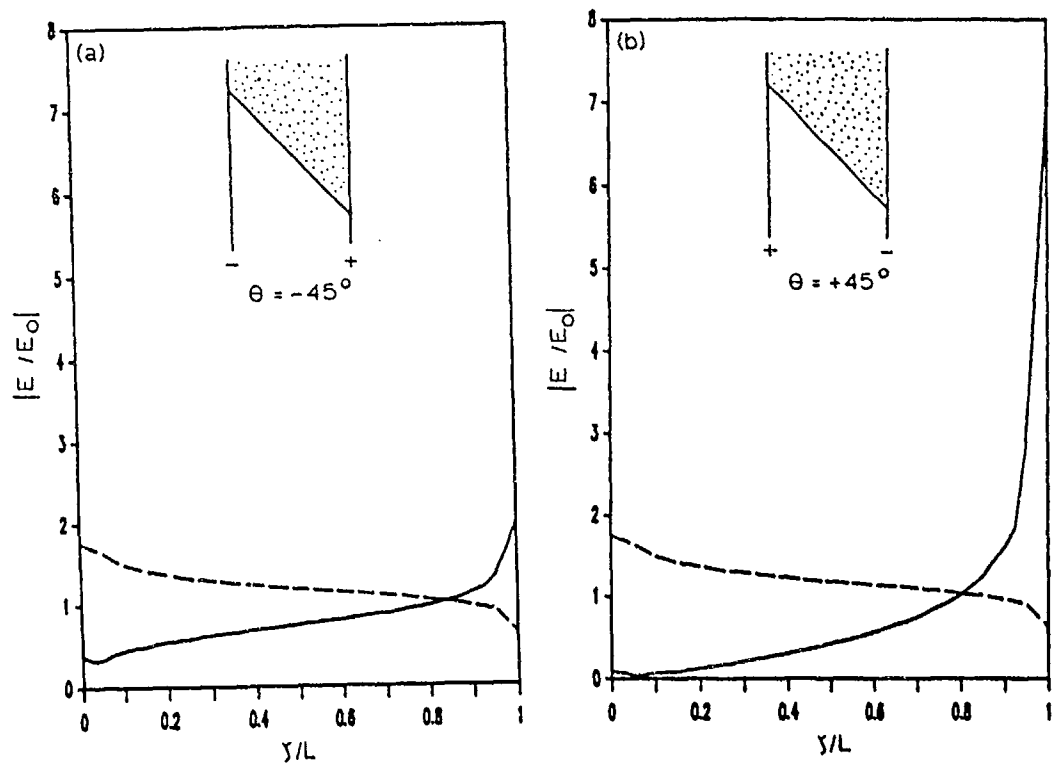


Figure 5.2. Total electric field enhancement versus position on the insulator surface. Solid line: charged. Broken line: uncharged.
 a) $\theta = -45^\circ$ (unconventional). b) $\theta = +45^\circ$ (conventional).

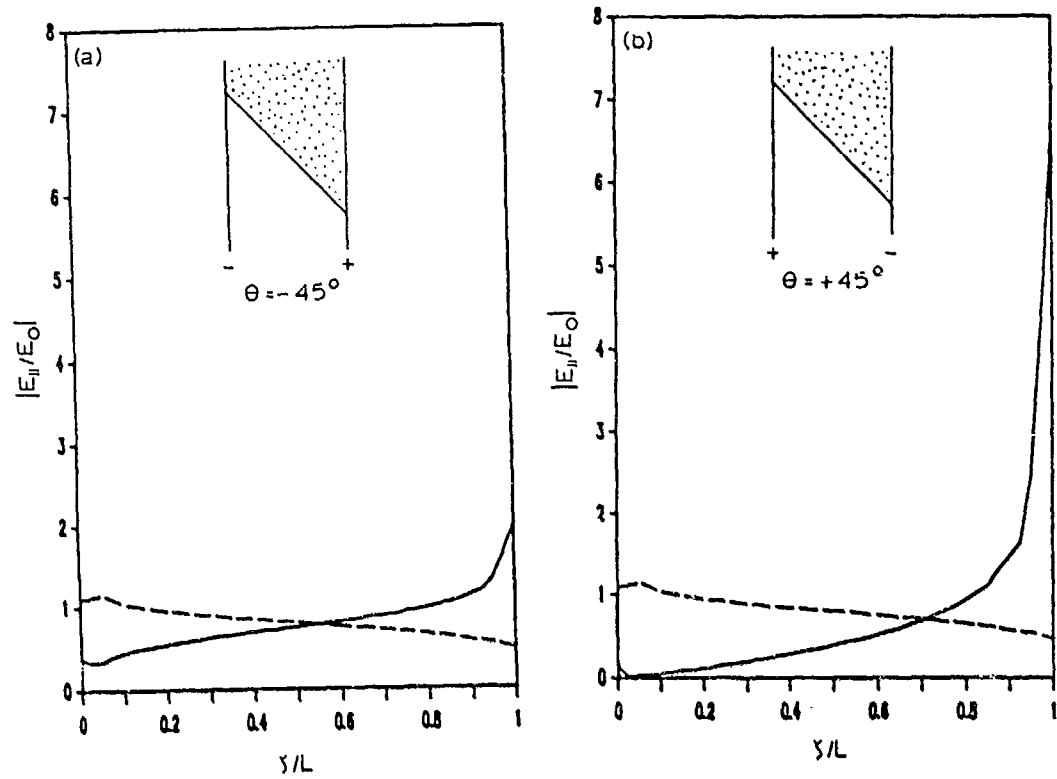


Figure 5.3. Parallel electric field enhancement versus position on the insulator surface. Solid line: charged. Broken line: uncharged. a) $\theta = -45^\circ$ (unconventional). b) $\theta = +45^\circ$ (conventional).

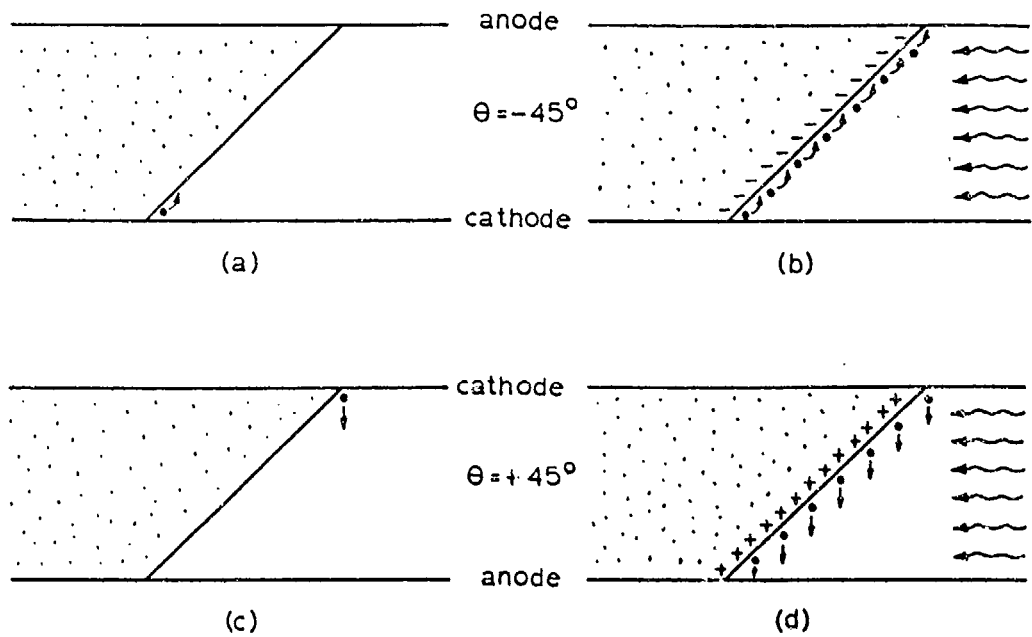


Figure 5.4. Surface charging mechanisms. At large insulator angles, field emission from the triple point (a and c) is an unlikely source of surface charging. Ultraviolet illumination (b and d) provides a source of primary electrons across the entire insulator surface

density is given in units of the charge density on the vacuum electrodes. Treating the vacuum electrodes as a capacitor, the surface charge Q on an area A of the electrode surface is just $Q = CV$, where C is the capacitance of the parallel plate electrodes and V is the applied voltage. Now, $C = \epsilon_0 A/L$, where L is the interelectrode distance. The surface charge density on the vacuum electrodes is then $\sigma_0 = CV/A = \epsilon_0 E$ since $E = V/L$. From Figure 5.5, the surface charge density required to modify the electric field so that $\theta_E \simeq 0^\circ$ is proportional to the dielectric constant of the material, and is on the order of

$$|\sigma|_{\theta_E=0^\circ} = \epsilon_r \sigma_0 \quad (5.1)$$

The magnitude of surface charging of insulators prior to flashover may be estimated from prebreakdown current measurements. For the polymers under consideration, $2 < \epsilon_r < 5$. For $E = 50 \text{ kV/cm}$, $\sigma_0 = 4.4 \text{ nC/cm}^2$. Prebreakdown currents observed are on the order of 0.5 A for 60 ns , so that the charge transferred in the interelectrode gap is on the order of 30 nC . The illuminated surface area of the insulator is approximately 1.5 cm^2 , which corresponds to $\sigma = 20 \text{ nC/cm}^2$. Therefore, the condition implied by Equation (5.1) is readily satisfied under ultraviolet illumination.

The induced surface charging theory of ultraviolet-induced insulator flashover in vacuum is consistent with the observation that fluence is the critical quantity in determining when flashover occurs. Since the surface charge density required to modify the interelectrode field is proportional to ϵ_r , it explains the dependence of F_c on ϵ_r . Since charging proceeds by secondary electron emission, it explains the dependence of F_c on K . The explanation of the fact that the unconventional configuration is more tolerant than the conventional is twofold. As shown in Figures 5.1–5.3, if the insulator surface is charged, it is the

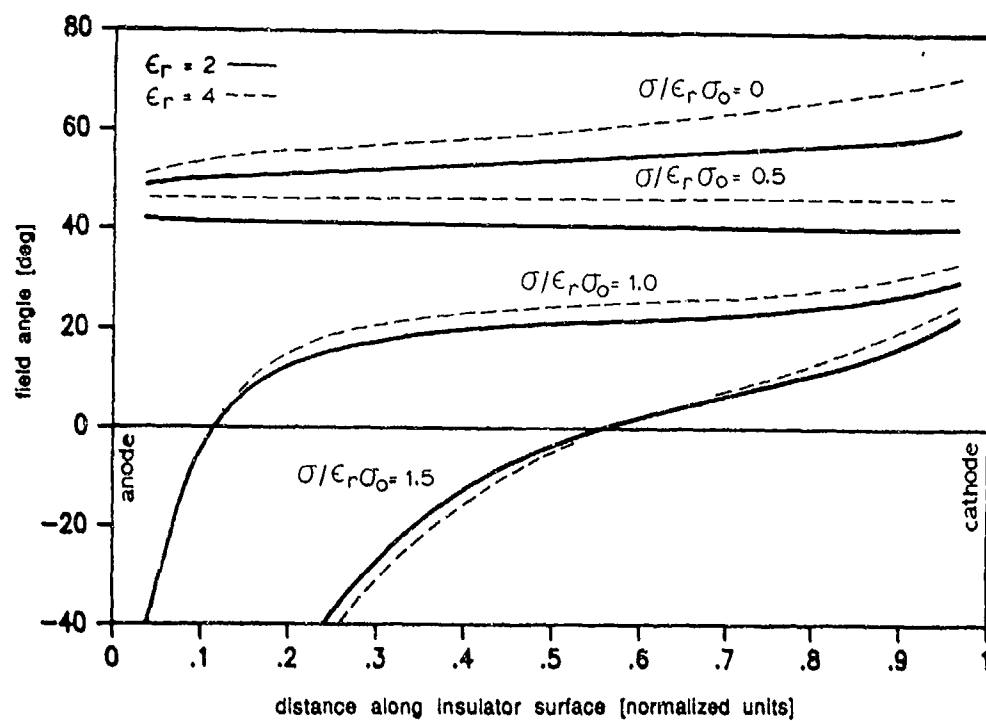


Figure 5.5. Angle of the electric field to the surface of the insulator versus magnitude of surface charge for $\epsilon_r = 2$ (solid line) and $\epsilon_r = 4$ (dashed line).

conventional configuration which is the weaker of the two configurations. Also, one may readily argue that the conventional configuration should be more readily charged than the unconventional. If a photoelectron is accelerated away from the surface of the insulator, as is the case for $\theta = +45^\circ$, it is straightforward to see that one elementary positive charge is left on the surface for every photoelectron. The efficiency of this charging mechanism is unity. However, if $\theta = -45^\circ$, electrons "hop" across the surface. For most insulators, $-45^\circ < \theta_c$, so that $\delta < 1$. The efficiency of this charging mechanism should be less than unity. The validity of this argument is borne out by the results shown in Figure 5.6, which indicate that for the same illumination, the prebreakdown current is greater for the conventional than for the unconventional configuration. The result of the surface acquiring a negative charge; namely, field enhancement at the wide end of the insulator, is also consistent with indications of explosive emission at that point from open shutter photographs of the induced flashover process.

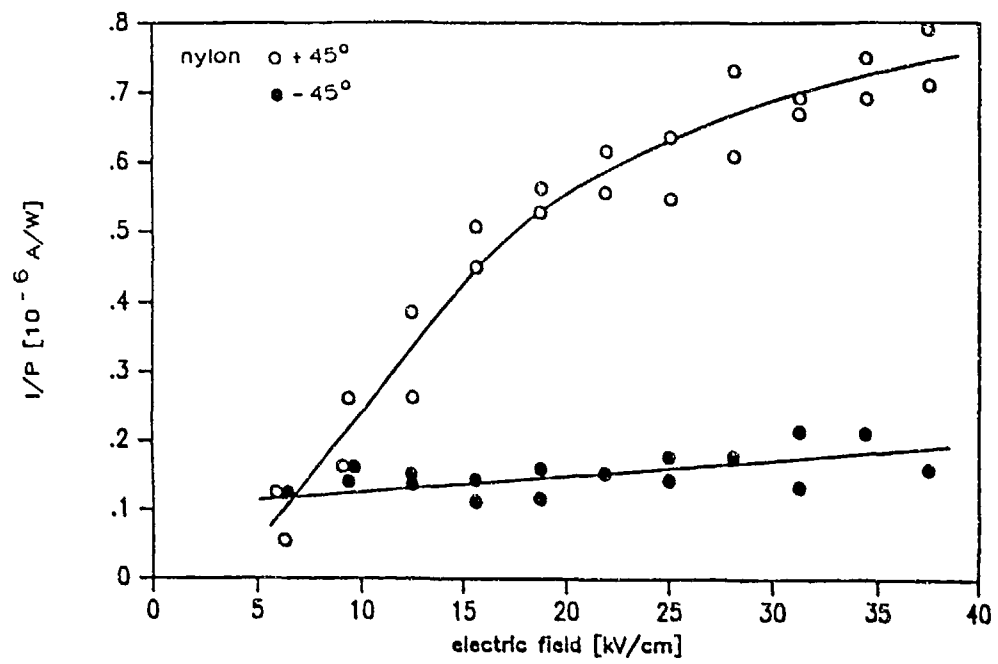


Figure 5.6. Peak prebreakdown current/peak laser power for conventional and unconventional configurations.

CHAPTER 6

CONCLUSIONS

Ultraviolet-induced flashover over polymeric insulators in vacuum depends on the ultraviolet fluence incident on the insulator surface. The negative-angle (unconventional) configuration exhibits superior ultraviolet tolerance compared to the positive-angle (conventional) configuration by approximately a factor of two in fluence. Insulating materials with high dielectric constants and low secondary electron emission coefficients exhibit superior ultraviolet tolerance. A model of ultraviolet-induced insulator flashover based on induced charging of the insulator surface is sufficient to explain the observed phenomena. The ultraviolet fluences required to initiate flashover are sufficiently low so that the contribution of neutral particles to the initiation of flashover may be disregarded, except perhaps at very low field stresses where the critical flashover fluences are correspondingly higher.

Insulating materials tested were polyethylene, polystyrene, acrylic, nylon-6, acetal, PVC, and teflon. Overall, of these materials nylon exhibited the best performance (that is, the highest critical fluence in both polarities) because of its high dielectric constant and low secondary electron emission, whereas teflon had the worst performance because of its low dielectric constant and high secondary electron emission.

It is important to note that this work was conducted using a single wavelength of ultraviolet light. Previous studies by this author, using a

broadband light source, found critical fluences which were much lower than those reported in this work. In those experiments, however, there was a significant component of ultraviolet with wavelengths shorter than the 248 nm KrF laser line. At these short wavelengths, the penetration depth of the ultraviolet in the material is a strong function of wavelength and decreases sharply as wavelength decreases. Therefore, shorter-wavelength ultraviolet should have a correspondingly larger effect on surface phenomena and induce flashover more readily. The previous measurements are therefore consistent with the data presented here.

APPENDICES

APPENDIX A

CHARGE SIMULATION TECHNIQUE

The charge simulation technique [Sin74] is one method which may be used to solve the Laplace and Poisson equations. Basically, it involves solving for the electric field inside a specified region as the superposition of the fields from a number of fictitious charges outside the boundary of that region. If the magnitude of these charges can be adjusted so that the total field on the boundaries of the region satisfies appropriate boundary conditions, then the total field inside the region is the desired solution.

For the two dimensional problem, the fictitious charges are line charges. The potential Φ at any point (x,y) due a charge of magnitude λ_i located at (x_i, y_i) is simply $\Phi = \lambda_i P_i$, where a form of P_i is the function [Sin74]

$$P_i(x,y) = K \ln \frac{\sqrt{(y+y_i)^2 + (x-x_i)^2}}{\sqrt{(y-y_i)^2 + (x-x_i)^2}} \quad (\text{A.1})$$

The constant K depends on the system of units which one is employing; for these calculations it is sufficient to set $K = 1$. Note that this particular form of P_i is invalid for $y_i = 0$. It follows from this form of P_i that the x - and y -components of the electric field are $E_x = \lambda_i X_i$ and $E_y = \lambda_i Y_i$, where [Sin74]

$$X_i(x,y) = K \left[\frac{(x-x_i)}{(y-y_i)^2 + (x-x_i)^2} - \frac{(x-x_i)}{(y+y_i)^2 + (x-x_i)^2} \right] \quad (\text{A.2})$$

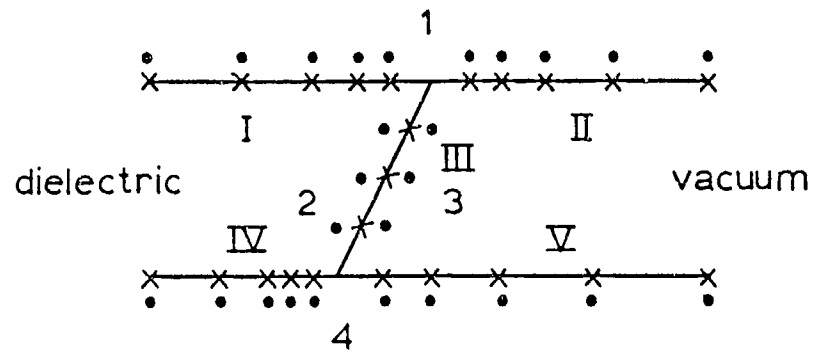
and

$$Y_i(x,y) = K \left[\frac{(y-y_i)}{(y-y_i)^2 + (x-x_i)^2} - \frac{(y+y_i)}{(y+y_i)^2 + (x-x_i)^2} \right] \quad (\text{A.3})$$

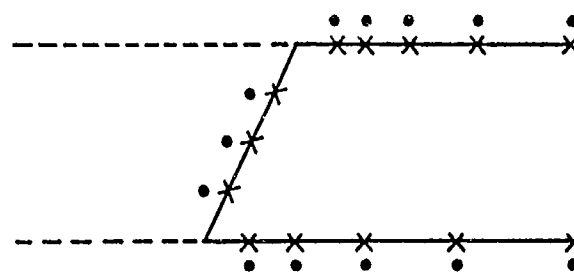
In order to solve for the magnitude of the fictitious charges, one selects a number of "contour points" on the boundaries, and for each contour point associates one fictitious charge for each boundary condition which must be satisfied at that point. A possible configuration for the problem of an insulator in vacuum between two electrodes is shown in Figure A.1. The boundary condition on the electrodes is that the potential be equal to a constant, so that there is one charge associated with each contour point on the electrode. There are two boundary conditions at the interface between the dielectric and the vacuum, however—the potential is continuous but the electric field is discontinuous, so that there are two charges associated with each contour point on the interface. Therefore, there are as many equations as there are unknown charges, so that a unique solution exists for the magnitudes of the charges. When the solution for each λ_i is obtained, then the potential and electric field at any point may be calculated by summing the contribution from each of the fictitious charges at that point.

One point should be noted—the charges contributing to the solution inside a particular region must themselves be outside that region. In Figure A.1(a), the charges are grouped into four groups (1-4). Groups 1 and 4 are exterior to the electrodes. Group 2 is exterior to the vacuum region, while group 3 is exterior to the dielectric. Similarly, the contour points are grouped into five groups (I-V) according to their positions. For example, the potential at a contour point (x,y) in group I is

$$\Phi = \sum_i \lambda_i P_i(x,y) \quad (\text{A.4})$$



(a)



(b)

Figure A.1. Contour point and fictitious charge placement for the solution to the problem of an insulator in vacuum via the charge simulation technique. Crosses are contour points, while points are line charges. a) For an uncharged insulator. b) For a charged insulator.

where i includes all of the charges in groups 1,3, and 4, which are exterior to the dielectric, but not group 2, which is interior to it.

The jump condition across the dielectric may be stated as [Sin74]

$$\begin{aligned}
 0 = & (\epsilon_r - 1) \sum_{\text{group 1}} \lambda_i N_i(x,y) \\
 & + (\epsilon_r - 1) \sum_{\text{group 2}} \lambda_i N_i(x,y) \\
 & + \epsilon_r \sum_{\text{group 3}} \lambda_i N_i(x,y) \\
 & - \sum_{\text{group 4}} \lambda_i N_i(x,y)
 \end{aligned} \tag{A.5}$$

where $N_i(x,y)$ generates the component of the electric field normal to the insulator surface. If the dielectric/vacuum interface is at an angle θ to the electrode normal, then

$$N_i(x,y) = X_i(x,y)\cos(\theta) - Y_i(x,y)\sin(\theta) \tag{A.6}$$

One advantage of the charge simulation technique is that it can readily account for the presence of non-uniform surface charge density, according to the requirement that the electric field be inclined at a particular critical angle θ_c to the surface of the insulator. This is accomplished by replacing the boundary condition expressed in Equation (A.5) with the condition that

$$\begin{aligned}
 0 = & \sum_{\text{groups 1,2,4}} \lambda_i Y_i(x,y) \\
 & - \tan(\theta^*) \sum_{\text{groups 1,2,4}} \lambda_i X_i(x,y)
 \end{aligned} \tag{A.7}$$

where $\theta^* = \theta \pm \theta_c$, depending on the polarity of the problem. One insight which falls out of this analysis is that the electric field configuration for a charged

insulator surface varies with δ , the secondary electron emission coefficient through θ_c , while in the uncharged configuration it varies with ϵ_r , the relative dielectric constant of the material.

Since the requirement that the electric field be inclined at the critical angle to the surface of the insulator applies to the vacuum side, it is redundant to calculate the field inside the dielectric, and much computing time can be saved by using the charge and contour point layout shown in Figure A.1(b) for the case of the charged insulator. The more contour points and charges are used, the more accurate the results. The equipotentials illustrated previously were calculated with 100 fictitious charges for the case of the uncharged insulator, and with 50 fictitious charges for the case of the charged insulator.

The source code for the programs used in these calculations, CHARGD, UNCHAR, and PLOTTER, follows. The code is written in Turbo Pascal 3.0 and may be run on the IBM PC or a compatible computer. Because of the large number of data points, the program UNCHAR cannot take advantage of the 8087 math coprocessor and is considerably slower than the program CHARGD. The program PLOTTER takes the output files generated by the other two programs and interpolates the equipotentials. The subroutines called by reference in the codes are those given by Press *et. al.* [Pre86]

Program CHARGD;

{ This program solves for the potential and electric field in the vicinity of a plane dielectric/vacuum interface between plane parallel electrodes, for the case of a charged insulator surface. The input parameter is the angle of the interface to the electrode normal. This angle may lie between -90 and $+90$ degrees. For ease of computation, the program places the narrow end of the insulator at the bottom electrode (which is by default at ground potential) and assigns the polarity of the upper electrode according to the convention that for positive angle, electrons are accelerated away from the insulator surface, while the opposite is true for negative

angles.

The program solves for the potentials and fields via the charge simulation technique (H. Singer, H. Steinbigler, and P. Weiss, IEEE Trans. Power Appar. Syst., vol. PAS-93, pp. 1660-1668 (1974)).

The program automatically places the contour points and unknown line charges, with increasing density near the triple points.

This program makes use of several subroutines taken from the book "Numerical Recipes" by W. H. Press, B. P. Flannery, S. A. Teukolsky, and W. T. Vetterling. (Cambridge: Cambridge University Press, 1986)

```
{ $U- }
{ $C- }
```

type

```
glyarray = array [1..256] of real;
gldarray = glyarray;
glnpbynp = array [1..50,1..50] of real;
glnarray = array [1..50] of real;
glindx = array [1..50] of integer;
```

var

```
filevar      : text;
input-filename : string[65];
output-filename : string[65];
{ Input and output file specifications }
A            : glnpbynp;
{ Matrix of the linear problem }
b            : glnarray;
{ Column vector of the linear problem }
indx        : glindx;
d            : real;
imax        : integer;
sum          : real;
dum          : real;
big          : real;
vv           : glnarray;
{ Required by procedure ludcmp }
ip           : integer;
ii           : integer;
{ Required by procedure lubksb }
n            : integer;
q            : glnarray;
qx           : glnarray;
qy           : glnarray;
{ Charge and position of the n simulated charges }
n1           : integer;
n2           : integer;
n3           : integer;
{ Number of charges in zones I through III }
m            : integer;
cx           : glnarray;
cy           : glnarray;
{ Position of the m contour points }
ma           : integer;
mb           : integer;
mc           : integer;
{ Number of contour points in zones 1 through 3 }
d1           : real;
d2           : real;
dchar        : char;
x            : glyarray;
y            : glyarray;
```

```

xx      : real;
yy      : real;
phixy   : real;
{Dummy variables}
i       : integer;
j       : integer;
k       : integer;
l       : integer;
{Indices}
E       : glyarray;
Ex      : glyarray;
Ey      : glyarray;
Eperp   : glyarray;
Epara   : glyarray;
{Electric field components along the insulator surface}
theta   : real;
{Angle of insulator}
thetaE   : real;
{Angle of electric field}
thetac   : real;
{Critical angle}
phi      : real;
{Potential of the top electrode}
phiu     : glyarray;
{Potential along the insulator surface}

{$! LUDCMP.PAS}
{$! LUBKSB.PAS}
{$! FOUR1.PAS}
{$! REALFT.PAS}
{$! SMOOFT.PAS}

function tan (x : real) : real;
begin
  tan := sin(x)/cos(x);
end;

function p (x,y : real; l : integer) : real;
{Potential at (x,y) due to the lth charge at (qx[l],qy[l])}
begin
  d1 := sqrt((y+qy[l])*(y+qy[l])+(x-qx[l])*(x-qx[l]));
  d2 := sqrt((y-qy[l])*(y-qy[l])+(x-qx[l])*(x-qx[l]));
  p := ln(d1/d2);
end;

function fx (x,y : real; l : integer) : real;
{Electric field along x at (x,y) due to the lth charge at (qx[l],qy[l])}
begin
  d1 := (x-qx[l])/((y-qy[l])*(y-qy[l])+(x-qx[l])*(x-qx[l]));
  d2 := (x-qx[l])/((y+qy[l])*(y+qy[l])+(x-qx[l])*(x-qx[l]));
  fx := (d1-d2);
end;

function fy (x,y : real; l : integer) : real;
{Electric field along y at (x,y) due to the lth charge at (qx[l],qy[l])}
begin
  d1 := (y-qy[l])/((y-qy[l])*(y-qy[l])+(x-qx[l])*(x-qx[l]));
  d2 := (y+qy[l])/((y+qy[l])*(y+qy[l])+(x-qx[l])*(x-qx[l]));
  fy := (d1-d2);
end;

procedure load-charged-negative-angle;
{Compute matrix elements corresponding to the condition that the electric
field be at the critical angle to the surface, for the case of a negative

```

```

insulator angle}
begin
  for i := ma+1 to ma+mb do
    begin
      clrscr;
      writeln ('Working on equation ',i,' (negative angle condition)');
      b[i] := 0;
      for j := 1 to n do
        begin
          A[i,j] := fx(cx[i],cy[i],j);
          A[i,j] := A[i,j] - tan(theta-thetac)*fy(cx[i],cy[i],j);
        end;
      end;
    end;
  end;

procedure load-charged-positive-angle;
{ Compute matrix elements corresponding to the condition that the electric
field be at the critical angle to the surface, for the case of a positive
insulator angle}
begin
  for i := ma+1 to ma+mb do
    begin
      clrscr;
      writeln ('Working on equation ',i,' (positive angle condition)');
      b[i] := 0;
      for j := 1 to n do
        begin
          A[i,j] := fx(cx[i],cy[i],j);
          A[i,j] := A[i,j] - tan(theta+thetac)*fy(cx[i],cy[i],j);
        end;
      end;
    end;
  end;

procedure load-matrix-elements;
{ Compute the elements of the matrix A, corresponding to n equations for the
n unknown line charges}
begin
  { Compute matrix elements corresponding to the condition that the
potential is a constant on the top electrode}
  for i := 1 to ma do
    begin
      clrscr;
      writeln ('Working on equation ',i,' (top electrode)');
      b[i] := phi;
      for j := 1 to n do
        A[i,j] := p(cx[i],cy[i],j);
      end;
    end;
  if (phi < 0)
  then
    load-charged-positive-angle
  else
    load-charged-negative-angle;
  for i := ma+mb+1 to ma+mb+mc do
    { Compute matrix elements corresponding to the condition that the
    potential is a constant on the bottom electrode}
    begin
      clrscr;
      writeln ('Working on equation ',i,' (bottom electrode)');
      b[i] := 0;
      for j := 1 to n do
        A[i,j] := p(cx[i],cy[i],j);
      end;
    end;
  end;
end;

```

```

procedure get-data-from-file;
{Load data from a file if something other than the default layout of
countour points and charges is desired}
begin
  clrscr;
  write ('Input data file. ');
  readln (input-filename);
  assign (filevar, input-filename);
  reset (filevar);
  readln (filevar, theta);
  if (theta > 0)
    then
      phi := -1
    else
      phi := 1;
  theta := abs(theta);
  theta := theta*(pi/180);
  readln (filevar, thetac);
  thetac := thetac*(pi/180);
  readln (filevar, ma, mb, mc, m);
  for i := 1 to m do
    readln (filevar, cx[i], cy[i]);
  readln (filevar, n1, n2, n3, n);
  for i := 1 to n do
    readln (filevar, qx[i], qy[i]);
  readln (output-filename);
  close (filevar);
end;

procedure generate-mesh;
{Lay out contour points and unknown line charges along the electrodes and
the surface of the insulator}
begin
  clrscr;
  write ('Angle of insulator (in degrees): ');
  readln (theta);
  {Determine the value of the potential on the top electrode according
to the convention of the angle of the insulator}
  if (theta > 0)
    then
      phi := -1
    else
      phi := 1;
  theta := abs(theta);
  theta := theta*(pi/180);
  write ('Critical angle (in degrees): ');
  readln (thetac);
  thetac := thetac*(pi/180);
  write ('Output file name: ');
  readln (output-filename);
  {Begin placing contour points}
  ma := 15;
  mb := 20;
  mc := 15;
  m := 50;
  {Place contour points along the top electrode}
  d1 := (2-(sin(theta)/cos(theta)));
  for i := 1 to 15 do
    begin
      cx[i] := 2-d1*(1-exp(-((i-1)/3.26)));
      cy[i] := 1;
    end;
  {Place contour points along the insulator surface}
  d1 := 1/40;

```

```

for i := 16 to 35 do
  begin
    cy[i] := d1+2*d1*(i-16);
    cx[i] := cy[i]*(sin(theta)/cos(theta));
  end;
{ Place contour points along the bottom electrode}
d1 := 2;
for i := 36 to 50 do
  begin
    cx[i] := 2-d1*(1-exp(-((i-36)/3.26)));
    cy[i] := 0;
  end;
{ End placing contour points}
{ Begin placing unknown charges}
n1 := 15;
n2 := 20;
n3 := 15;
n := 50;
{ Place unknown charges slightly above the top electrode}
for i := 1 to 15 do
  begin
    qx[i] := cx[i];
    qy[i] := cy[i]+0.025;
  end;
{ Place unknown charges slightly inside the insulator}
for i := 16 to 35 do
  begin
    qx[i] := cx[i]-0.025*cos(theta);
    qy[i] := cy[i]+0.025*sin(theta);
  end;
{ Place unknown charges slightly below the bottom electrode}
for i := 36 to 50 do
  begin
    qx[i] := cx[i];
    qy[i] := cy[i]-0.025;
  end;
{ End placing charges}
{ Shift the entire grid upward by 1.0 to avoid singularities}
for i := 1 to m do
  begin
    cy[i] := cy[i]+1;
  end;
for i := 1 to n do
  begin
    qy[i] := qy[i]+1;
  end;
end;

procedure input-data;
{ User interface}
begin
  clrscr;
  write ('Input from file or keyboard [F/K]: ');
  read (kbd, dchar);
  if (dchar = 'F') or (dchar = 'f')
  then
    get-data-from-file
  else
    if (dchar = 'K') or (dchar = 'k')
    then
      generate-mesh
    else
      input-data;
end;

```

```

procedure move;
begin
  for i := 1 to n do
    q[i] := b[i];
end;

procedure solve-for-field-quantities;
{ Calculate the field quantities along the insulator surface }
begin
  clrscr;
  writeln ('Back-substituting');
  assign (filevar, output-filename);
  rewrite (filevar);
  writeln (filevar, 'Potential and field along the surface of an insulator');
  writeln (filevar);
  writeln (filevar, 'This information from file: ', output-filename);
  writeln (filevar, 'Insulator angle in degrees: ', (theta*(180/pi)):4:1);
  if (phi < 0)
  then
    begin
      begin
        writeln (filevar, 'Polarity: conventional (positive)');
      end
    end
  else
    begin
      writeln (filevar, 'Polarity: unconventional (negative)');
    end;
  writeln (filevar, 'Potential on the lower electrode: ground');
  writeln (filevar, 'Potential on the upper electrode: ', phi:3:1);
  writeln (filevar);
  for i := 1 to 41 do
    begin
      y[i] := 1+0.025*(i-1);
      x[i] := (y[i]-1)*tan(theta);
      phiu[i] := 0;
      for j := 1 to n do
        phiu[i] := phiu[i] + q[j]*p(x[i],y[i],j);
      ex[i] := 0;
      for j := 1 to n do
        ex[i] := ex[i] + q[j]*fx(x[i],y[i],j);
      ey[i] := 0;
      for j := 1 to n do
        ey[i] := ey[i] + q[j]*fy(x[i],y[i],j);
      e[i] := sqrt(ex[i]*ex[i] + ey[i]*ey[i]);
      eperp[i] := ex[i]*cos(theta)-ey[i]*sin(theta);
      epara[i] := ex[i]*sin(theta)+ey[i]*cos(theta);
    end;
  writeln (filevar);
  writeln (filevar, 'Raw data:');
  writeln (filevar);
  write (filevar, '...zeta... ..phi... ..Ex... ..Ey... ');
  writeln (filevar, '....E.... .E.perp.. .E.para..');
  for i := 1 to 41 do
    begin
      write (filevar, y[i]-1:9:2, ' ', phiu[i]:9:2, ' ', ex[i]:9:2, ' ', ey[i]:9:2, ' ');
      writeln (filevar, e[i]:9:2, ' ', eperp[i]:9:2, ' ', epara[i]:9:2);
    end;
  clrscr;
  { Smooth data }
  writeln ('Smoothing Phi');
  smooft (phiu,41,3);
  clrscr;
  writeln ('Smoothing Ex');
  smooft (ex,41,3);

```

```

clrscr;
writeln ('Smoothing Ey');
smooft (ey,41,3);
clrscr;
writeln ('Smoothing E');
smooft (e,41,3);
clrscr;
writeln ('Smoothing E perp');
smooft (eperp,41,3);
clrscr;
writeln ('Smoothing E para');
smooft (epara,41,3);
writeln (filevar);
writeln (filevar, 'Smoothed data:');
writeln (filevar);
write (filevar, '...zeta... ..phi... ..E.x... ..E.y... ');
writeln (filevar, '...E.... .E.perp... .E.para..');
for i := 1 to 41 do
begin
write (filevar, y[i]-1:9:2, ' ', phi[i]:9:2, ' ', ex[i]:9:2, ' ', ey[i]:9:2, ' ');
writeln (filevar, e[i]:9:2, ' ', eperp[i]:9:2, ' ', epara[i]:9:2);
end;
writeln (filevar);
writeln (filevar, '*');
writeln (filevar, theta:9:4);
clrscr;
{ Compute potentials on a rectilinear grid for later manipulation}
writeln ('Computing equipotentials');
for i := 0 to 20 do
begin
for j := 0 to 10 do
begin
xx := 0.1*i;
yy := 1 + 0.1*j;
phixy := 0;
for k := 1 to n do
phixy := phixy + q[k]*p(xx,yy,k);
writeln (filevar, xx:9:4, ' ', yy-1:9:4, ' ', phixy:9:4);
end;
end;
close (filevar);
end;

procedure beep;
{ Make a sound when the computation is complete}
begin
clrscr;
writeln ('Done');
sound(880);
delay(125);
nosound;
delay(25);
sound(880);
delay(125);
nosound;
end;

begin
{ Main program}
input-data;
load-matrix-elements;
ludcmp(A,50,50,indx,d);
lubksb(A,50,50,indx,b);
move;

```

```

solve-for-field-quantities;
beep;
end.

```

Program UNCHAR;

{ This program solves for the potential and electric field in the vicinity of a plane dielectric/vacuum interface between plane parallel electrodes, for the case of an uncharged insulator surface. The input parameters are the relative dielectric constant of the insulating material and the angle of the interface to the electrode normal. This angle may lie between -90 and $+90$ degrees. For ease of computation, the program places the narrow end of the insulator at the bottom electrode (which is by default at ground potential) and assigns the polarity of the upper electrode according to the convention that for positive angle, electrons are accelerated away from the insulator surface, while the opposite is true for negative angles.

The program solves for the potentials and fields via the charge simulation technique (H. Singer, H. Steinbigler, and P. Weiss, IEEE Trans. Power Appar. Syst., vol. PAS-93, pp. 1660-1668 (1974)). The program automatically places the contour points and unknown line charges, with increasing density near the triple points.

This program makes use of several subroutines taken from the book "Numerical Recipes" by W. H. Press, B. P. Flannery, S. A. Teukolsky, and W. T. Vetterling. (Cambridge: Cambridge University Press, 1986)

```

{$U-}
{$R-}

```

```

type
    glnpbypn = array [1..100,1..100] of real;
    glnarray = array [1..100] of real;
    glindx = array [1..100] of integer;
var
    filevar : text;
    input-filename : string[65];
    output-filename : string[65];
    { Input and output file specifications}
    A : glnpbypn;
    { Matrix of the linear problem}
    b : glnarray;
    { Column vector of the linear problem}
    indx : glindx;
    d : real;
    imax : integer;
    sum : real;
    dum : real;
    big : real;
    vv : glnarray;
    { Required by procedure ludcmp}
    ip : integer;
    ii : integer;
    { Required by procedure lubksb}
    n : integer;
    q : glnarray;
    qx : glnarray;
    qy : glnarray;
    { Charge and position of the n simulated charges}
    n1 : integer;

```

```

n2      : integer;
n3      : integer;
n4      : integer;
{ Number of charges in zones I through IV}
m       : integer;
cx      : glnarray;
cy      : glnarray;
{ Position of the m contour points}
ma      : integer;
mb      : integer;
mc      : integer;
md      : integer;
me      : integer;
{ Number of contour points in zones A through E}
d1      : real;
d2      : real;
dchar   : char;
x       : real;
y       : real;
{ Dummy variables}
i       : integer;
j       : integer;
k       : integer;
l       : integer;
{ Index variables}
E       : real;
Ex      : real;
Ey      : real;
Eperp   : real;
Epara   : real;
{ Electric field components along the insulator surface}
epsirel : real;
{ Relative dielectric constant of insulator}
theta   : real;
{ Angle of insulator}
thetaE  : real;
{ Angle of electric field}
phi     : real;
{ Potential on the top electrode}
phiu    : real;
{ Potential along the insulator surface}

{$! LUDCMP.PAS}
{$! LUBKSB.PAS}

function tan (x : real) : real;
begin
  tan := sin(x)/cos(x);
end;

function p (x,y : real; l: integer) : real;
{ Potential at (x,y) due to the lth charge at (qx[l],qy[l])}
begin
  d1 := sqrt((y+qy[l])*(y+qy[l])+(x-qx[l])*(x-qx[l]));
  d2 := sqrt((y-qy[l])*(y-qy[l])+(x-qx[l])*(x-qx[l]));
  p := ln(d1/d2);
end;

function fx (x,y : real; l : integer) : real;
{ Electric field along x at (x,y) due to the lth charge at (qx[l],qy[l])}
begin
  d1 := (x-qx[l])/((y-qy[l])*(y-qy[l])+(x-qx[l])*(x-qx[l]));
  d2 := (x-qx[l])/((y+qy[l])*(y+qy[l])+(x-qx[l])*(x-qx[l]));
  fx := (d1-d2);

```

end;

```
function fy (x,y : real; l : integer) : real;
{ Electric field along y at (x,y) due to the lth charge at (qx[l],qy[l]) }
begin
  d1 := (y-qy[l])/((y-qy[l])*(y-qy[l])+(x-qx[l])*(x-qx[l]));
  d2 := (y+qy[l])/((y+qy[l])*(y+qy[l])+(x-qx[l])*(x-qx[l]));
  fy := (d1-d2);
end;
```

```
function fn (x,y : real; l : integer) : real;
{ Normal electric field at (x,y) due to the lth charge at (qx[l],qy[l]) }
begin
  fn := fx(x,y,l)*cos(theta)-fy(x,y,l)*sin(theta);
end;
```

```
procedure load-matrix-elements;
{ Compute the elements of the matrix A, corresponding to n equations for the
n unknown line charges }
begin
```

```
  { Compute matrix elements according to the condition that the
  potential is a constant on the top electrode }
  for i := 1 to ma do
```

```
    begin
      clrscr;
      writeln ('Working on equation ',i,' (top electrode)');
      b[i] := phi;
      for j := 1 to n1 do
        A[i,j] := p(cx[i],cy[i,j]);
      for j := n1+1 to n1+n2 do
        A[i,j] := 0;
      for j := n1+n2+1 to n1+n2+n3 do
        A[i,j] := p(cx[i],cy[i,j]);
      for j := n1+n2+n3+1 to n1+n2+n3+n4 do
        A[i,j] := p(cx[i],cy[i,j]);
    end;
```

```
  { Compute matrix elements according to the condition that the
  potential is a constant on the top electrode }
  for i := ma+1 to ma+mb do
```

```
    begin
      clrscr;
      writeln ('Working on equation ',i,' (top electrode)');
      b[i] := phi;
      for j := 1 to n1 do
        A[i,j] := p(cx[i],cy[i,j]);
      for j := n1+1 to n1+n2 do
        A[i,j] := p(cx[i],cy[i,j]);
      for j := n1+n2+1 to n1+n2+n3 do
        A[i,j] := 0;
      for j := n1+n2+n3+1 to n1+n2+n3+n4 do
        A[i,j] := p(cx[i],cy[i,j]);
    end;
```

```
  { Compute matrix elements according to the condition that the
  potential continuous across the insulator surface }
  for i := ma+mb+1 to ma+mb+mc do
```

```
    begin
      clrscr;
      writeln ('Working on equation ',i,' (insulator)');
      b[i] := 0;
      for j := 1 to n1 do
        A[i,j] := 0;
      for j := n1+1 to n1+n2 do
        A[i,j] := -p(cx[i],cy[i,j]);
      for j := n1+n2+1 to n1+n2+n3 do
```

```

        A[i,j] := p(cx[i],cy[i]j);
    for j := n1+n2+n3+1 to n1+n2+n3+n4 do
        A[i,j] := 0;
    end;
{ Compute matrix elements according to the jump condition on the
electric field across the insulator surface}
for i := ma+mb+mc+1 to ma+mb+2*mc do
    begin
        clrscr;
        writeln ('Working on equation ',i,' (jump condition)');
        b[i] := 0;
        for j := 1 to n1 do
            begin
                A[i,j] := fn(cx[i-mc],cy[i-mc]j)*(epsirel-1);
            end;
        for j := n1+1 to n1+n2 do
            begin
                A[i,j] := -fn(cx[i-mc],cy[i-mc]j);
            end;
        for j := n1+n2+1 to n1+n2+n3 do
            begin
                A[i,j] := fn(cx[i-mc],cy[i-mc]j)*epsirel;
            end;
        for j := n1+n2+n3+1 to n1+n2+n3+n4 do
            begin
                A[i,j] := fn(cx[i-mc],cy[i-mc]j)*(epsirel-1);
            end;
        end;
    end;
{ Compute matrix elements according to the condition that the
potential is a constant on the bottom electrode}
for i := ma+mb+2*mc+1 to ma+mb+2*mc+md do
    begin
        clrscr;
        writeln ('Working on equation ',i,' (bottom electrode)');
        b[i] := 0;
        for j := 1 to n1 do
            A[i,j] := p(cx[i-mc],cy[i-mc]j);
        for j := n1+1 to n1+n2 do
            A[i,j] := 0;
        for j := n1+n2+1 to n1+n2+n3 do
            A[i,j] := p(cx[i-mc],cy[i-mc]j);
        for j := n1+n2+n3+1 to n1+n2+n3+n4 do
            A[i,j] := p(cx[i-mc],cy[i-mc]j);
        end;
    end;
{ Compute matrix elements according to the condition that the
potential is a constant on the bottom electrode}
for i := ma+mb+2*mc+md+1 to ma+mb+2*mc+md+me do
    begin
        clrscr;
        writeln ('Working on equation ',i,' (bottom electrode)');
        b[i] := 0;
        for j := 1 to n1 do
            A[i,j] := p(cx[i-mc],cy[i-mc]j);
        for j := n1+1 to n1+n2 do
            A[i,j] := p(cx[i-mc],cy[i-mc]j);
        for j := n1+n2+1 to n1+n2+n3 do
            A[i,j] := 0;
        for j := n1+n2+n3+1 to n1+n2+n3+n4 do
            A[i,j] := p(cx[i-mc],cy[i-mc]j);
        end;
    end;
end;

procedure get-data-from-file;
{ Load data from a file if something other than the default layout of

```

countour points and charges is desired}

```
begin
  clrscr;
  write ('Input data file: ');
  readln (input-filename);
  assign (filevar, input-filename);
  reset (filevar);
  readln (filevar, theta, epsirel);
  if (theta > 0)
    then
      phi := -1
    else
      phi := 1;
  theta := abs(theta);
  theta := theta*(pi/180);
  readln (filevar, ma, mb, mc, md, me, m);
  for i := 1 to m do
    readln (filevar, cx[i], cy[i]);
  readln (filevar, n1, n2, n3, n4, n);
  for i := 1 to n do
    readln (filevar, qx[i], qy[i]);
  readln (output-filename);
  close (filevar);
end;
```

procedure generate-mesh;

{Lay out contour points and unknown line charges along the electrodes and the surface of the insulator}

```
begin
  clrscr;
  write ('Angle of insulator (in degrees): ');
  readln (theta);
  {Determine the value of the potential on the top electrode according
  to the convention of the angle of the insulator}
  if (theta > 0)
    then
      phi := -1
    else
      phi := 1;
  theta := abs(theta);
  theta := theta*(pi/180);
  write (' Relative dielectric constant: ');
  readln (epsirel);
  write (' Output file name: ');
  readln (output-filename);
  {Begin placing contour points}
  ma := 15;
  mb := 15;
  mc := 20;
  md := 15;
  me := 15;
  m := 80;
  {Place contour points along the top electrode}
  d1 := (1+(sin(theta)/cos(theta)));
  for i := 1 to 15 do
    begin
      cx[i] := -1+d1*(1-exp(-(i-1)/3.26));
      cy[i] := 1;
    end;
  {Place contour points along the top electrode}
  d1 := (2-(sin(theta)/cos(theta)));
  for i := 16 to 30 do
    begin
      cx[i] := 2-d1*(1-exp(-(i-16)/3.26));
```

```

        cy[i] := 1;
    end;
    {Place contour points along the insulator surface}
    d1 := 1/40;
    for i := 31 to 50 do
        begin
            cy[i] := d1 + 2*d1*(i-31);
            cx[i] := cy[i]*(sin(theta)/cos(theta));
        end;
    {Place contour points along the bottom electrode}
    d1 := 1;
    for i := 51 to 65 do
        begin
            cx[i] := -1 + d1*(1-exp(-(i-51)/3.26));
            cy[i] := 0;
        end;
    {Place contour points along the bottom electrode}
    d1 := 2;
    for i := 66 to 80 do
        begin
            cx[i] := 2*d1*(1-exp(-(i-66)/3.26));
            cy[i] := 0;
        end;
    {End placing contour points}
    {Begin placing charges}
    n1 := 30;
    n2 := 20;
    n3 := 20;
    n4 := 30;
    n := 100;
    {Place unknown charges slightly above the top electrode}
    for i := 1 to 30 do
        begin
            qx[i] := cx[i];
            qy[i] := cy[i] + 0.025;
        end;
    {Place unknown charges slightly inside the insulator}
    for i := 31 to 50 do
        begin
            qx[i] := cx[i] - 0.025;
            qy[i] := cy[i];
        end;
    {Place unknown charges slightly outside the insulator}
    for i := 51 to 70 do
        begin
            qx[i] := cx[i-20] + 0.025;
            qy[i] := cy[i-20];
        end;
    {Place unknown charges slightly below the bottom electrode}
    for i := 71 to 100 do
        begin
            qx[i] := cx[i-20];
            qy[i] := cy[i-20] - 0.025;
        end;
    {End placing charges}
    {Shift upward by 1.0 to avoid singularities}
    for i := 1 to m do
        begin
            cy[i] := cy[i] + 1;
        end;
    for i := 1 to n do
        begin
            qy[i] := qy[i] + 1;
        end;

```

```

end;

procedure input-data;
{User interface}
begin
  clrscr;
  write ('Input from file or keyboard [F/K]: ');
  read (kbd, dchar);
  if (dchar = 'F') or (dchar = 'f')
  then
    get-data-from-file
  else
    if (dchar = 'K') or (dchar = 'k')
    then
      generate-mesh;
    else
      input-data;
  end;
end;

procedure move;
begin;
  for i := 1 to n do
    q[i] := b[i];
  end;
end;

procedure solve-for-field-quantities;
{Calculate the field quantities along the insulator surface}
begin
  clrscr;
  writeln ('Back-substituting');
  assign (filevar, output-filename);
  rewrite (filevar);
  writeln (filevar, 'Potential and field along the surface of an insulator');
  writeln (filevar);
  writeln (filevar, '    This information from file: ', output-filename);
  writeln (filevar, '    Insulator angle in degrees: ', (theta*(180/pi)): 4: 1);
  writeln (filevar, '    Relative dielectric constant: ', epsirel: 3: 1);
  writeln (filevar, 'Potential on the lower electrode: ground');
  writeln (filevar, 'Potential on the upper electrode: ', phi: 3: 1);
  writeln (filevar);
  write (filevar, '...zeta... ..phi... ..E.x... ..E.y... ');
  writeln (filevar, '....E.... .E.perp.. .E.para. ');
  for i := 1 to 21 do
    begin
      y := 1+0.05*(i-1);
      x := (y-1)*tan(theta);
      phiu := 0;
      for j := 1 to n1 do
        phiu := phiu + q[j]*p(x,y,j);
      for j := n1+1 to n1+n2 do
        phiu := phiu + q[j]*p(x,y,j);
      for j := n1+n2+1 to n1+n2+n3 do
        phiu := phiu;
      for j := n1+n2+n3+1 to n1+n2+n3+n4 do
        phiu := phiu + q[j]*p(x,y,j);
      ex := 0;
      for j := 1 to n1 do
        ex := ex + q[j]*fx(x,y,j);
      for j := n1+1 to n1+n2 do
        ex := ex + q[j]*fx(x,y,j);
      for j := n1+n2+1 to n1+n2+n3 do
        ex := ex;
      for j := n1+n2+n3+1 to n1+n2+n3+n4 do
        ex := ex + q[j]*fx(x,y,j);
    end;
  end;
end;

```

```

ey := 0;
for j := 1 to n1 do
  ey := ey + q[j]*fy(x,y,j);
for j := n1+1 to n1+n2 do
  ey := ey + q[j]*fy(x,y,j);
for j := n1+n2+1 to n1+n2+n3 do
  ey := ey;
for j := n1+n2+n3+1 to n1+n2+n3+n4 do
  ey := ey + q[j]*fy(x,y,j);
e := sqrt(ex*ex + ey*ey);
eperp := ex*cos(theta)-ey*sin(theta);
epara := ex*sin(theta)+ey*cos(theta);
write (filevar,(y-1):9:2,' ',phiu:9:2,' ',ex:9:2,' ',ey:9:2,' ');
writeln (filevar,e:9:2,' ',eperp:9:2,' ',epara:9:2);
end;
writeln (filevar);
writeln (filevar, '*');
writeln (filevar, theta:9:4);
clrscr;
writeln ('Computing equipotentials');
for i := 0 to 20 do
  begin
    for k := 0 to 10 do
      begin
        x := 0.1*i;
        y := 1 + 0.1*k;
        phiu := 0;
        for j := 1 to n1 do
          phiu := phiu + q[j]*p(x,y,j);
        for j := n1+1 to n1+n2 do
          phiu := phiu + q[j]*p(x,y,j);
        for j := n1+n2+1 to n1+n2+n3 do
          phiu := phiu;
        for j := n1+n2+n3+1 to n1+n2+n3+n4 do
          phiu := phiu + q[j]*p(x,y,j);
        writeln (filevar,x:9:4,' ',y-1:9:4,' ',phiu:9:4);
      end;
    end;
    close (filevar);
  end;

procedure beep;
{ Make a sound when the computation is complete}
begin
  clrscr;
  writeln ('Done');
  sound(980);
  delay(125);
  nosound;
  delay(25);
  sound(880);
  delay(125);
  nosound;
end;

begin
{ Main program}
  input-data;
  load-matrix-elements;
  ludcmp(A,100,100,indx,d);
  lubksb(A,100,100,indx,b);
  move;
  solve-for-field-quantities;
  beep;

```

end.

Program PLOTTER;

{ This program takes the output files generated by the programs CHARGD and UNCHAR and interpolates points along the equipotential contours, evenly spaced both in the potential phi and along the x-axis. The points may be connected to plot the equipotential contours. }

var

```
input-file      : string[40];
output-file     : string[40];
filevar         : text;
{ Input/output file specifications }
phi             : array[0..20,0..10] of real;
{ Input array }
input-string    : string[80];
ratio           : real;
throw           : real;
{ Dummy variables }
phi0            : real;
{ Equipotential value }
theta           : real;
{ Angle of the insulator }
xeq             : real;
yeq             : real;
{ Calculated points along the equipotentials }
i               : integer;
j               : integer;
k               : integer;
{ Indices }
```

procedure input-data;

{ Get data from previously-created file }

begin

```
  clrscr;
  write (' Input file: ');
  readln (input-file);
  assign (filevar, input-file);
  reset (filevar);
  repeat
    readln (filevar, input-string);
  until input-string[1] = '*';
  read (filevar, theta);
  for i := 0 to 20 do
    begin
      for j := 0 to 10 do
        read (filevar, throw, throw, phi[i,j]);
      end;
    end;
  close (filevar);
  if (phi[10,5] < 0)
  then
    begin
      for i := 0 to 20 do
        begin
          for j := 0 to 10 do
            phi[i,j] := -phi[i,j];
          end;
        end;
      end;
    end;
```

end;

```

procedure solve;
{Interpolate to find points along equipotentials}
begin
  write ('Output file: ');
  readln (output-file);
  assign (filevar, output-file);
  rewrite (filevar);
  writeln (filevar, 'This data in file: ',output-file);
  writeln (filevar);
  writeln (filevar, '...phi... ..x... ..y...');
  for k := 1 to 9 do
    begin
      phi0 := 0.1*k;
      for i := 0 to 20 do
        begin
          for j := 1 to 10 do
            begin
              if (j > i/((sin(theta)/cos(theta))+0.01))
              then
                begin
                  end
                end
              else
                begin
                  if (phi[i,j] > phi0) and (phi[i,j-1] < phi0)
                  then
                    begin
                      xeq := 0.1*i;
                      ratio := (phi0-phi[i,j-1])/(phi[i,j]-phi[i,j-1]);
                      yeq := 0.1*(j-1)+0.1*ratio;
                      writeln (filevar,phi0:9:1, ' ',xeq:9:2, ' ',yeq:9:2);
                    end
                  else
                    begin
                      end;
                    end;
                  end;
                end;
              end;
            end;
          end;
        end;
      end;
    end;
  close (filevar);
end;

begin
{Main program}
  input-data;
  solve;
end.

```

APPENDIX B

USING "LAPLACE"

The computer code LAPLACE [LAP86] provides the capability to solve the Poisson and Laplace equations on a personal computer, rather than having to access a mainframe computer. Essentially, the code sacrifices the ability to generate the solution mesh for an arbitrary problem (as codes such as JASON are capable of doing) in order to be small enough to run on a personal computer, leaving the mesh generation to the user. LAPLACE provides the facility of generating primitive mesh shapes (the "scratchpad meshes") and attaching these together to form the solution mesh (the archival "LAPLACE mesh"). As such, there may be several ways to generate the solution mesh, all equally valid, which way is most convenient may vary from user to user.

Unfortunately, the documentation provided with the user's manual does not make it clear exactly how these primitives are used, leaving the user to flounder for some time until he realizes what the program is doing. The first difficulty arises in realizing how the logical boundaries are assigned to the physical boundaries when a primitive mesh is generated.

The most common shape is surely the four-sided mesh. It is defined by the coordinates of its four corners, as shown in Figure B.1(a). Note that point (4) is opposite point (1). If one attempts to define the coordinates counterclockwise around the rectangle, then an error will result. The logical boundaries are defined by default as shown, with 1 opposite 3 and 2 opposite 4.

The three sided mesh is similarly defined by the coordinates of its three corners, as shown in Figure B.1(b). Here the boundary 1 is between points (1) and

(2), boundary 2 is between points (1) and (3), and boundary 3 is between points (2) and (3).

Confusion arises when the user attempts to create a trapezoidal primitive. This may be accomplished in two ways—by defining the four-sided primitive in the shape of a trapezoid, as in Figure B.1(c) (there is no requirement that the primitive be rectilinear), or by first defining a three sided primitive and removing rows of the mesh from the top, as in Figure B.1(d). Two points are salient. The y-coordinate of the top of the trapezoid in the later example will be determined by the number of mesh points which are retained along the side 2. If there were 21 mesh points along side 2 (counting the end points) and 11 rows were kept, then the height of the trapezoid will be half the height of the original triangle. Also, rows are counted from side one, so that irrespective of the orientation of the triangle, point (3) will always be eliminated.

The resulting trapezoidal meshes will have the same shape, but there will be a subtle difference between them. The logical boundaries of the four-sided mesh are assigned in ascending order clockwise from the bottom. The logical boundaries of the truncated three-sided mesh are different, since the original assignments of sides 1 to 3 are retained while a new side 4 is created. The result is that comparing the two, boundaries 3 and 4 are interchanged. Either is a valid mesh, but it is important to know which boundary one is referring to when placing the scratchpad mesh into the archival mesh, since LAPLACE provides no visual aid in determining which logical boundaries correspond to which physical boundaries.

A drawback to the code is that while it readily creates circular meshes which may be used to form convex regions, creating the concave regions with

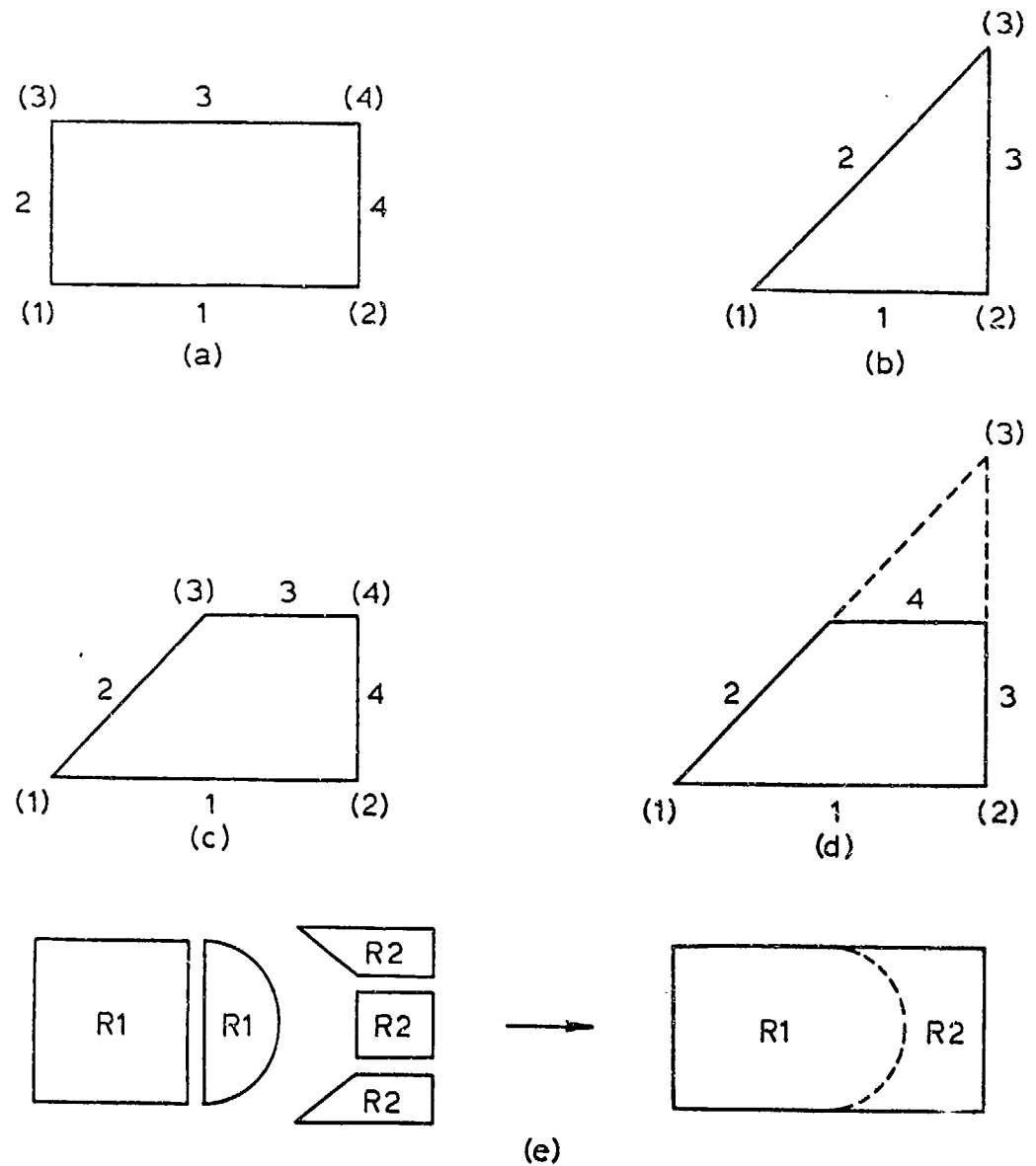


Figure B.1. LAPLACE scratchpad meshes. a) Four-sided mesh. b) Three-sided mesh. c) A trapezoidal four-sided mesh. d) A trapezoidal mesh created by truncating a three-sided mesh. e) Assembling a mesh with a circular boundary between regions.

which these may mate is a more difficult problem. Effectively, one must use the node-level editor to determine the position of each of the nodes on the circular boundary of the convex region. Then, one must use primitives to build the concave region. Since the boundaries of the convex region and the primitives are only approximately the same, it is necessary to again use the node-level editor to match the nodes on the primitives to those on the convex region.

Another difficulty arises when attaching the scratchpad mesh to the archival mesh. Logical boundary (and region) assignments can be changed at will in the scratchpad mesh, but not at all in the archival mesh. Even this must be done carefully. If one wishes to switch the assignments of boundaries 1 and 2, one cannot blithely change 1 to 2 and then expect to change 2 to 1. The first operation destroys the original identity of boundary 2. Rather, one must change 2 to 12 (or some "dummy" number < 20), change 1 to 2, and finally change 12 to 1.

The procedure of attaching a scratchpad mesh to an archival mesh is best illustrated by example, as shown in Figure B.2. First, a trapezoidal four-sided scratchpad mesh is created. By default, it is region R1. The default logical boundary assignment of boundary 4 is changed to 5, and the scratchpad mesh is added to the archival mesh. Another scratchpad mesh is created, and now the logical boundary 2 is changed to 5, while the default region R1 is changed to R2. This scratchpad mesh is added to the archival mesh, using the "zip-up" option. The resulting archival mesh has four logical boundaries and two logical regions. Now, the dielectric constant of one of the regions may be changed (to model an insulator) and the potential on boundaries 1 and 3 may be specified (to model high-voltage electrodes). Note that the boundary between regions does not carry a logical boundary number; boundary number 5 disappeared when the second

archival mesh was added. LAPLACE takes the boundary conditions between regions into account automatically.

One final difficulty may be overcome by careful mesh generation. LAPLACE allows the addition of space charge in specified regions, but does not allow for surface charge. However, surface charge may be simulated by placing space charge in a region which is thin, compared to the other dimensions of the problem. Figure B.3 illustrated the technique by modelling a capacitor. In Figure B.3(a), the capacitor is modelled by a unit potential across a unit distance. In Figure B.3(b), the potential across the unit distance is not defined; rather, a region of space charge of unit charge density and unit thickness replaces the upper boundary. Finally, in Figure B.3(c), the thickness of the space-charged region is reduced and the charge density is increased, keeping (charge density) \times (thickness) constant. The resulting potential distributions in the are equivalent. In general, surface charge of charge density σ may be replaced by a thin region of thickness l and space charge of charge density ρ , such that $\rho l = \sigma$, as long as l is smaller than the other pertinent dimensions in the problem.

One final note is appropriate—in adding a thin region to the archival mesh, it is necessary to use the “zip-up with modifications” option and to set the “zip-up factor” on the order of the ratio of the thickness of the thin region to the typical mesh spacing in the archival mesh. Otherwise, the scratchpad mesh will effectively disappear when attached to the archival mesh. A typical mesh used to model the problem of a vacuum insulator with a uniform charge density on the surface is shown in Figure B.4.

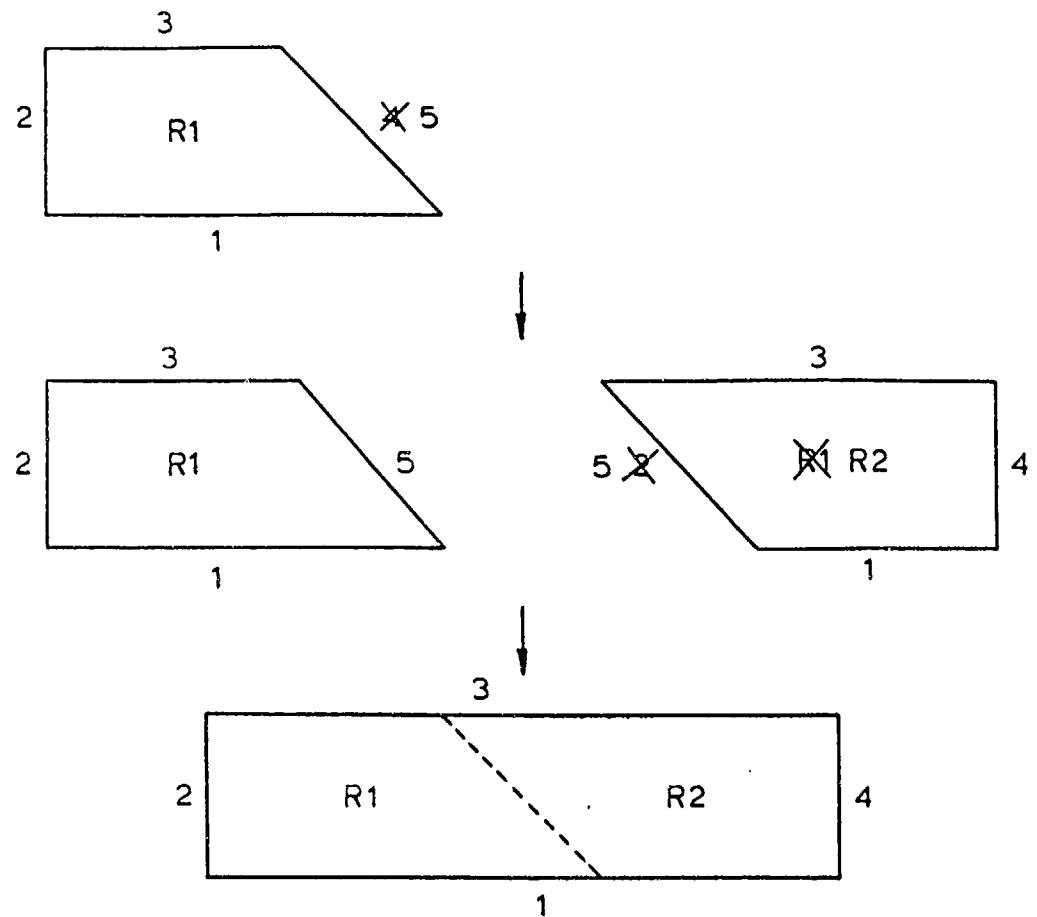


Figure B.2. Adding a scratchpad mesh to an archive mesh.

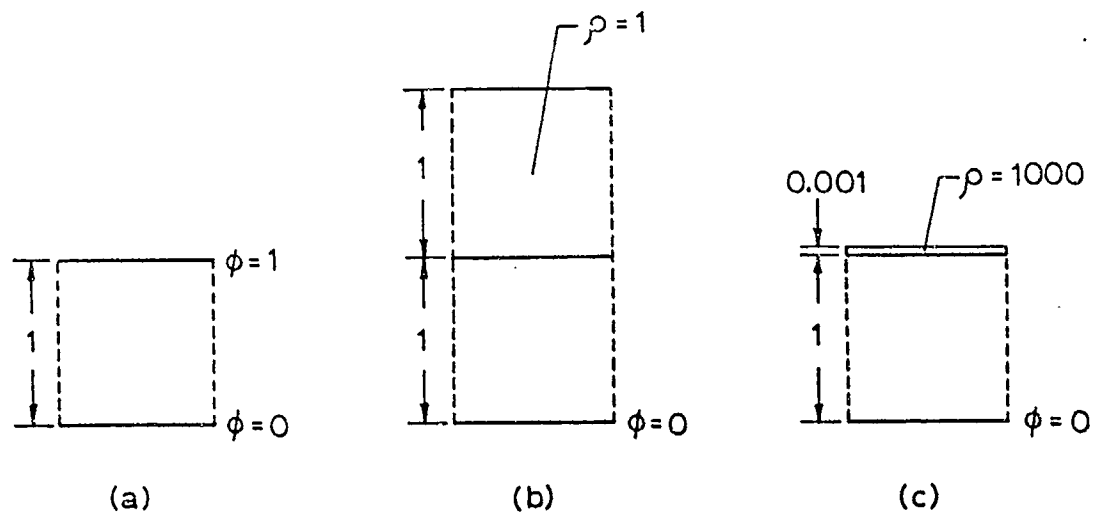


Figure B.3. Simulating surface charge with thin regions of volume charge in three equivalent ways. a) By defining the potential. b and c) By defining the charge density.

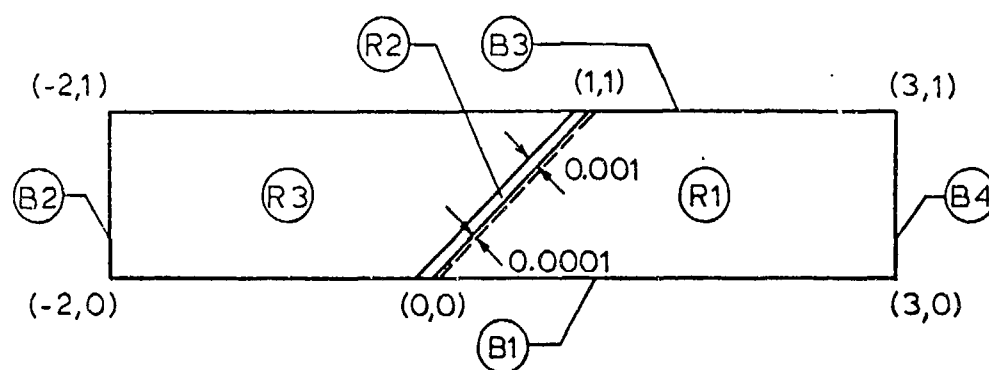


Figure B.4. A typical LAPLACE mesh used to solve the problem of a vacuum insulator with a uniform surface charge density.

APPENDIX C

OPERATING THE KRF EXCIMER LASER

Included in this appendix are formulas for the gas mixtures used in the KrF excimer laser and a checklist for laser operations. Although the user's manual supplied with the laser should be consulted if any questions arise concerning operation or especially maintenance of the laser, a few points deserve emphasis:

- 1) The fluorine gas is supplied as a 10% mixture of fluorine in helium. Although it is buffered, it is nevertheless highly corrosive and should be handled with caution.
- 2) The mixing cell is metered by two gauges, one a vacuum gauge for measuring pressures below atmosphere, and another a pressure gauge for measuring pressure above atmosphere. The valve connecting the vacuum gauge to the mixing cell must be closed before applying greater-than-atmosphere pressure to the cell; otherwise, a pressure relief valve will vent excess (and presumably corrosive) gas into the vent line.
- 3) The PVC vent line for the laser cabinet is pressurized by the exhaust fan of the laser, and exits the building above the roofline. In order to make sure that corrosive fumes do not enter the experimental bay, the laser and the mixing cell must not be exhausted or evacuated unless the laser power is on and the exhaust fan is running. The exhaust fan is on continuously while the laser is on. Also, the laser should be allowed to run for 20 minutes after the last corrosive mixture is vented in order to insure that the exhaust line is clear. The laser power must

be on any time that a corrosive mixture is in the laser, to vent the experimental bay in case of accidental release of a corrosive mixture.

- 4) The laser is interlocked to both the front and the back experimental bay doors. If the interlock is broken, high voltage is shut off, although laser power is still on. Nevertheless, if the laser power is on do not remove laser goggles in the experimental bay without covering the output of the laser or confirming that the "high voltage off" (green) light on the control panel is lighted.
- 5) Do not look into the laser any time when an active lasing mixture is in it, even if the interlock is open. If it becomes necessary to align the laser by eye, replace the active mixture with an inert on (He) and wear safety glasses when looking down the optical axis.

KrF Laser Operations Checklist

SETUP SEQUENCE

- ___ Laser power on
- ___ Vacuum pump on
- ___ Gas bottles open
- ___ Verify regulator settings (charging 22 PSIG, firing 25 PSIG)
- ___ Wait for laser to warm up

MIXING SEQUENCE

- ___ Evacuate mixing tank (bypass to 5 PSIG)
- ___ Fill mixing tank with desired mixture (lasing or hot passivation)

FIRING SEQUENCE

- ___ Evacuate laser (bypass to 20 PSIA)
- ___ Fill laser with gas mixture
- ___ Open gas flow into switches (15 SCFH for repetitive pulses)
- ___ Adjust laser charge voltage (maximum for lasing, 25 kV for hot passivation)
- ___ Fire laser

*MIXING AND FIRING SEQUENCES MAY BE REPEATED AS DESIRED

SHUTDOWN SEQUENCE

- ___ Evacuate mixing tank (bypass to 5 PSIG)
- ___ Fill mixing tank with desired mixture
- ___ Evacuate laser (bypass to 20 PSIA)
- ___ Fill laser with gas mixture (He or static passivation to 20 PSIA)
- ___ Vent excess from mixing tank (to 5 PSIG)
- ___ Close all valves
- ___ Gas bottles closed
- ___ Vacuum pump off
- ___ Wait 20 minutes
- ___ Laser power off unless passivation mixture is used

Table C.1. Gas Mixtures for the KrF Excimer Laser

	Lasing		Hot Passivation		Static Passivation	
begin with	83 Torr	He	500 Torr	F/He	40 PSIG	F/He
add	517 Torr	Kr	balance	He	160 PSIG	He
to get	600 Torr	Mix	200 PSIG	Mix	200 PSIG	Mix
add	156 Torr	F/He				
to get	756 Torr	Mix				
add	balance	He				
to get	200 PSIG	Mix				
fill laser to	35-45 PSIA	Mix	10 PSIA	Mix	45 PSIA	Mix

REFERENCES

REFERENCES

- And75 R. A. Anderson, "Role of the Secondary Electron Emission Avalanche in Surface Flashover or [sic] Insulators in Vacuum," in *1974 Annual Report, Conference on Electrical Insulation and Dielectric Phenomena* (Washington, D.C.: National Academy of Sciences, 1975), 435.
- And77 R. A. Anderson, "Propagation velocity of cathode-initiated surface flashover," *J. Appl. Phys.* **48** (10), 4210 (1977).
- And78 R. A. Anderson, "Time-Resolved Measurements of Surface Flashover of Conical Insulators," in *1975 Annual Report, Conference on Electrical Insulation and Dielectric Phenomena* (Washington, D.C.: National Academy of Sciences, 1978), 475.
- And79 R. A. Anderson and J. P. Brainard, "Insulator Surface Charging During Fast Pulsed Surface Flashover in Vacuum," in *1977 Annual Report, Conference on Electrical Insulation and Dielectric Phenomena* (Washington, D.C.: National Academy of Sciences, 1979), 128.
- And80 R. A. Anderson and J. P. Brainard, "Mechanism of pulsed surface flashover involving electron-stimulated desorption," *J. Appl. Phys.* **51** (3), 1414 (1980).
- And85 R. A. Anderson and K. W. Tucker, "Vacuum surface flashover from bipolar stress," *J. Appl. Phys.* **58** (9), 3346 (1985).
- Avd77a A. A. Avdienko, "Surface breakdown of solid dielectrics in vacuum. I. Characteristics for breakdown of insulators along the vacuum surface," *Sov. Phys. Tech. Phys.* **22** (8), 982 (1977).
- Avd77b A. A. Avdienko and M. D. Malev, "Surface breakdown of solid dielectrics in vacuum. II. Mechanism for surface breakdown," *Sov. Phys. Tech. Phys.* **22** (8), 986 (1977).
- Avd79 A. A. Avdienko and M. D. Malev, "Surface breakdown of solid dielectrics in vacuum. III. Quantitative model," *Sov. Phys. Tech. Phys.* **24** (5), 581 (1979).
- Bak78 W. L. Baker, M. C. Clark, J. H. Degnan, G. F. Kiuttu, C. R. McClenahan, and R. E. Reinovsky, "Electromagnetic-implosion generation of pulsed high-energy-density plasma," *J. Appl. Phys.* **49** (9), 4694 (1978).

- Ber77 K. D. Bergeron, "Theory of the secondary electron avalanche at electrically stressed insulator-vacuum interfaces," *J. Appl. Phys.* **48** (7), 3073 (1977).
- Boe63 H. Boersch, H. Hamisch, and W. Ehrlich, "Oberflächenentladungen über Isolatoren in Vakuum," *Z. Angew. Phys.* **15**, 518 (1963).
- Bor58 E. S. Borovik and B. P. Batrakov, "Investigations of Breakdown in Vacuum," *Sov. Phys. Tech. Phys.* **3**, 1811 (1958).
- Bov58 F. A. Bovey, *The Effects of Ionizing Radiation on Natural and Synthetic High Polymers*, (New York: Interscience Publishers, 1958).
- Bra74 J. P. Brainard and D. Jensen, "Electron avalanche and surface charging on alumina insulators during pulsed high voltage stress," *J. Appl. Phys.* **45** (8), 3260 (1974).
- Bra75 J. P. Brainard and D. Jensen, "Measurements of the Charge Distributions on an Alumina Insulator in Vacuum Resulting from High Voltage Stress," in *1975 Annual Report, Conference on Electrical Insulation and Dielectric Phenomena* (Washington, D.C.: National Academy of Sciences, 1978), 475.
- Bra78 J. P. Brainard, "Local Fields at the Cathode-Insulator Junction as a Cause of Breakdown of Shaped Insulators in Vacuum," in *1975 Annual Report, Conference on Electrical Insulation and Dielectric Phenomena* (Washington, D.C.: National Academy of Sciences, 1978), 482.
- Bug68 S. P. Bugaev, A. M. Iskol'dskii, and G. A. Mesyats, "Investigations of the Pulsed Breakdown Mechanism at the Surface of a Dielectric in a Vacuum. I. Uniform Field," *Sov. Phys. Tech. Phys.* **12** (16), 1368 (1968).
- Bur80 E. A. Burke, "Secondary Emission from Polymers," *IEEE Trans. Nucl. Sci.*, **NS-27** (6), 1760 (1980).
- Cha67 A. Charlesby, "Radiation Mechanisms in Polymers," in *Irradiation of Polymers*, ed. R. F. Gould (Washington, D.C.: American Chemical Society, 1967), 1.
- Cro74 J. D. Cross and T. S. Sudarshan, "The Effect of Cuprous Oxide Coatings on Surface Flashover of Dielectric Spacers in Vacuum," *IEEE Trans. Electr. Insul.* **EI-9** (4), 146 (1974).
- DeT72 C. H. DeTourreil, K. D. Srivastava, and U. J. Woelke, "Experimental Observation of Surface Charging of High-Voltage Insulators for Vacuum Apparatus," *IEEE Trans. Electr. Insul.* **EI-7** (4), 176 (1972).
- DeT73 C. H. DeTourreil and K. D. Srivastava, "Mechanism of Surface Charging of High-Voltage Insulators in Vacuum," *IEEE Trans. Electr. Insul.* **EI-8** (1), 17 (1973).

- Dio73 G. F. Dionne, "Effects of secondary electron scattering on secondary emission yield curves," *J. Appl. Phys.* **44** (12), 5361 (1973).
- Dio75 G. F. Dionne, "Origin of secondary-electron-emission yield-curve parameters," *J. Appl. Phys.* **46** (8), 3347 (1975).
- Ekd80 C. A. Ekdahl, "Voltage and current sensors for a high-density z-pinch experiment," *Rev. Sci. Instrum.* **51** (12), 1645 (1980).
- Enl82 C. Enloe, R. Blaher, M. Coffing, and R. E. Reinovsky, "Vacuum Ultra-Violet Effects on Power Transport Across a Vacuum/Solid Dielectric Interface," *Proc. Xth International Symposium on Discharge and Electrical Insulation in Vacuum*, Columbia, SC, 1982, 308.
- Enl83 C. L. Enloe and R. E. Reinovsky, "Ultra-Violet Induced Insulator Flashover as a Function of Material Properties," *Proc. 4th IEEE Pulsed Power Conference*, Albuquerque, NM, 1983, 682.
- Enl85 C. L. Enloe, "An Ultraviolet Laser Shadowgraphy System for the SHIVA-Star Fast Capacitor Bank," Air Force Weapons Laboratory technical report AFWL-TR-85-82 (1985).
- Enl87a C. L. Enloe and R. M. Gilgenbach, "Ultraviolet-Induced Flashover of a Plastic Insulator Using a Pulsed Excimer Laser," *Plasma Chem. and Plasma Process.* **7** (1), 89 (1987).
- Enl87b C. L. Enloe and R. M. Gilgenbach, "Ultraviolet-Induced Insulator Flashover Experiments at the University of Michigan," *Proc. 6th IEEE Pulsed Power Conference*, Arlington, VA, 1987 (to be published).
- Enl87c C. L. Enloe, R. M. Gilgenbach, and J. S. Meachum, "Fast, sensitive laser deflection system suitable for transient plasma analysis," *Rev. Sci. Instrum.* **58** (9), 1597 (1987).
- Flo69 P. J. Flory, *Statistical Mechanics of Chain Molecules* (New York: Interscience, 1969), 41.
- Gil83 R. M. Gilgenbach, O. E. Ulrich, and L. D. Horton, "Localized metallic melting and hole boring by laser guided discharges," *Rev. Sci. Instrum.* **54** (1), 109 (1983).
- Gle51a P. H. Gleichauf, "Electrical Breakdown Over Insulators in High Vacuum," *J. Appl. Phys.* **22** (5), 535 (1951).
- Gle51b P. H. Gleichauf, "Electrical Breakdown Over Insulators in High Vacuum," *J. Appl. Phys.* **22** (6), 766 (1951).
- Gra85 E. W. Gray, "Vacuum surface flashover: a high-pressure phenomenon," *J. Appl. Phys.* **58** (1), 132 (1985).

- Gre82 M. A. Greenspan and K. V. Reddy, "A laser deflection technique for sensitive measurement of a reduced-density channel in neutral gas," *Appl. Phys. Lett.* **40** (7), 576 (1982).
- Grz72 S. Grzybowski, E. Kuffel, and J. P. C. McMath, "The Flashover Voltage of Polymethylmethacrylate in Vacuum Under Direct, Alternating, and Surge Voltages of Various Front Durations," *IEEE Trans. Electr. Insul.* **EI-7** (4), 180 (1972).
- Han88 S. G. Hansen and T. E. Robitaille, "Formation of polymer films by pulsed laser evaporation," *Appl. Phys. Lett.* **52** (1), 81 (1988).
- Haw68 R. Hawley, "Solid Insulators in Vacuum: A Review," *Vacuum* **18** (7), 383 (1968).
- Hud65 R. H. Huddleston and S. L. Leonard, *Plasma Diagnostic Techniques* (New York: Academic, 1965).
- Jac83 G. L. Jackson, L. L. Hatfield, M. Kristiansen, J. Marx, and A. Bowling, "Pulse Flashover of Solid Dielectrics in Vacuum," *IEEE Trans. Electr. Insul.* **EI-18** (3), 310 (1983).
- Kea83 A. J. Kearsley, A. J. Andrews, C. E. Webb, K. Errey, and J. Coutts, "Cryogenic Gas Purification and Lifetime Extension of ArF, KrF, and XeF Laser Gas Mixtures," in *Excimer Lasers-1983*, ed. C. K. Rhodes, H. Egger, and H. Pummer (New York: American Institute of Physics, 1983), 107.
- Kir85 *Kirk-Othmer Concise Encyclopedia of Chemical Technology*, ed. M. A. Grayson, (New York: John Wiley and Sons, 1985).
- Kno79 G. F. Knoll, *Radiation Detection and Measurement* (New York: John Wiley and Sons, 1979).
- LAP86 *LAPLACE Version 2.5 Manual*, P. L. Hagelstein and Associates, P.O. Box 2723, Livermore, CA 94550 (1986).
- Lat81 R. V. Latham, *High Voltage Vacuum Insulation: The Physical Basis* (London: Academic Press, 1981), 229ff.
- Loc68 W. Lochte-Holtgreven, *Plasma Diagnostics*, (Amsterdam: North-Holland, 1968).
- Lyn75, *CRC Handbook of Materials Science*, ed. C. T. Lynch (Cleveland: CRC Press, 1975).
- Mil72 O. Milton, "Pulsed Flashover of Insulators in Vacuum," *IEEE Trans. Electr. Insul.* **EI-7** (1), 9 (1972).

- Mil78 H. C. Miller and E. J. Furno, "The effect of Mn/Ti surface treatment on voltage-holdoff performance of alumina insulators in vacuum," *J. Appl. Phys.* **49** (11), 5416 (1978).
- Mil80 H. C. Miller, "Improving the Voltage Holdoff Performance of Alumina Insulators in Vacuum Through Quasimetallizing," *IEEE Trans. Electr. Insul.* **EI-15** (5), 419 (1980).
- Mil85 H. C. Miller, "The Effect of Doping on the Voltage Holdoff Performance of Alumina Insulators in Vacuum," *IEEE Trans. Electr. Insul.* **EI-20** (3), 505 (1985).
- Nas79 V. Nassisi and A. Luches, "Rogowski coils: theory and experimental results," *Rev. Sci. Instrum.* **50** (7), 900 (1979).
- Nik63 T. S. Nikitina, E. V. Zhuravskaya, and A. S. Kuzminsky, *Effect of Ionizing Radiation on High Polymers* (New York: Gordon and Breach, 1963).
- Pea41 R. W. B. Pearse and A. G. Gaydon, *The Identification of Molecular Spectra* (London: Chapman and Hall, 1941).
- Pel80 D. G. Pellinen, M. S. DiCapua, S. E. Sampayan, H. Gerbracht, and M. Wang, "Rogowski coil for measuring fast, high-level pulsed currents," *Rev. Sci. Instrum.* **51** (11), 1535 (1980).
- Phi86 H. R. Philipp, H. S. Cole, Y. S. Liu, and T. A. Sitnik, "Optical absorption of some polymers in the region 240-170 nm," *Appl. Phys. Lett.* **48** (2), 192 (1986).
- Pil82 A. S. Pillai and R. Hackam, "Surface flashover of solid dielectric in vacuum," *J. Appl. Phys.* **53** (4), 2983 (1982).
- Pil83 A. S. Pillai and R. Hackam, "Modifications of electric field at the solid insulator-vacuum interface arising from surface charges on the solid insulator," *J. Appl. Phys.* **54** (3), 1302 (1983).
- Pil84 A. S. Pillai and R. Hackam, "Surface flashover of conical insulators in vacuum," *J. Appl. Phys.* **56** (5), 1374 (1984).
- Pil85a A. S. Pillai and R. Hackam, "Surface flashover of solid insulators in atmospheric air and in vacuum," *J. Appl. Phys.* **58** (1), 146 (1985).
- Pil85b A. S. Pillai and R. Hackam, "Effects of Glow Discharge Conditioning and Addition of Gases on Surface Flashover," *IEEE Trans. Electr. Insul.* **EI-20** (4), 763 (1985).
- Pre86 W. H. Press, B. P. Flannery, S. A. Teukolsky, and W. T. Vetterling, *Numerical Recipes* (Cambridge: Cambridge University Press, 1986).

- Rån67 B. Rånby and P. Carstensen, "Free Radicals in Polyolefins Initiated with Ultraviolet and Ionization Radiation," in *Irradiation of Polymers*, ed. R. F. Gould (Washington, D.C.: American Chemical Society, 1967), 256.
- Rea80 J. Reader, C. H. Corliss, W. L. Wiese, and G. A. Martin, *Wavelengths and Transition Probabilities for Atoms and Atomic Ions*, National Bureau of Standards Report NSRDS-NBS68 (1980).
- Sha65 J. P. Shannon, S. F. Philip, and J. G. Trump, "Insulation of High Voltage Across Solid Insulators in Vacuum," *J. Vac. Sci. Tech.* **2**, 234 (1965).
- Sin74 H. Singer, H. Steinbigler, and P. Weiss, "A Charge Simulation Method for the Calculation of High Voltage Fields," *IEEE Trans. Power Appar. Syst.* **PAS-93**, 1660 (1974).
- Sri87 R. Srinivasan, B. Braren, and R. W. Dreyfus, "Ultraviolet laser ablation of polyimide films," *J. Appl. Phys.* **61** (1), 372 (1987).
- Sud76 T. S. Sudarshan and J. D. Cross, "The Effect of Chromium Oxide Coating on Surface Flashover of Alumina Spacers in Vacuum," *IEEE Trans. Electr. Insul.* **EI-11** (1), 32 (1976).
- Sud77 T. S. Sudarshan, J. D. Cross, and K. D. Srivastave, "Prebreakdown Processes Associated with Surface Flashover of Solid Insulators in Vacuum," *IEEE Trans. Electr. Insul.* **EI-12** (3), 200 (1977).
- Sut86 E. Sutcliffe and R. Srinivasan, "Dynamics of UV laser ablation of organic polymer surfaces," *J. Appl. Phys.* **60** (9), 3315 (1986).
- Tho80 J. E. Thompson, J. Lin, K. Mikkelsen, and M. Kristiansen, "Investigations of Fast Insulator Surface Flashover in Vacuum," *IEEE Trans. Plasma Sci.* **PS-8** (3), 191 (1980).
- Van82 J. P. VanDevender, "Magnetic inhibition of insulator flashover," *J. Appl. Phys.* **53** (6), 4441 (1982).
- Wat67 A. Watson, "Pulsed Flashover in Vacuum," *J. Appl. Phys.* **38** (5), 2019 (1967).
- Wea85 *CRC Handbook of Chemistry and Physics*, ed. R. C. Weast (Boca Raton: CRC Press, 1985).
- Win83 H. J. Wintle, "Conduction Processes in Polymers," in *Engineering Dielectrics*, vol. IIA, ed. R. Bartnikas and M. Eichorn (Philadelphia, American Society for Testing and Materials, 1983), 239.